Synthesis of GaN Film from Aqueous Solution

Jae-Wook Kang

Synthesis of GaN Film from Aqueous Solution

Advisor: Professor Masazumi Okido

by

Jae-Wook Kang
Department of Materials Science and Engineering
Nagoya University

A dissertation submitted to the faculty of the Nagoya University in partial fulfillment of the requirements for the degree of Doctor of Philosophy in the Department of Materials Science and Engineering.

Nagoya, Japan
2019. 1. 15
Approved by

_____
Professor Masazumi Okido

Abstract

Gallium nitride (GaN) is a direct bandgap semiconductor and one of the most interesting materials in the optoelectronic device and high-power electronic device field. GaN has a wide bandgap energy of 3.39 eV at room temperature which can cover the entire UV visible range, thus it emits blue light efficiently and has been successfully employed in optoelectronics industry. In addition, GaN having a stable wurtzite structure has attracted attention as an alternative to silicon semiconductors since its high electron transfer speed and stability in high frequency region. Thus, for decades, many researchers have been trying various researches for high quality GaN, and have recently succeeded in producing single crystal GaN using by various dry methods such as MOCVD, MBE, HVPE, etc.

Nevertheless, high-cost of GaN manufacturing technologies are proposed as a challenge to overcome in its wide application and commercialization. Expensive equipment for high vacuum and high temperature environments and ultrapure source materials requiring complex processing are the main challenges in the commercialization of GaN. The main key for GaN commercialization is to reduce the costs used for high vacuum, high temperature environments and ultrapure sources. Due to these demands, electrochemical methods are again attracting attention, and electrodeposition has been proposed as one of the possible methods for GaN fabrication by its low-temperature and low-cost characteristics. Therefore, I tried to synthesize GaN film by applying electrochemical deposition method.

GaN films were synthesized on n-type-silicon (111) substrates using a low-cost and low-temperature technique of electrochemical deposition. The electrochemical behavior of gallium, ammonium, and nitrate ions in the aqueous solutions used as sources of GaN were confirmed by cyclic voltammetry. The scanning electron microscopy images showed that the films deposited at a current density of 3.5 mA cm^{-2} or greater have plate-like surface morphologies on the silicon substrate. The energy dispersive X-ray spectroscopy results showed that oxygen, gallium, and nitrogen coexist in these plate-like films. In the X-ray diffraction patterns, the sample synthesized at a current density of 3.5 mA

cm^{-2} for 24 h exhibited peaks of cubic-GaN (c-GaN) and hexagonal-GaN (h-GaN) phases. Also, the peaks corresponding to gallium and gallium oxide phase were observed. Photoluminescence analysis revealed the peaks at 3.2 and 3.39 eV, which corresponds to the band gap energy of GaN, as well as a broad peak at around 2.5 eV at room temperature.

Next, the electrodeposition of GaN film has been attempted on various substrate materials. And electrochemical behavior of gallium and nitrogen ions on different electrodes. A cathodic current corresponding to the reduction reaction of each ion on different four substrates was confirmed. The hydrogen overpotential of electrodes influenced the reduction reactions of gallium and nitrogen species ions, and it was confirmed that the formation of adsorbed nitrogen on the substrate with high hydrogen overvoltage was easy. Reduction reaction of gallium occurred along with hydrogen evolution, and CV analysis confirmed the peaks of the reduction reaction of each ion separated on gallium and aluminum electrode. Nitrogen content of 20 mol% or more was observed from the films deposited on gallium and aluminum electrodes, and a peak due to reflection of GaN was detected by X-ray diffraction. In particular, a sharp peak corresponding to GaN was observed on Al substrate.

As previous research has confirmed that the properties of substrates affect the formation of GaN film, and the presence of high content of gallium and nitrogen in the film deposited on the aluminum substrate was confirmed. Therefore, the films were synthesized on aluminum substrates heat-treated at various temperatures to investigate the effect of aluminum. Deposited films showed that the plate-like polygonal structure and irregular cauliflower-like morphology. The presence of h-GaN and gallium oxide phases was confirmed by X-ray diffraction. Composition analysis revealed that more than 35 mol% of gallium and nitrogen are present with oxygen in the film. It was confirmed that the amount of oxygen in the electrodeposited films was significantly reduced by the effect of boric acid added into the solution as a buffer. The X-ray photoelectron spectroscopy and Raman analysis revealed that the signals due to h-GaN, and the stronger signals appeared for the films formed on heat-treated aluminum substrate. In particular, the GaN film is more easily grown in the presence of alumina formed by heat treatment. The growth characteristics of electrodeposited GaN are strongly influenced by the composition and

orientation of Al substrate. It is confirmed that the GaN film grows in a direction perpendicular to the preferred orientation of Al substrate and the GaN grows in the direction of making lattice mismatch small. In other words, it has been found that GaN growth can be controlled depending on substrate conditions.

Although the synthesis of single crystal GaN was not achieved, the possibility of synthesis of GaN from room temperature aqueous solution by electrodeposition was confirmed. Therefore, this is a simple one-step method for the synthesis of GaN, and this is possible to apply as the economical method for preparation of next generation materials.

Table of Contents

Chapter 2. Low-temperature Synthesis of GaN Films from Aqueous Solution by Electrodeposition

Chapter 3. Influence of Substrate on Formation of Electrodeposited GaN Film

List of Tables

List of Figures

Chapter 1

Introduction

Chapter 1 – General introduction

1.1 Overview of GaN material

Since its appearance in the early 1990s gallium nitride (GaN) has been regarded as a very interesting and highly promising material system for both optical and microwave high-power electronic applications [1–9]. For dozens of years researchers all around the world have made great efforts to meet these interesting [10–14]. GaN-based optical devices have reached the commercialization stage and commercial innovation is expected with the application of single crystal GaN substrates, an interesting alternative to silicon wafers. The GaN device market was valued at $400 million in 2018 and is expected to reach $3 billion by 2025 [15]. This chapter will start with general introduction of GaN material. An overview of the advantages of GaN and some of the possible areas of application will highlight the importance of this research.

1.1.1 Characteristics and Applications of GaN

Gallium nitride (GaN) and its alloys with aluminum (Al) or indium (In) are very promising materials which have stable wurtzite structure for optoelectronic devices and high-power electronic devices [16–18]. Specifically, III-nitrides semiconductors are also suitable for ultraviolet (UV) detectors, waveguides, UV and visible light-emitting diodes (LEDs), and laser diodes (LDs) for digital data read-write applications [19]. Especially, GaN has a wide bandgap energy, E_g, of 3.39 eV at room temperature which can cover the entire UV visible range (see Figure 1.1), thus it has been successfully employed in optoelectronic devices field [20–24]. GaN has bandgap energy about two to three times those of conventional semiconductors such as silicon (Si), gallium arsenide (GaAs), and indium phosphide (InP), and wide bandgap energy results in high electric breakdown fields, E_c, which enable the applications requiring high supply voltages.

GaN provide many advantages over organic materials for optoelectronic device applications,

including high operating temperature, high carrier mobility and radiative recombination rates, as well as long-term stability and reliability [25–30]. The excitement over GaN stems from their better material and electronic properties compared to silicon and other III-V compounds, like GaAs. GaN has also a breakdown voltage of ~5.0 × 10^6 V cm^{-1} approximately 10 times greater than that of Si [31,32], and a saturation electron velocity is ~3.15 × 10^7 cm s^{-1} [33], which is much higher than Si, GaAs, and silicon carbide (SiC) [34]. In addition, when comparing physical properties with SiC, which is attracting attention as a semiconductor material at the same time, all values excluding thermal conductivity exceed SiC [9,35]. Furthermore, unlike compound semiconductors using phosphorus (P) or arsenic (As), nitrides are harmless to the human body and the environment [36].

These properties enable the use of GaN based devices in a broad range of applications in various fields, including the automotive, military and space industries as well as in high power amplifiers for wireless base stations, and high voltage electronics for power transmission lines [37].

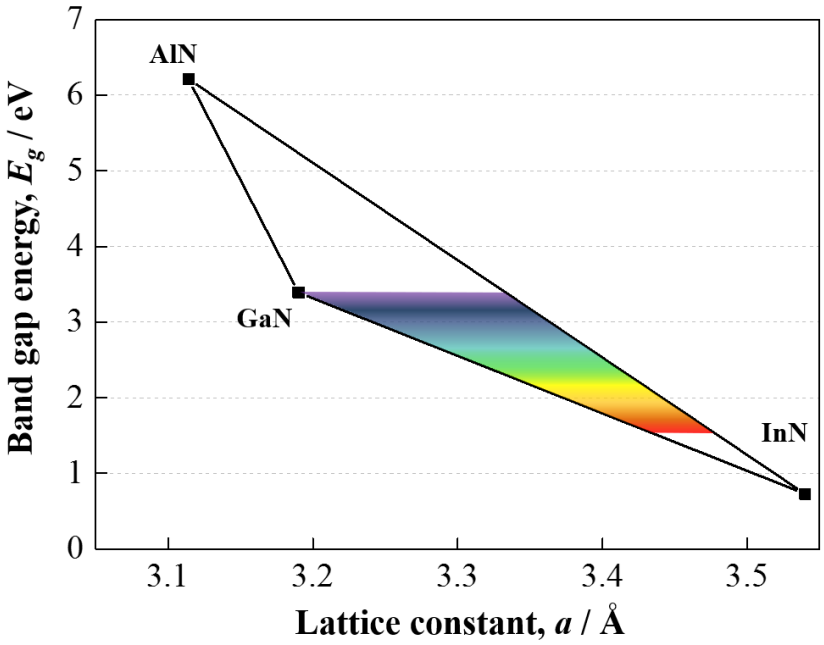

Fig. 1.1 Bandgap energies of III-nitride semiconductors as a function of the lattice parameters. The range of visible spectrum is shown in colors [38].

Table 1.1 Material properties of conventional and wide-bandgap semiconductors at 300 K [18,39,40].

Property	GaN, AlGaN/ GaN	GaAs, AlGaAs/ InGaAs	InP, InAlAs/ InGaAs	SiC	Si
Bandgap Energy, E_g (eV)	3.44	1.43	1.35	3.26	1.12
Electric breakdown field, E_c (MV/cm)	3	0.4	0.5	3	0.3
Electron mobility, μ_n ($cm^2/V{\cdot}s$)	900, 2000^{α}	8500, 10000^{β}	5400, 10000^{χ}	700	1500
Thermal conductivity, κ (W/cm·K)	1.3–2.1	0.5	0.7	3.7–4.5	1.5

$^{\alpha, \beta, \chi}$ values for the corresponding heterostructures

1.1.2 Crystal Structure of GaN

GaN can have wurtzite and zinc blende structures. Under ambient conditions, the thermodynamically stable structure is wurtzite [41,42]. However, at ambient conditions the wurtzite structure is the thermodynamically stable phase consisting of two interpenetrating hexagonal close-packed lattices [43]. The chemical bonds of III-nitride compounds such as GaN are predominantly covalent, which means that each atom is tetrahedrally bonded to four atoms of the other type [44]. Because of the large difference in the electronegativity of Ga and N atoms, there is a significant ionic strength dependence on the bond between two atoms, which determines their structural stability. The unit cell of the wurtzite lattice is hexagonal with a basis of four atoms, two of each kind. This lattice has no inverse symmetry along the [0001] direction or the *c*-axis, which is typically the direction shown by

a vector pointing to the nearest N atom from the Ga atom. No inversion symmetry means that when defining atomic positions in a dense plane with coordinates (x, y, z), it is invariant with position (−x, -y, -z) because inversion replaces the result. Group III atoms are N atoms, and vice versa. Due to the lack of reverse symmetry, all atoms in the same plane on each side of the bond are the same. Thus, Urgite GaN crystals have two distinct faces, commonly known as Ga-planes and N-planes, which correspond to (0001) and (0001) crystal planes [45,46].

Figure 1.2 shows the atomic arrangement in Ga-face GaN crystals and the three parameters that define the wurtzite lattice [47,48]. These are the edge length of the basal hexagon (a_0), the height of the hexagonal lattice cell (c_0), and the cation-anion bond length ratio (u_0) along the [0001] direction in units of c_0. The subscript "0" indicates that these values are those of the equilibrium lattice. In an ideal wurtzite crystal, the c_0/a_0 ratio equals $\sqrt{8/3}$ = 1.633 and the value for u_0 is 0.375 [15,49,50]. Table 2.1 gives an overview of the lattice parameters of some important wurtzite III-nitrides at 300 K [6,19,51]. From Table 2.1, it is clear that that GaN is closest to the ideal wurtzite structure compared to other III-nitrides.

Considering the other possible structure, the zinc blende structure for GaN has been stabilized by epitaxial growth of thin films on (011) crystal planes of cubic substrates such as Si, SiC, MgO, and GaAs [52,53]. In these cases, the intrinsic tendency for the formation of wurtzite structure is to be overcome by topological compatibility. The chemical bonds of GaN are predominantly covalent, which means that each atom is tetrahedrally bonded to four atoms of the other type. Because of the large difference in electronegativity of Ga and N atoms, there is a significant ionic contribution to the bond which determines the stability of the respective structural phase [54]. The wurtzite and zincblende structures are somewhat similar but different. In both cases, each Ga atoms is coordinated by four N atoms. Conversely, each N atom is coordinated by four Ga atoms. The main difference between these two structures lies in the stacking order of the nearest charged diatomic plane [9,44,45]. The wurtzite structure consists of alternating diatomic close-packed (0001) planes of Ga and N pairs, thus the stacking sequence of the (0001) plane is AaBbAa [55]. In contrast, a zincblende structure is formed when a hexagonal double-layers are periodically stacked of AaBbCcAaBbCc (see Fig. 1.3). Moreover, the

wurtzite structure is more stable and easier to grow than zincblende structure [56]. Therefore, most researchers have been focusing on the preparation of wurtzite GaN. Therefore, scientific attention and industrial interest have been focused on the wurtzite form [57,58]. This work considers consequently wurtzite GaN.

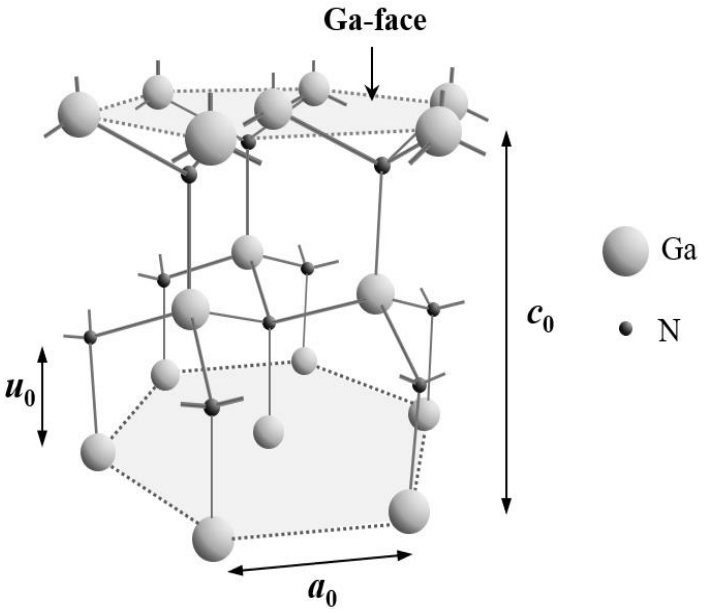

Fig. 1.2 Atomic arrangement in Ga-face GaN crystals and the parameters that define the wurtzite lattice [44,45].

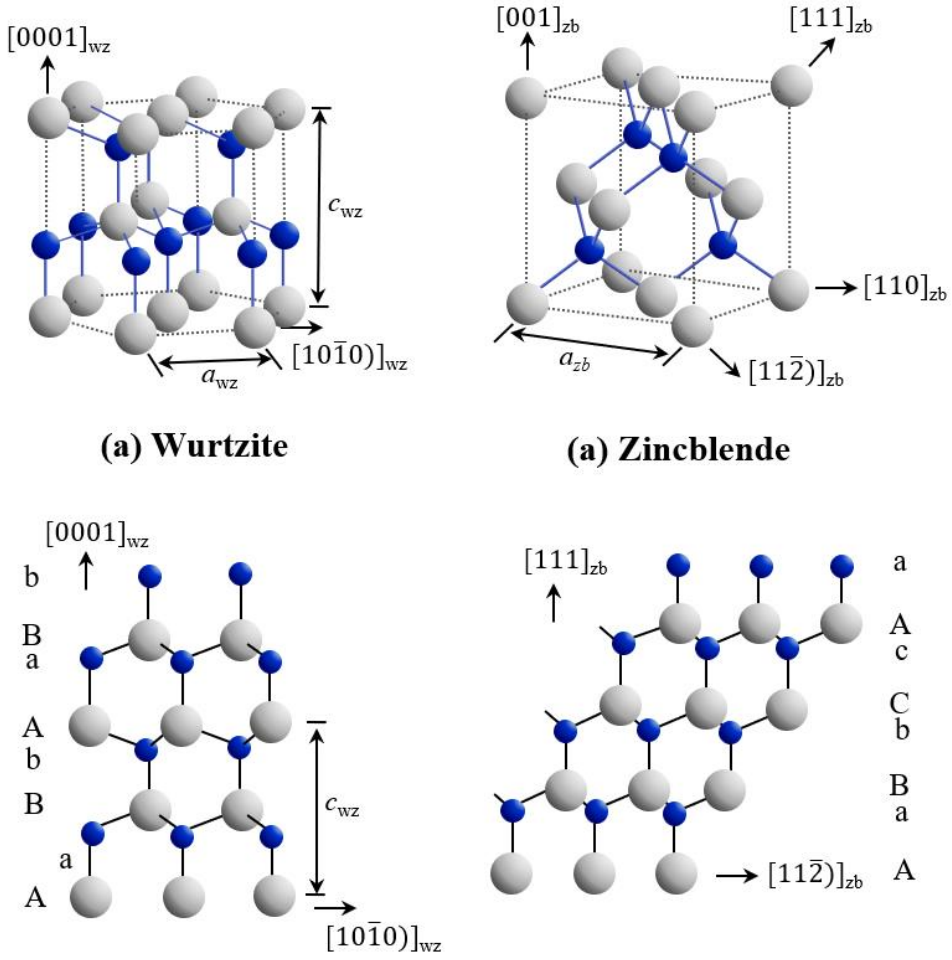

Fig. 1.3 Crystal structure of (a) wurtzite and zincblende GaN. The projections show the different stacking sequences of the close packed planes of Ga (grey) and N (blue) atoms [19].

Table 1.2 Lattice parameters of wurtzite III-nitrides at 300 K [19].

Parameter	Ideal	GaN	AlN	InN
a_0 (Å)		3.189	3.112	3.540
c_0 (Å)		5.185	4.982	5.705
c_0/a_0 (exp.)		1.626	1.601	1.612
c_0/a_0 (cal.)	1.633	1.634	1.619	1.627
u_0	0.375	0.376	0.380	0.377

1.2 Current Techniques for Preparation of GaN

GaN and its alloys are usually grown at a high temperature by various deposition techniques on foreign substrates. These substrates include silicon carbide for RF applications, silicon for power electronic applications, and sapphire for optical devices.

1.2.1 Metalorganic Chemical Vapor Deposition Method (MOCVD)

The MOCVD is one of the most useful methods for fabrication of GaN. This is a vapor phase growth method that crystallizes GaN by flowing trimethylgallium (TMGa) and ammonia (NH_3) gases onto a heated substrate at a temperature of 1000–1100 °C. TMGa has a structure in which three methyl groups ($-CH_3$) are bonded to Ga, and the methyl group dissociates from TMGa as it approaches the heated substrate. As a result, the remaining Ga atoms and ammonia-derived nitrogen atoms combine to form GaN [58].

$$Ga(CH_3)_3\,(g) + NH_3\,(g) \rightarrow GaN\,(s) + 3CH_4\,(g)$$

Figure 1.2 shows a schematic diagram of the MOCVD [58]. When the source gases are blown from a direction parallel to the substrate, the source gas rises due to thermal convection near the substrate heated to 1000 °C [59]. In order to prevent this, Shuji Nakamura et al. (Nichia at the time of 1989) and others introduced a device that suppresses the source gas rising by convection with a mixture of N_2 and H_2 from the direction perpendicular to the substrate. The introduced subflow gas effectively prevented the rise of the main gases, and the epitaxial growth of GaN proceeds by the two-step reaction.

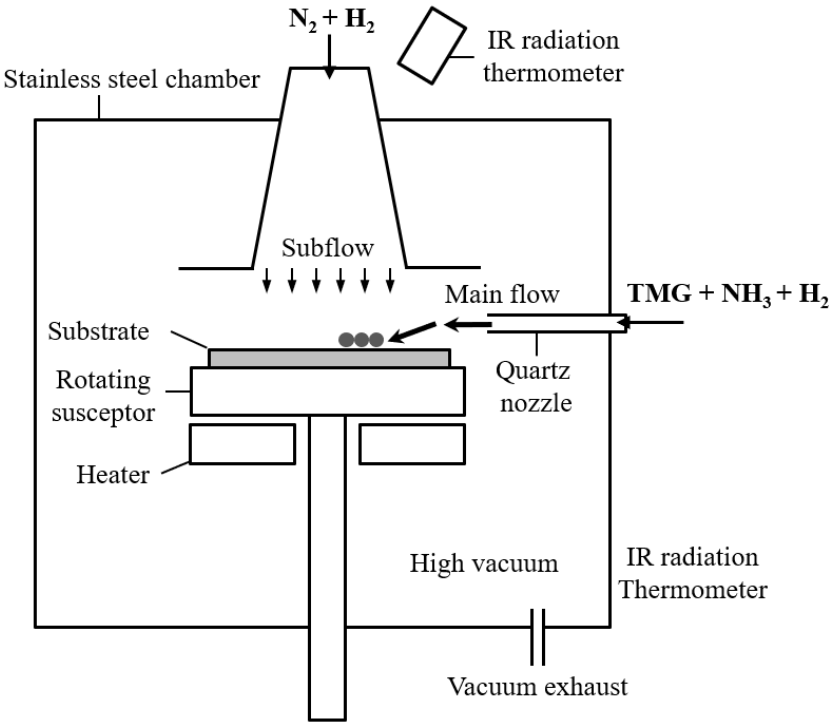

Fig. 1.4 Schematic of metalorganic chemical vapor deposition method [58].

1.2.2 Hydride Vapor Phase Epitaxy (HVPE)

The hydride vapor phase epitaxy which is one of the current methods for producing GaN. It grows crystals by blowing a metal hydride, which is produced by reacting a high-temperature halide gas with a metal, onto the heated substrate. This is a phase growth method. Figure 1.5 shows a schematic diagram of the HVPE device used for GaN fabrication [60]. This equipment consists of a raw material part that generates group III raw material molecules and a growth part that grows and precipitates GaN crystals. When hydrochloric acid (HCl) is supplied onto the raw material Ga, gallium chloride (GaCl (g)) is produced by the reaction of following equation.

$$Ga\ (l) + HCl\ (g) \rightarrow GaCl\ (g) + 1/2\ H_2\ (g)$$

After that, GaCl (g) reacts independently with NH_3 supplied to the growth part, and GaN grows on the substrate [61].

$GaCl\,(g) + NH_3\,(g) \rightarrow GaN\,(s) + HCl\,(g) + H_2\,(g)$

For reproducibility of crystal growth and rapid growth, a temperature of GaCl (g) should be maintained at 700–900 °C., and liquid Ga needs sufficient surface area. In addition, the growth part requires a growth temperature of 1000–1100 °C [62]. Due to the high temperature growth, the reaction rate at the outermost surface of the crystal is fast, and the crystal growth takes place in areas where material transport is restricted.

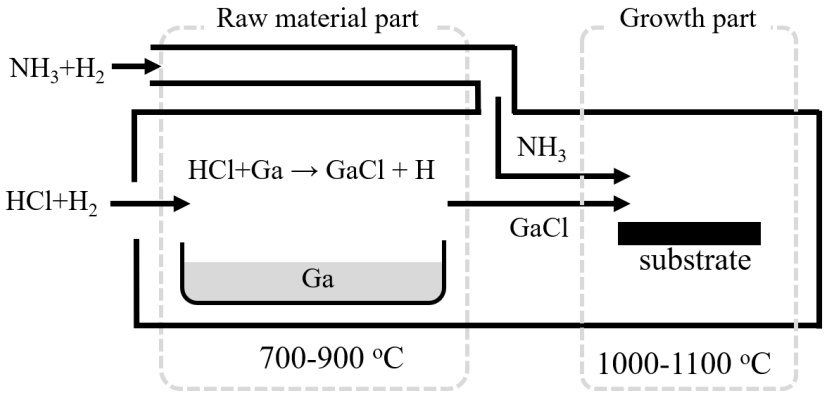

Fig. 1.5 Schematic of hydride vapor phase epitaxy method [62]

1.2.3 Molecular-Beam Epitaxy (MBE)

Molecular beam epitaxy (MBE) is normally regarded as an epitaxial technique for the growth of very thin layers with monolayer control of their thickness. It is a crystal growth method that epitaxially grows using a molecular beam in an ultra-high vacuum of 10 torr or less, and is mainly used to form a compound single crystal film. This is basically the same in the current dry deposition method and the growth mechanism of the film, but the molecules elements from the evaporation source are incident on the surface of the substrate in a beam state and the scattered molecules do not form a residual layer [63–65]. Compared with other crystal growth methods, the MBE method separates the crystal growth zone and the source of growth material so that both can be monitored and controlled separately. By opening and closing the shutter, the start and stop of the molecular beam can be made instantaneously, and it is

easy to precisely control the growth film thickness or to make rapid compositional changes in the growth direction.

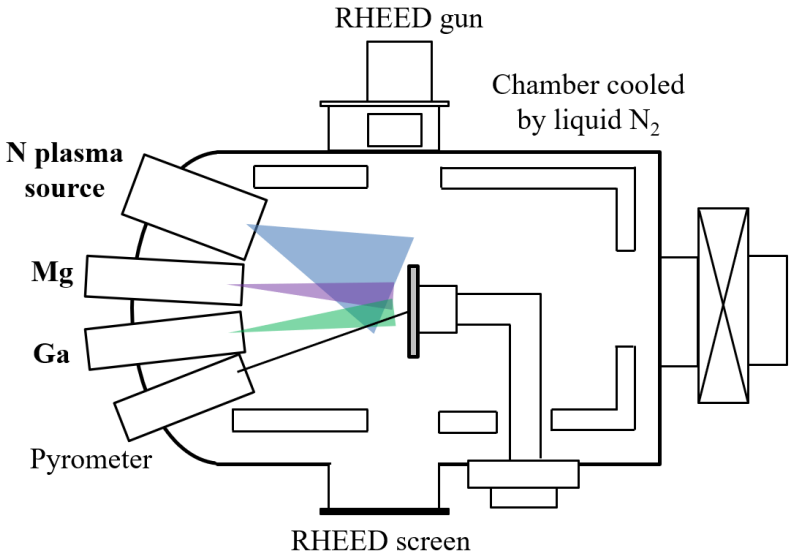

Fig. 1.6 Schematic of molecular-beam epitaxy method [64]**.**

1.2.4 Main Challenges in Current Techniques

Although GaN has been fabricated by various dry processes, these methods have some limitations. As described above, most current techniques are typically performed in well-defined environments such as those entailing ultra-high vacuum and high temperatures. And these methods need very high-cost equipment, ultrapure source and complicated multi-step processes that require a high level of understanding by operator. Moreover, the size of materials produced by the process in the vacuum chamber is limited. Therefore, an economical and low-cost/temperature method for synthesizing GaN is required to ensure its widespread application and commercialization.

1.3 Electrochemical Deposition

Electrodeposition is a process of coating a thin layer of another metal on top of a metal to modify the surface properties of the metal material. It is generally carried out to achieve the desire electrical and corrosion resistance, reduce wear and friction, improve heat tolerance and for decoration.

1.3.1 Principles of Electrodeposition

Electrodeposition is a well-known conventional surface modification method to improve the surface characteristics, decorative and functional, of a wide variety of materials [66]. At present, electrodeposition has emerged as a versatile technology for the preparation of nanomaterials and metal-compound composites [67]. This method employs electricity to reduce cations of a desired material from an electrolyte and coat the material with a thin film on a conductive substrate. This principle is applied in accordance with Faraday's law of electrolysis, and the coating rate can vary depending on the material to be coated and the type of electrodes. Electrodeposition has very low production cost and can flexibly adjust the thickness and morphology of films. Fig. 1.7 represents a general electrodeposition system. The "electro" part of the system contains the voltage/current source and the system, and the "chemical" part contains the electrolyte and electrodes (anode and cathode) immersed in the electrolyte, and the circuit is completed by the flow of ions. The metal to be deposited may be the anode and be ionized and go into the electrolyte, or come from the composition of the deposition bath [66,68,69].

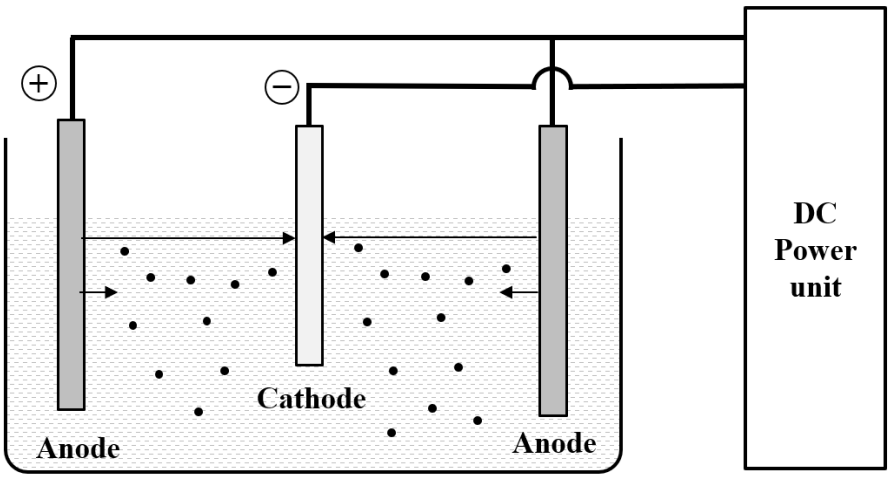

Fig. 1.7 Schematic of the general electrodeposition system.

The electrodeposition process proceeds as follows:

1. The power supply supplies electrons to the cathode.

2. An electron from the cathode transfers to a positively charged metal ion in the electrolyte.

3. Ionic conduction through the deposition bath completes the circuit to the anode.

4. At the anode, two different processes occur depending on whether the anode material is soluble, a source of metal to be deposited, or an inert that is insoluble. If the anode material is soluble, the metal atoms lose their electrons and enter into the solution to replenish the content of metal ions in the plating bath as positively charged metal ions. If the anode is inert, negatively charged ions from the plating bath provide electrons to the anode.

5. Electrons flow from the anode to the power source, completing the circuit. The metal deposition requires electrons, so the deposition rate depends on the flow of electrons, i.e. the current flowing from the rectifier. Thus, the thickness of the deposit depends on the current and the time the current is applied. This relationship is the result of Faraday's law in which the weight of the material produced by the cathode or anode electrode reaction during electrolysis as being directly proportional to the quantity of electricity passed through the cell.

Faraday‘s Law

From Faraday's experiment, two fundamental laws for controlling electrolysis has been proposed. These are:

(i) First Law. The mass of ions liberated at an electrode is directly proportional to the quantity of electricity i.e. charge which passes through the electrolyte.

or

The weight of a substance liberated from an electrolyte in a given time is proportional to the quantity of electricity passing through the electrolyte. That is $W \propto Q \propto It$, where I is the current and t is the time.

$W = Zit$

Where Z is a constant called electro-chemical equivalent.

If I = 1 ampere and T= one second then,

$Z = W$, which gives a definition of Z.

The electrochemical equivalent of a substance is the amount of that substance by weight liberated in unit time by unit current [69].

(ii) Second Law. The masses of ions of different substances liberated by the same quantity of electricity are proportional to their chemical equivalent weights.

or

If the same current flows through several electrolytes, the weights of ions liberated are proportional to their chemical equivalents. The chemical equivalent of a substance is the weight of the substance which can displace or combine with unit weight of hydrogen. Obviously, the chemical equivalent of hydrogen is 1 by definition.

Definitions

1) Current Efficiency

On account of the impurities which cause secondary reactions, the quantity of a substance liberated is less than that calculated from Faraday‘s Law. Current efficiency is the ratio of the actual mass of material formed by the passage of the current to the theoretical mass of material determined according to Faraday's law. Current efficiency can be used in measuring electro deposition thickness on materials in electrolysis. And current efficiency can be used to measure the deposited film thickness of the material.

2) Energy Efficiency

On account of secondary reactions, the voltage actually required for the deposition or liberation of metal is higher than the theoretical value which increases the actual energy required.

Energy efficiency is defined as = $\frac{\text{theoretical energy}}{\text{actual energy required}}$

It is a process by which a metal is deposited over another metal or non-metal. Electro-plating is a very common example of such process. Conditions have to be provided so that the deposit will be fine grained and will have a smooth appearance. The factors which affect the electro-deposition of metals are: (i) Current Density (ii) Electrolyte concentration (iii) Temperature (iv) Addition agents (v) Nature of

electrolyte (vi) Nature of the metal on which the deposit is to be made (vii) Throwing power of the electrolyte

(i) Current density

- At low values of current density the ions are released at a slow rate and the rate of growth of nuclei is more than the rate at which the new nuclei form themselves. Electro-deposition depends upon the rate at which crystals grow and the rate at which fresh nuclei are formed. Therefore, at low current densities the deposit will be coarse and crystalline in nature. At higher current density, the quality of deposit becomes more uniform and fine-grained on account of the greater rate of formation of nuclei. If the current density is so high that it exceeds the limiting value for the electrolyte hydrogen is released and spongy and porous deposit is obtained.

(ii) Electrolytic Concentration

- This is more or less complementary to the first factor, i.e. current density, since by increasing the concentration of the electrolyte higher current density can be achieved. Increase of concentration tends to give better deposits.

(iii) Temperature

- The temperature of the electrolyte has two contradictory effects. One, at comparatively high temperature there is more diffusion and even at relatively high current density smooth deposits may be produced. Two, the rate of crystal growth increases the possibility of coarse deposits. At moderate temperatures the deposits are good. In chromium plating the temperature is maintained at 35 °C, and in nickel between 50 °C to 60 °C.

(iv) Addition Agents

- the quality of a deposit is improved by the presence of an addition agent which may be colloidal matter or an organic compound, otherwise the metal deposits in the form of large crystals and the surface becomes rough. Materials used as addition agents are gelatin, agar, glue, gums, rubber, alkaloids, sugar etc. The addition agents are supposed to be absorbed by crystal nuclei

and prevent their growth into large crystals. The discharged ions start to build up new nuclei and the deposit of metal is fine-grained.

(v) Nature of electrolyte

- Smooth deposits can be obtained from the solutions with complex ions, e.g., cyanides. Silver forms a coarse precipitate from nitric acid solution, while forms a smooth deposit in cyanide solution. Thus, the formation of deposits is highly dependent on the nature of the electrolyte.

(vi) Nature of the metal on which deposit is to be made

- Factors such as the intrinsic potential and resistance of metals affect the growth of crystals. Metals with very negative potential are not easily deposited from aqueous solution due to their high activity in aqueous solutions.

(vii) Throwing Power

- The throwing power of an electrolyte may be regarded as the quality which produces a uniform deposit on a cathode having an irregular shape. Since the shape is irregular, The distance of the various parts of the cathode from the anode is not the same and therefore the conductance of the electrolyte is not the same for all parts of the cathode. The phenomenon of throwing power has not been clearly understood so far. In an electrolyte of low conductance, the current will concentrate on the parts of the cathode which are nearer the cathode resulting in poor throwing power. If the electrolyte has good conductance, the throwing power will also be good. One way to improve the throwing power is to keep a good distance between the cathode and the anode thereby providing more or less the same conductance for all parts of cathode. Presence of colloidal matter improves the throwing power but increase of temperature may produce the opposite effect

The plating bath generally contains other ions to facilitate current flow between the electrodes. The deposition of metal takes place at the cathode. The overall plating process occurs in the following sequence:

If anode and cathode electrodes were immerged in an electrolyte and let current flow between two

electrodes, then the electrons will carry charge along the external circuit (electronic conductor) and the ions transport charge in electrolyte (ionic conductor). The continuous current flow allows charge transfer between the electrode and electrolyte interface, through this process, the cations in the electrolyte receive electrons and are reduced at the cathode. The amount of metal ion reduced at the cathode is proportional to the current flow and is calculated in accordance with Faraday's law. The reduction potential of metal at the cathode during electroplating varies with the type of metal and each type has an eigenvalue. At a normal state, the equilibrium electrode potential of metals is called the standard reduction potential, and the higher the standard reduction potential, the easier the reducing process and vice versa. For metal to be reduced at the cathode, cathode potential should be lower than the standard reduction potential which varies with the activity of metal ion, temperature, and pH, etc. each of which is a key factor in the deposition process.

1.3.2 Electrodeposition of Semiconductors

Semiconductors are classically manufactured by high temperature solidification methods from the bulk form element, or vapor phase methods. Electrodeposition can be applied as a process of fabricating the semiconductors on a conductive substrate from an ion electrolyte including source ions of a semiconductor material as well as the metals. The fabrication of semiconductors by electrodeposition technique has some advantages over other physical and chemical dry processes. It is eco-friendly and economical, because it is possible to prepare the semiconductor with waste-free or small material [70]. Because of the purification effect often caused by electrodeposition process, there is no need to use ultra-pure source materials as in the case of other methods. Simple and accurate control of electrochemical parameters such as deposition current and plating time allows semiconductor properties to be controlled to the accuracy of μC and ms, respectively.

Many researchers have reported on the growth of semiconductor materials in bulk or thin film form by electroplating from liquid solutions using water or other solvents (organic, ionic liquids, molten salts) [70–75]. There are some reports on the synthesis of IV, III-V and II-VI semiconductor materials by

electrodeposition. These materials can be deposited in bulk or thin film form on the surface of cathode electrode, starting from a precursor (mainly in ionic form) dissolved in solution, and examples of possible reactions are the following [70,71]:

IV: $SiF_6^{2-} + 4e^- \rightarrow Si + 6F-$

III–V: $Ga^{3+} + H_3AsO_4 + 5H^+ + 8e \rightarrow GaAs + 4H_2O$

II–VI: $Cd^{2+} + HTeO_2^+ + 3H^+ + 6e^- \rightarrow CdTe + 2H_2O$

I–III–VI_2: $Cu^{2+} + In^{3+} + 2H_2SeO_3 + 8H^+ + 13e^- \rightarrow CuInSe_2 + 6H_2O$

As such, the manufacture of various semiconductor materials by electrodeposition has been attempted and applied. However, there are few reports on nitride semiconductors such as GaN because nitrogen is not stable as a single reactor in the solution. Electrodeposition of nitride semiconductors thus represents a new challenge, not only from the academic point of view, but also from the industrial point of view.

1.3.3 Application of Electrodeposition for GaN synthesis

As mentioned above, MOCVD, HVPE and MBE methods, etc. are the mainstream as the current main GaN fabrication methods. These processes have problems in terms of raw material yield, expensive equipment costs, and production costs. On the other hand, there are only a limited number of reports of low-temperature and low-cost synthesis of GaN, and it has not yet been put to practical use. Electrodeposition from an aqueous solution is a process carried out at low temperatures of below 100 °C [70] and has the advantages of low cost and low environmental dependence. Therefore, the development of electrodeposition of GaN from aqueous solution leads to the application of low-cost and innovative fabrication processes for next-generation semiconductor devices, and its academic and industrial significance is deep. Furthermore, it is essential to elucidate the mechanism and electrochemical behavior of redox reactions involving Ga and N source chemicals in an aqueous solution. The investigation on the mechanism and electrochemical behavior of the redox reactions of ions that are

expected to form GaN from aqueous solutions has significant value for the low-temperature synthesis of GaN. The achievement of this study is thought to be helpful in the development of future material field.

1.4 Outline of Thesis

The goal of this work is to synthesis GaN material from aqueous solution by low-cost/temperature and economical method in order to its application for widespread industrial field. This dissertation is divided into six chapters, including the current introductory chapter. Chapter 2 introduces the results of electrodeposition of GaN on n-type silicon wafer. In Chapter 3, I investigate the influence of the substrate materials to expand the theoretical study of the growth mechanism of GaN films. In Chapter 4, synthesis of GaN is tried on heat-treated aluminum substrate from boric acid solution to improve the quality of deposition film. In addition, the effect of crystal orientation on the formation of GaN film in aqueous solution is confirmed. Chapter 5 summarizes the work with the main achievements and presents an outlook for further studies.

Reference

[1] B. Ozpineci, L. M. Tolbert, *in Oak Ridge National Laboratory Report* (2003)

[2] J. I. Pankove, *J. Lumin.* **7** (1973) 114

[3] B. J. Baliga, *Microelectron. J.* **24** (1993) 31

[4] B. J. Baliga, *IEEE Trans. on Electron Devices* **43** (1996) 1717

[5] H. Amano, M Kito, K Hiramatsu, I Akasaki, *Jpn. J. Appl. Phys.* **28** (1989) 2112

[6] H. Amano, M. Kitoh, K. Hiramatsu, I. Akasaki, *J. Electrochem. Soc.* **137** (1990) 1639

[7] S. Nakamura, M. Senoh, T. Mukai, *Jpn. J. Appl. Phys.* **32** (1993) 8

[8] S. Nakamura, M. Senoh, T. Mukai, *Appl. Phys. Lett.* **62** (1993) 2390

[9] H. Morkoç, S. Strite, G. B. Gao, M. E. Lin, B. Sverdlov, M. Burns, *J. Appl. Phys.* **76** (1994) 1363

[10] S Nakamura, *Solid State Commun.* **102** (1997) 237

[11] S. Nakamura, M. Senoh, N. Iwasa, S. Nagahama, T. Yamada, T. Mukai, *Jpn. J. Appl. Phys. Lett.* **34** (1995) 1332

[12] S. Nakamura, M. Senoh, S. Nagahama, N. Iwasa, T. Yamada, T. Matsushita, H. Kiyoku, Y. Sugimoto, *Jpn. J. Appl. Phys.* **35** (1996) 217

[13] S. Nakamura, M. Senoh, S. Nagahama, N. Iwasa, T. Yamada, T. Matsushita, H. Kiyoku, Y. Sugimoto, *Jpn. J. Appl. Phys.* **68** (1996) 2105

[14] S. Nakamura, T. Mukai, M. Senoh, *Jpn. J. Appl. Phys.* **30** (1998) 1998

[15] A. Bhutani, P. Bhardwaj, *in Global Market Insights* (2019)

[16] I Akasaki, H Amano, M Kito, K Hiramatsu, *J. Lumin.* **48** (1991) 666

[17] T. Kakeuchi, H Takeuchi, S Sota, H Sakai, H Amano, I. Akasaki*, Jpn. J. Appl. Phys.* **36** (1997) 177

[18] K. Takahashi, A. Yoshikawa, A. Sandhu, *in Wide Bandgap Semiconductors* (2007)

[19] R.A. Ferreyra, C. Zhu, A. Teke, H. Morkoç, *in Springer Handbook of Electronic and Photonic Materials (Springer, Cham)* (2017) 1

[20] Sh. Valedbagi, S.M. Elahi, M.R. Abolhasani, A. Esfandiar, *Optical Mater.* **47** (2015) 44

[21] B. Damilano, N. Grandjean, F. Semond, J. Massies, M. Leroux, *Appl. Phys. Lett.* **75** (1999) 962

[22] K. Chung, C.H. Lee, G.C. Yi, *Science* **330** (2010) 655

[23] S. Chang, N.B. Rex, R.K. Chang, G. Chong, L.J. Guido, *Appl. Phys. Lett.* **75** (1999) 166

[24] X.H. Yang, T.J. Schmidt, W. Shan, J.J. Song, *Appl. Phys. Lett.* **66** (1995) 1

[25] R. Dingle, R.B. Zetterstrom, K.L. Shaklee, R.F. Leheny, *Appl. Phys. Lett.* **19** (1971) 5

[26] X. Duan, C.M. Lieber, *J. Am. Chem. Soc.* **122** (2000) 188

[27] W. Han, S. Fan, Q. Li, Y. Hu, *Science* **277** (1997) 1287

[28] S. Bidnyk, T.J. Schmidt, B.D. Little, J.J. Song, *Appl. Phys. Lett.* **74** (1999) 1

[29] N.A. Preschilla, S. Major, *Appl. Phys. Lett.* **77** (2000) 1861

[30] J. C. Johnson, H.J. Choi, K. P. Knutsen, R. D. Schaller, P. Yang, R. J. Saykally, *Nature Materials* **1** (2002) 106

[31] W Saito, Y Takada, M Kuraguchi, K. Tsuda, I. Omura, T. Ogura, H. Ohashi, *IEEE Transactions on Electron Devices* **50** (2003) 2528

[32] B.J. Baliga, R. Ehle, J.R. Shealy, W. Garwacki, *IEEE Electron Device Letters* **2** (1981) 302

[33] K. Park, M.A. Stroscio, C. Bayram, *J. Appl. Phys.* **121** (2017) 245109

[34] H.S. Lee, *Ph. D Thesis,* KTH, Royal Institute of Technology, Sweden (2008)

[35] T.P.Chow, V. Khemka, J. Fedison, N. Ramungul, K. Matocha, Y. Tang, R.J. Gutmann, *Solid State Electron.* **44** (2000) 277

[36] I. Akasaki, *J. Crys. Grow.* **237–239** (2002) 905

[37] N. Hasegawa, *Ph. D Thesis*, Kyoto University, Japan (2018)

[38] K.S. Boutros, R. Chu, B. Hughes, *IEEE Energytech* (2012) 29

[39] R. T. Kemerley, H. B. Wallace, M. N. Yoder, *Proceedings of the IEEE* **90** (2002) 1059

[40] L. M. Tolbert, B. Ozpineci, S. K. Islam, M. S. Chinthavali, *in Power and Energy Systems. ACTA Press*, USA, (2003)

[41] R.C. Powell, N.E. Lee, Y.W. Kim, J.E. Greene, *J. Appl. Phys.* **73** (1993) 189

[42] L.E. Ramos, L.K. Teles, L.M.R Scolfano, J.L.P. Castineira, A.L. Rosa, J.R. Leite, *Phys. Rev. B* **63** (2001) 165210

[43] A. Trampert, O. Brandt, K.H. Ploog, *Semiconduct. Semimet.* **50** (1997) 167

[44] A.R. Acharya, *in HJS*. **5** (2014) 22

[45] K.W. Böer, U.W. Pohl, *in Semiconductor Physics* (2018) 59

[46] M.H. Lin, H.C. Wen, Y.R. Jeng, C.P. Chou, *Nanoscale Res. Lett.* **5** (2010) 1812

[47] M.G. Ganchenkova, V.A. Borodin, K. Laaksonen, R.M. Nieminen, *Phys. Rev. B* **77** (2008) 075207

[48] M.C.J.C.M. Krämer, *Ph. D Thesis*, *AMS, Netherlands* (2006)

[49] O. Ambacher, J. Majewski, C. Miskys, A. Link, M. Hermann, M. Eickhoff, M. Stutzmann, F. Bernardini, V. Fiorentini, V. Tilak, B. Schaff, L. F. Eastman, *J. Phys.-Condens. Mat.* **14** (2002) 3399

[50] M. Xie, *Ph. D Thesis*, *Linkoping, Sweden* (2012)

[51] http://www.ioffe.ru/SVA/NSM/Semicond/GaN/basic.html

[52] V. R. Velasco, J.T. Sanchez, H.R. Coppola, *Surf. Sci.* **565** (2004) 259

[53] T. Kurobe, Y. Sekiguchi, J. Suda, M. Yoshimoto, *Appl. Phys. Lett.* **73** (1998) 2305

[54] H. Morkoç, *in Handbook of Nitride Semiconductors and Devices: Materials Properties, Physics and Growth* (2009)

[55] J. Piprek*, in Nitride semiconductor devices: principles and simulation* (2007)

[56] J. Derluyn et al, *in Gallium Nitride-enabled High Frequency and High Efficiency Power Conversion* (2018)

[57] J. Piprek*, in Nitride semiconductor devices: principles and simulation* (2007)

[58] A.N. Hattori, K. Endo, *in Stoichiometry and Materials Science: Structure, Morphology, and Stoichiometry of GaN(0001) Surfaces Through Various Cleaning Procedures* (2012) 83

[59] I. Halidou, A. Touré, B. El Jani, *Indian J. of Phys.* **93** (2019) 1137

[60] A.S.Segal, A.V. Kondratyev, S.Yu. Karpov, D. Martin, V. Wagner, M. Ilegems, *J. Crys. Growth* **270** (2004) 384

[61] A. S. Segal, D. S. Bazarevskiy, M. V. Bogdanov, E. V. Yakovlev, *Phys. Status Solidi C* **6**, (2009) 329

[62] C.T. Tash, W.K. Wang, T.T. Yen, S.Y. Huang, *Materials* **10** (2017) 605

[63] K. Alavi, *in Encyclopedia of Materials: Science and Technology* (2001)

[64] Mircea Guina, Shu Min Wang, *in Molecular Beam Epitaxy* (2013)

[65] H. Adachi, K. Wasa, *in Handbook of Sputtering Technology (Second Edition)* (2012)

[66] A. Brenner, *in Electrodeposition of alloys: principles and practice* (1963)

[67] V.B. Singh, D.K. Singh, *Matrix Nanocomposites Nanosci. Technol.* **1** (2014) 1

[68] M. Schwartz, *in Deposition Technologies for Films and Coatings* (1994) 506

[69] *Studies in Surface Science and Catalysis*, *Electrodeposition* (2010)

[70] D. Lincot, *Thin Solid Films* **487** (2005) 40

[71] C.D. Lokhande, S.H. Pawar, *Phys. Stat. Sol. (a)* **111** (1989) 17

[72] T. Pauporté, D. Lincot*, Electrochimica Acta* **45** (2000) 3345

[73] G.F. Fulop, R.M. Taylor, *Ann. Rev. Mater. Sci.* **15** (1985) 197

[74] F. Endres, *Chem. Phys. Chem.* **3** (2002) 144

[75] G. Riveros, H. Gomez, R. Henrıquez, R. Schrebler, R.E. Marotti, E.A. Dalchiele, *Sol. Energ. Mat. Sol.* C **70** (2001) 255

Chapter 2

Low-temperature Synthesis of GaN Film from Aqueous Solution by Electrodeposition

Chapter 2 – Low-temperature Synthesis of GaN Film from Aqueous Solution by Electrodeposition

2.1 Introduction

GaN is a direct wide band gap semiconductor with high stability due to its wurtzite structure [1,2]. Since GaN has a broadband gap energy (3.39 eV) at room temperature, it can cover most of the visible light region and efficiently emit blue light. Moreover, InGaN with indium (In) added to GaN can be used for various LEDs such as green, yellow and orange depending on the composition [3–5]. Also, as is well known, direct band gap semiconductors are very efficient in terms of energy since they do not require a change in the momentum accompanying phonons for electron transfer from the valence band to the conduction band. Since these unique characteristics, GaN is innovating the world of power engineering by achieving high speed, efficiency and power density that was previously impossible with silicon MOSFETs [6, 7], and are gaining attention as a promising material of the future industry [8–15].

Various manufacturing techniques have been studied by many researchers for several decades to produce high performance GaN, and dry methods such as molecular beam epitaxy [16,17], metalorganic chemical vapor deposition [18], hydride vapor phase epitaxy [19], and reactive sputtering [20] are now generally used. At present, ammonothermal growth is the best possible method for GaN synthesis, in terms of the size and quality of crystals obtained [21]. However, most of the techniques for manufacturing GaN have been conducted in ultra-high vacuum and high temperature environment [22]. In addition, these techniques require expensive source materials, production costs and complex multi-step processes [21]. In view of this aspect, there is a need for a new synthesis method that is economically advantageous for the enlargement and commercialization of GaN [23,24].

Electrodeposition has been proposed as one of the effective techniques due to its low cost and simple operation characteristics [25,26]. This method is a low-cost technique with several advantages,

such as being able to control deposition rate, film thickness and surface morphology by simply changing the electrochemical parameters [27]. Moreover, since the film can be formed from low temperature solution under the standard condition, it is very advantageous in terms of economics.

There have been several reports on the synthesis of GaN over the last decade. Wang et al. [28] have recently reported on the synthesis of GaN film by electrodeposition. However, it differs from the method used in this study because it involves an additional process of annealing with high temperature ammonium gas after electrodeposition. Roy et al. [23] showed the possibility of GaN synthesis via a single-step electrodeposition method, but the purity of deposition film is insufficient. Since then, electrodeposition of GaN is being studied by some researchers. However, few papers have been published on this topic, and the low temperature synthesis of GaN films is still a challenge [29].

Therefore, the synthesis of GaN using simple and inexpensive electrodeposition technique was studied in this study. In addition, since the confirmation of the electrochemical behavior of ions in the solution during the deposition process is very importance, the synthesis of GaN has been studied by focusing on the ionic behavior. The electrochemical synthesis of GaN film was tried on n-type silicon (111) substrate from an aqueous solution containing mixture of gallium nitrate and ammonium nitrate. The electrodeposited GaN film was characterized by several analysis methods, and the optical property of the GaN films was also confirmed by photoluminescence analysis.

2.2 Experimental Procedures

All the electrochemical experiments were performed using a potentiostat (Hokuto Denko, HZ-7000) in a three-electrode cell configuration at atmospheric pressure and room temperature. Figure 2.1 shows a schematic diagram of the system used in this experiment.

The working electrode was an n-type silicon (111) wafer and a platinum (Pt) coil was used as the counter electrode. An Ag|AgCl|sat'd-KCl electrode was used as the reference electrode. The working and counter electrodes were approximately 1.0 cm apart. The n-type Si wafers were immersed in a mixture solution of deionized water and 50 mM hydrofluoric acid (HF, 46–48%, Junsei Chemical Co.,

Ltd.) for 10 min to remove the surface oxides (M = mol dm^{-3}). They were then ultrasonically cleaned with acetone and ethanol for 10 min, respectively. The Si electrode only exposed the surface area of 1.0×1.0 cm^2 and the other part was well covered with Nitoflon adhesive tape (Nitto Denko).

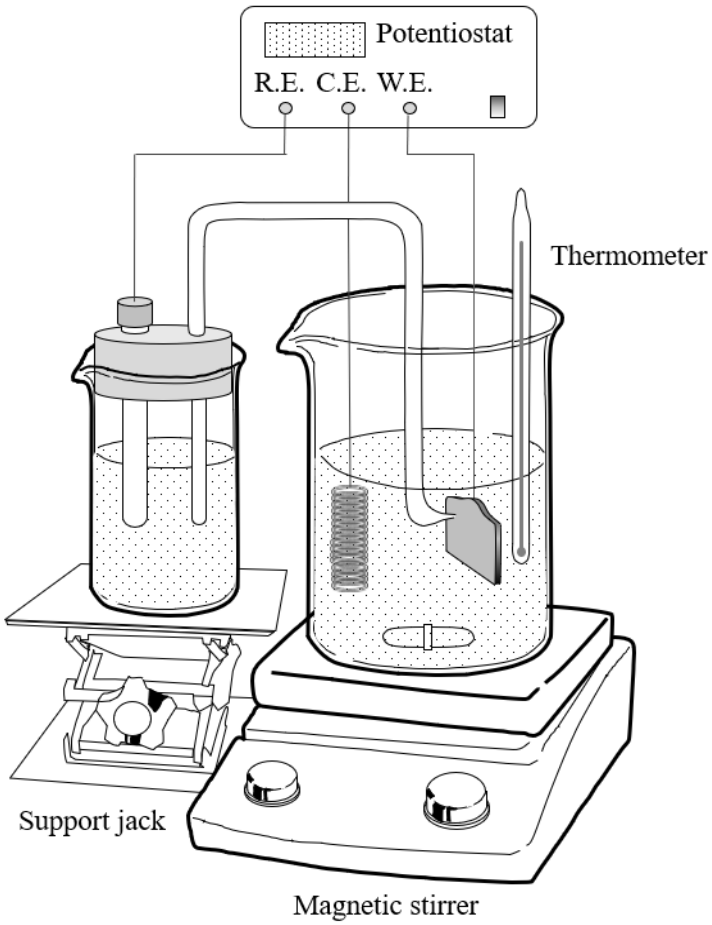

Fig.2.1 Schematic diagram of in a three-electrode cell configuration for electrochemical experiment.

Prior to deposition, the cyclic voltammetry was conducted to confirm the redox behavior of each ion on the Si electrode in aqueous solution. A first scan started in the negative direction and scans were repeated 10 times with a scan rate of 20 mV s^{-1}. Sodium chloride (NaCl, ≥99%, Sigma Aldrich), sodium nitrate ($NaNO_3$, ≥98%, Nacalai Tesque), ammonium chloride (NH_4Cl, ≥98.5%, Nacalai Tesque), and ammonium nitrate (NH_4NO_3, ≥98%, Sigma Aldrich) were used for the CV measurements. Additionally,

gallium (III) chloride ($GaCl_3$, ≥99.9%, Wako Pure Chemical Industries), and gallium (III) nitrate hydrate ($Ga(NO_3)_3 \cdot xH_2O$, ≥99.9%, Sigma Aldrich) were used. The ions present in the experimental solutions are summarized in Table 2.1.

Table 2.1 Bath conditions for cyclic voltammetry measurement.

Concentration of ion (M)						
No.	Ga^{3+}	NH_4^+	NO_3^-	Adjusting ion		
				Na^+	Cl^-	H^+
1	-	-	-	1.000	1.032	0.032
2	-	1.000	-	-	1.032	0.032
3	-	-	1.032	1.000	-	0.032
4	-	1.000	1.032	-	-	0.032
5	0.100	-	-	1.000	1.126	0.026
6	0.100	1.000	-	-	1.128	0.028
7	0.100	-	1.129	1.000		0.029
8	0.100	1.000	1.130	-		0.030

The electrochemical deposition to synthesis GaN film was carried out at current densities in the range 3.5–8 mA cm^{-2} in mixed solutions of deionized water, $Ga(NO_3)_3$, and NH_4NO_3. The pH of each solution was adjusted to 1.5 through dropwise addition of concentrated nitric acid (HNO_3, 70.0%, Nacalai Tesque) to prevent the formation of gallium oxides. Immediately after deposition, the sample was washed with distilled water and dried at room temperature.

The surface morphology and composition were confirmed by scanning electron microscopy (SEM, Hitachi, S-4800) and energy dispersive X-ray spectroscopy (EDX, HORIBA, EMAX ENERGY, EX-350) at an acceleration voltage of 12 kV and current of 10 μA. The crystalline properties of the deposited films were characterized by X-ray diffraction (XRD, Rigaku, Ultima IV) with Cu-K-alpha radiation (λ

= 1.54 Å). The optical property of deposited films was analyzed by a low-temperature photoluminescence using a He-Cd laser with a wavelength of 325 nm. The beam diameter of the laser was 1.0 mm and integral time was 3000 ms. In addition, the bandgap energy of the deposited films was calculated from the obtained PL results.

2.3. Results and Discussion

2.3.1. Electrochemical Properties of Gallium

The electrochemical properties of gallium ions (Ga^{3+}) was confirmed to select suitable bath conditions for the deposition of gallium (Ga) from an aqueous solution. The open circuit potential (OCP) was measured using solid and liquid Ga electrodes in the aqueous solutions containing 0.1 M $GaCl_3$ at 20 °C and 80 °C while the pH value was varied. Since Ga has a very low melting point of 29 °C, we fabricated a J-shaped Ga electrode shown in Fig. 2.2 and used in this experiment. The results represent in the E-pH (Pourbaix) diagram in Fig. 2.3 [30]. The potential values of the solid and liquid Ga electrodes shown in the figure exhibited similar or slightly negative potentials than those of the hydrogen evolution reaction (HER), so the Ga electrode can be slowly dissolved in the solution. It can be seen that in the neutral solution at around pH 7, the potentials of Ga electrodes were very close to the HER potential. Such HER can reduce current efficiency during electrodeposition and lead to defects in the deposited film [31]. In contrast, the Ga electrodes immersed in acidic and basic solutions with pH values of 0, 1, and 11 exhibited significantly lower potential than HER, and these values were close to the solid Ga line. Thus, the redox reaction between Ga and gallium ions (Ga^{3+}) can be expected to occur at these pH values. However, in a basic solution with a pH of 11 or higher, a low potential of -1.2 V or lower is required for the Ga precipitation. Furthermore, it was confirmed that nitrogen (N) is not included in the films electrodeposited from the basic solution from our previous studies. Therefore, in this study, all depositions were conducted in an acidic solution at room temperature to synthesize GaN films.

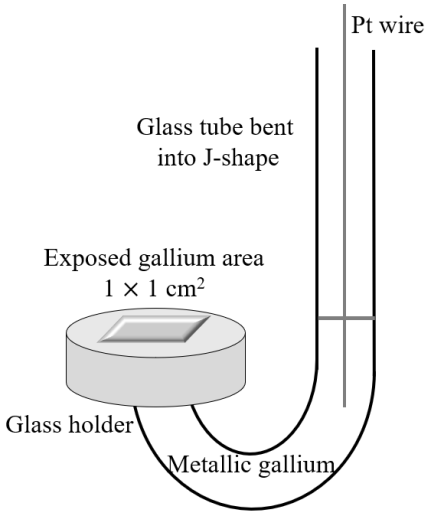

Fig. 2.2 Schematic of a J-shape gallium electrode.

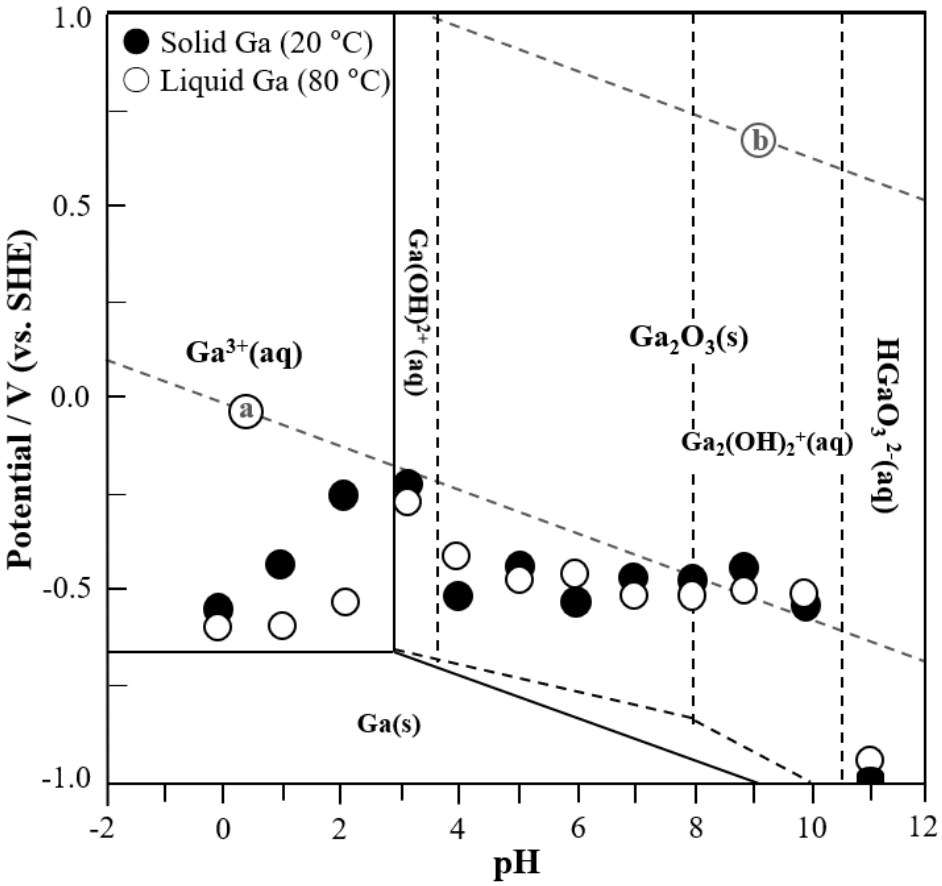

Fig. 2.3 Pourbaix diagram of gallium and potential values of gallium electrodes in 0.1 M $GaCl_3$ solutions with different pH value [ref. 30].

2.3.2. Cyclic Voltammetry

Figure 2.4 shows the results of CV for the aqueous solutions containing NaCl, NH_4Cl, $NaNO_3$, and NH_4NO_3 (corresponding to No.1–No.4 solutions in Table 2.1, respectively) without Ga to examine the electrochemical behavior of ions that can be used as sources of nitrogen (N). To unify the ion species present in the bath, hydrochloric acid (HCl) was used to adjust the pH of the solutions containing NaCl or NH_4Cl, and HNO_3 was used for the solutions containing $NaNO_3$ or NH_4NO_3 severally. The current response was recorded against the voltage applied (V vs. Ag/AgCl), which is scanned in a triangular waveform. The cathodic scan was first measured from self-potential to −5.0 V and back to 0 V. Although the standard reduction potentials of Ga and N are −1 V or more, CV was measured until a very low potential region because the reaction did not easily occur on the Si electrode due to its high resistance.

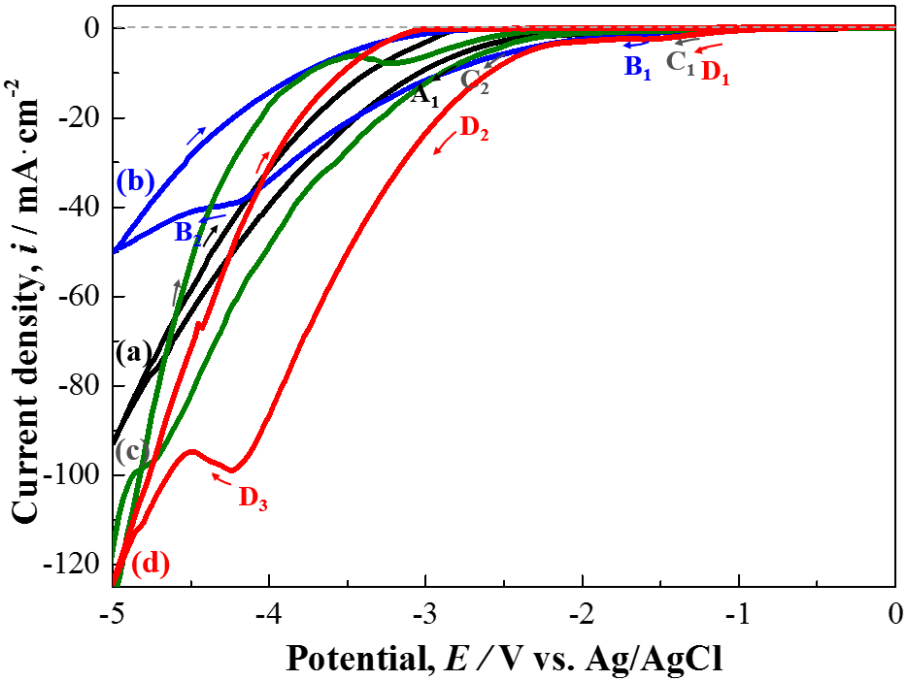

Fig. 2.4 Comparison of CVs from No. 1–No. 4 in Table 2.1 aqueous solutions containing, (a) 1 M NaCl; (b) 1M NH_4Cl; (c) 1 M $NaNO_3$; (d) 1 M NH_4NO_3.

As can be seen in Fig. 2.4, no apparent cathodic peak was observed in all CVs, but a gradual increase in cathodic current appeared from ca. -1.1 V (B_1, C_1 and D_1). It can be considered that this increase in current is due to the HER occurred from HNO_3 added in solution for pH control. From these CV results, two remarkable facts could be confirmed. Firstly, the cathodic current significantly decreased with the addition of ammonium (NH_4^+) ions (in Fig. 2.4 (b)). And current densities were increased in the solutions containing nitrate (NO_3^-) ions (Figs. 2.4 (c), (d)). This trend suggests that the reduction of NO_3^- ions occurs mainly with HER and that the NH_4^+ ions do not change to other species in the solution. Secondly, weak cathodic peaks were observed only in the solutions containing NH_4^+ ions at ca. -4.1 V (B_2 and D_3) in Figs. 2.4 (b), (d). This cathodic current can be attributed to the reduction reaction of NO_3^- ions to other species influenced by NH_4^+ ions. In general, the process of electrochemical reduction of NO_3^- ions in an aqueous solution is known to be very complex, and different nitrogen-containing compounds can be formed by various factors [32, 33]. However, the reactions between NO_3^- and NH_4^+ ions on the Si surface can be clearly established under these conditions. As expected from the Pourbaix diagram of N, the NO_3^- ions can be changed to NO2 or NH4+ ions, easily. That is, although it is not clear about the kind of ions that are formed electrochemically, the following reactions can be expected to occur in the solution.

$$NO_3^- + 2H^+ + 2e^- \rightarrow NO_2^- + H_2O \quad (2.1)$$

$$NO_3^- + 10H^+ + 8e^- \rightarrow NH_4^+ + 3H_2O \quad (2.2)$$

If NO_2^- ions are produced in the solution containing NH_4^+ ions, a reaction of comproportionation, as shown in Eq. (2.3), is expected thermodynamically based on the Frost diagram shown in Fig. 2.5 (b) [35]. It is likely that the N atom reacts with Ga atom to form GaN, as shown in Eqs. (2.4) and (2.5).

$$NO_2^- + NH_4^+ \rightarrow 2N_{ads} + 2H_2O \quad (2.3)$$

$$Ga^{3+} + 3e^- \rightarrow Ga_{ads} \quad (2.4)$$

$$Ga_{ads} + N_{ads} \rightarrow GaN \quad (2.5)$$

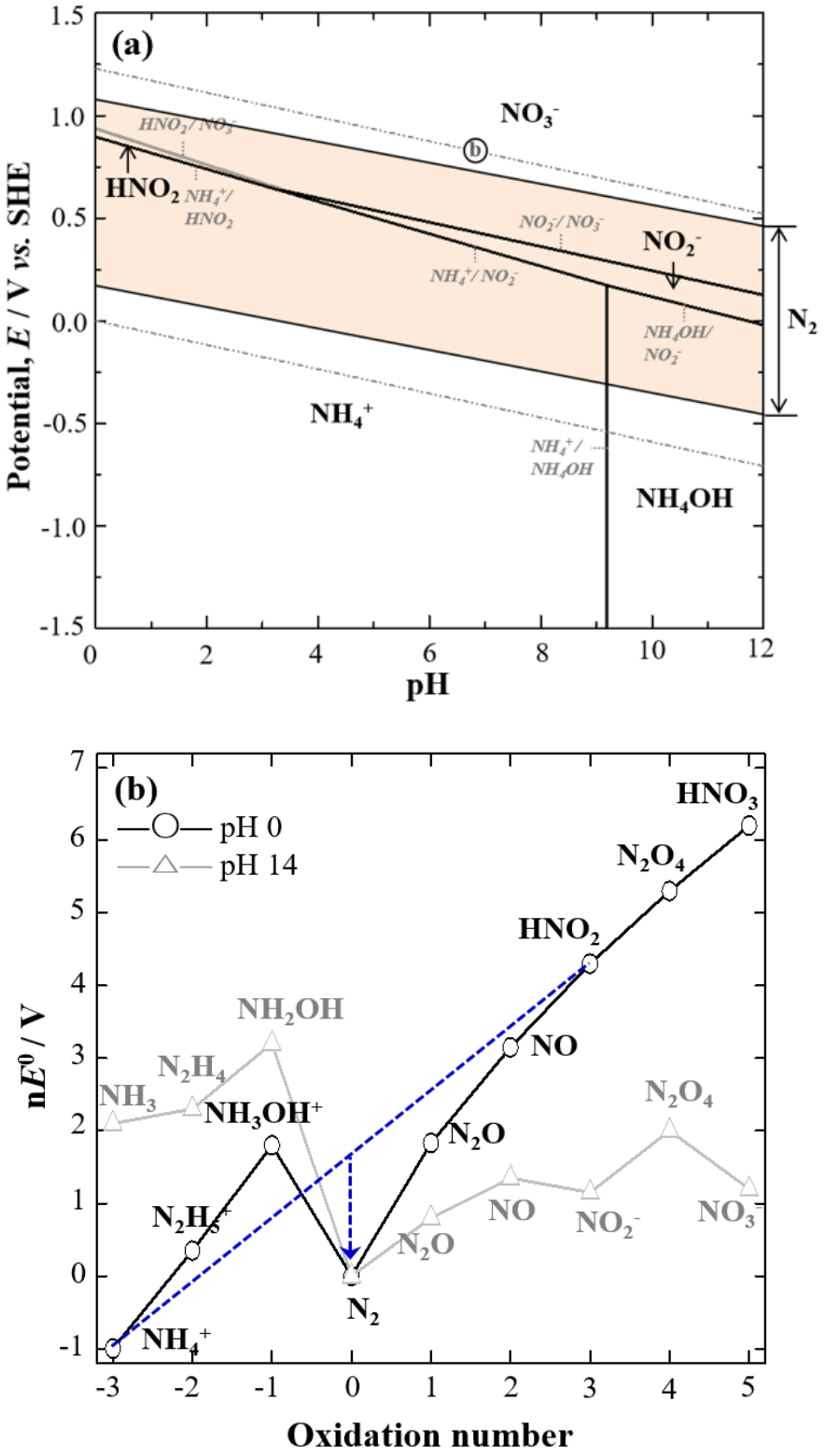

Fig. 2.5 (a) Pourbaix diagram of the dissolved compounds of nitrogen at 25 °C and (b) Frost diagram of nitrogen at different pH levels (ref. 34, 35).

The electrochemical behavior of Ga^{3+} ions from the solution containing Ga^{3+} ions was examined and the results are shown in Fig. 2.6. The solutions were No. 5–No. 8 solutions shown in Table 2.1. In the solution containing Ga^{3+} and Na^{+} ions (graph (a)), an increase in the cathode current starting at ca. −0.8 V is observed, which corresponds to the reduction of Ga^{3+} ions to solid Ga. However, in the solution containing only NH_4^{+} ions (Fig. 2.6 (b)), the flow of current is significantly lower than that seen in the case of Fig. 2.6 (a). When NH_4^{+} and Ga^{3+} ions coexist, the reactivity of Ga^{3+} ions declined and the amount of electric current which flows between two electrodes decreased.

In the solutions containing $Ga(NO_3)_3$ (Figs. 2.6 (c) and (d)), the reduction current began to increase from about −0.8 V (C_1 and D_1) and the reduction peak was observed at −1.6 V (C_2 and D_2). The highest cathodic current density was observed in the mixed solution of $Ga(NO_3)_3$ and NH_4NO_3. It is likely that the NO_3^{-} ions were transformed into other species via electrochemical reaction in the solution as described above, and thus the reduction effect of NH_4^{+} on the reactivity of Ga^{3+} ions in this system can be controlled.

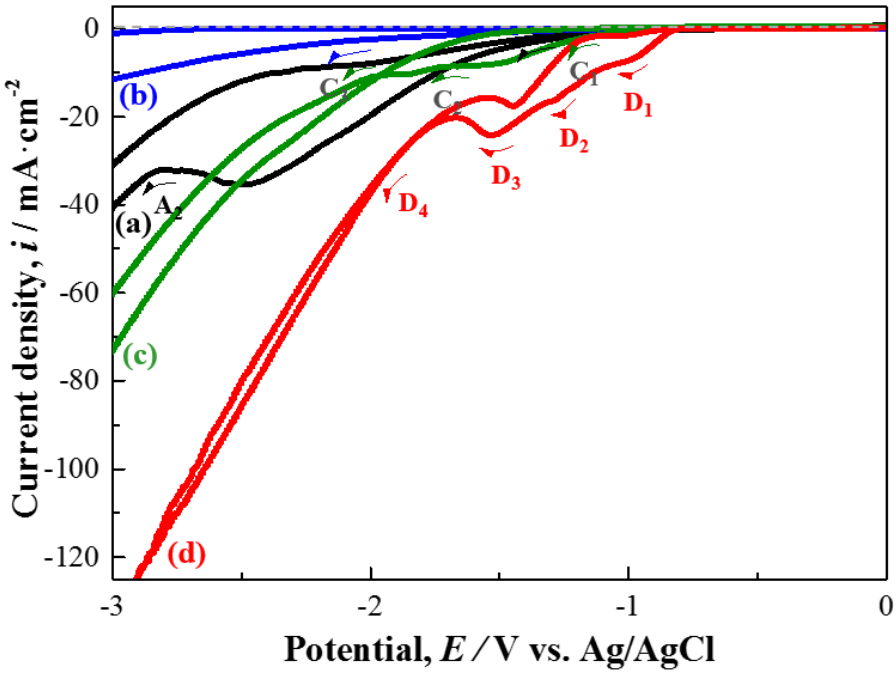

Fig. 2.6 Comparison of CVs from No. 5–No. 8 aqueous solutions in Table 2.1 containing the mixture of, (a) 1 M NaCl and 0.1 M $GaCl_3$; (b) 1 M NH_4Cl and $GaCl_3$; (c) 1 M $NaNO_3$ and $Ga(NO_3)_3$ (d) 1 M NH_4NO_3 and $Ga(NO_3)_3$.

2.3.3 Potential Variation during Deposition Process

The electrodeposition was conducted in the solutions comprising a mixture of $Ga(NO_3)_3$ and NH_4NO_3. The molarities of $Ga(NO_3)_3$ and NH_4NO_3 were selected to be 0.1 M and 2.5 M, respectively. These values of molarities were chosen based on the work reported by Al-Heuseen et al [29, 36]. The depositions were attempted at several current densities because the value of current density at which the N source reacts is not clearly known. Although electrodeposition was carried out using other solutions such as $Ga(NO_3)_3$ and a mixture of $GaCl_3$ and NH_4Cl, GaN was not obtained from these trials.

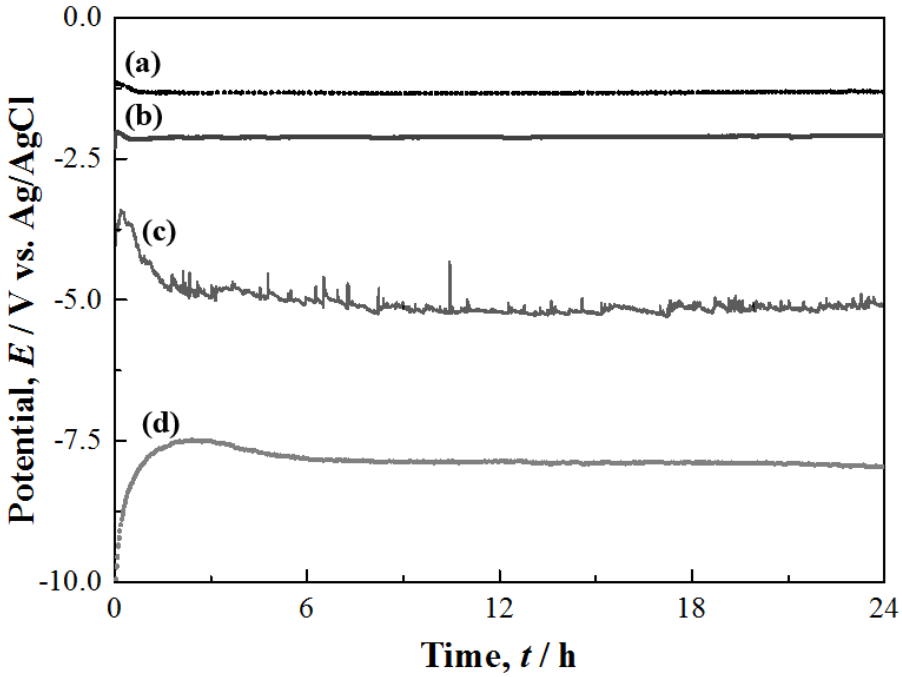

Fig. 2.7 Galvanostatic potential vs. elapsed time curves obtained during deposition at different current densities, (a) 2.5 mA cm^{-2}; (b) 3.5 mA cm^{-2}; (c) 8 mA cm^{-2}; (d) 10 mA cm^{-2}; for 24 h.

Figure 2.7 shows the potential-time curves obtained during the deposition process in the aqueous solutions and the applied current densities were from 2.5 mA cm^{-2} to 10 mA cm^{-2} for 24 h. As seen from the graph, the potential curves shift in a positive direction instantaneously, then slowly shift in a negative direction slightly, finally reach a steady-state potential. At an applied current density of 2.5 mA cm^{-2} (Fig. 2.7 (a)), the potential value was ca. −1.3 V which was lower than the reduction peak of −1.6 V

obtained from CV result (D_2 in Fig.2.6). A stable potential of ca. −2.1 V was observed when a current density of 3.5 mA cm^{-2} was applied and a large amount of noise appeared on the graph with a low potential below −5.0 V at an applied current density of −8 mA cm^{-2} in Figs. 2.7 (b) and (c). At 10 mA cm^{-2}, the initial potential values exceeded the equipment limit (± 10 V), and subsequently maintained a low potential value of −7.5 V or less.

2.3.4 Morphology of Deposited Films

Figure 2.8 shows the SEM images of the films obtained at current densities in the range 2.5–10 mA cm^{-2}. These current densities were chosen based on the results of previous study on electrodeposition of GaN from aqueous solutions by R.K. Roy [23]. As shown in Fig. 2.8 (a), film formation starts with the formation of small clusters of critical sizes, and these clusters begin to grow with increase in current. In contrast to the report by K. Al-Heuseen et al. [37], a film was not formed on the silicon surface even though it was deposited for a longer period under the same conditions. It could be considered that the potential value was not enough to reduce Ga and N when the current density of 2.5 mA cm^{-2} was applied as shown in Fig. 2.7 (a). It can be confirmed that the plate-like morphologies of the films were observed when current densities of 3.5 mA cm^{-2} and greater were applied (Fig. 2.8 (b)). Denser films were formed on the substrates grown at current densities of 8 mA cm^{-2} and 10 mA cm^{-2} (Figs. 2.8 (c) and (d)).

These films were observed to have island-shaped structures with many wide cracks. These are likely due to hydrogen gas evolution during the process of deposition. The island-like growth identified in the GaN fabrication process under vacuum conditions is the same, but the hydrogen generated in the solution interfere the connection of the GaN islands in the next step [38]. Moreover, it is well known that the surface morphology of a substrate exhibits different sensitivities toward various chemical treatments [39, 40]. Therefore, it is difficult to expect uniformity in film growth rate because large bubbles generated and adsorbed on the electrode surface affect the surface state of Si electrode.

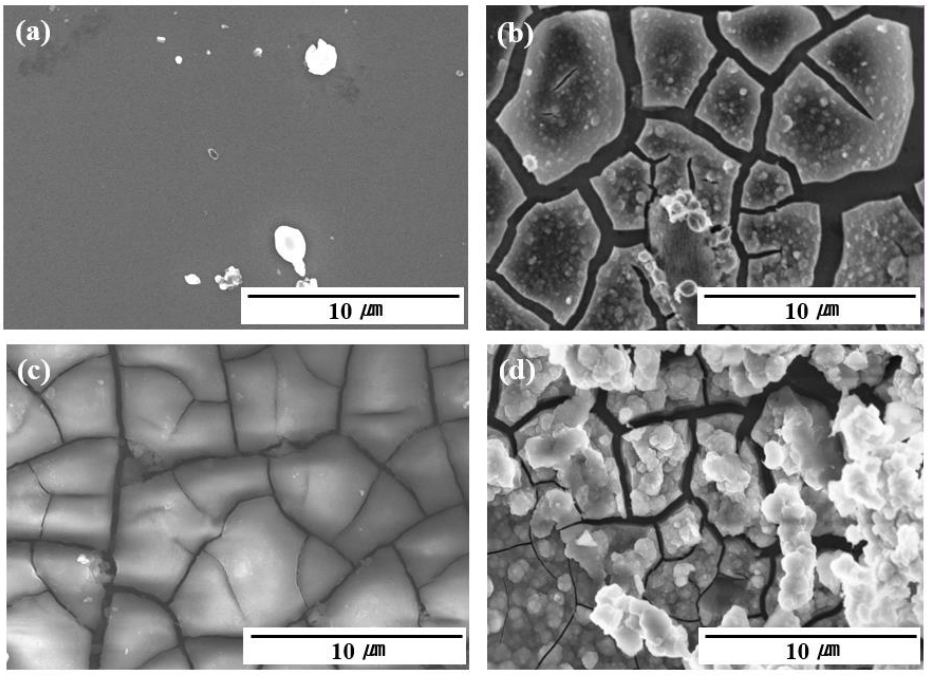

Fig. 2.8 SEM images of the films deposited at different current densities of, (a) 2.5 mA cm^{-2}; (b) 3.5 mA cm^{-2}; (c) 8 mA cm^{-2}; (d) 10 mA cm^{-2}; for 24 h.

2.3.5 Composition and Phase Analysis

EDX results as seen in Table 2.2 clearly reveal that more than 10 mol% of N is present alongside Ga and O in the film grown in these conditions. This indicates that the GaN compound film was formed according to Eq. (2.5). On the contrary, when a high current density of 10 mA cm^{-2} was applied, spherical particles were formed on the plate-like film and these particles were Ga_2O_3. Furthermore, the atomic concentration of N was lower than 3 mol% at any given position, while the concentration of Ga increased. The Ga was oxidized during precipitation even though the reductive reaction occurred at the working electrode. Therefore, it should be postulated that Ga is oxidized according to the following process. At the working electrode, besides the reduction of NO_3^- and Ga^{3+} ions, there is also a dominant reduction of the H^+ ions present in the solution. When the applied current is high, a large amount of hydrogen gas interferes with the precipitation of other ions on the surface of the electrode, H^+ ions near the surface are suddenly depleted, and the pH value increases as the reaction progresses. Therefore, the

following reaction between Ga^{3+} ions and water molecules proceeds via hydrolysis.

$$2Ga^{3+} + 3H_2O \rightarrow Ga_2O_3 + 6H^+ \quad (2.6)$$

Accordingly, it is likely that the reaction described in Eq. (2.4) did not proceed and only gallium oxide layer was formed on the substrate when hydrogen reduction was rapidly accelerated with increase in current. Therefore, it is inferred that the deposition must be attempted at a low current density or be conducted only for a short time at high current densities to prevent the reaction in Eq. (2.6) from proceeding. Hence, the synthesis of GaN was performed at current densities of 3.5 mA cm^{-2} and 8 mA cm^{-2}.

Table 2.2 EDX results of the films deposited on Si at different current densities for 24 h.

Element	Applied current density			
(mol%)	2.5 mA cm^{-2}	3.5 mA cm^{-2}	8.0 mA cm^{-2}	10.0 mA cm^{-2}
Ga	0.00	11.7	41.01	63.02
N	1.66	12.9	2.23	1.23
O	1.57	43.2	51.51	32.56
Si	96.77	32.1	5.25	3.19

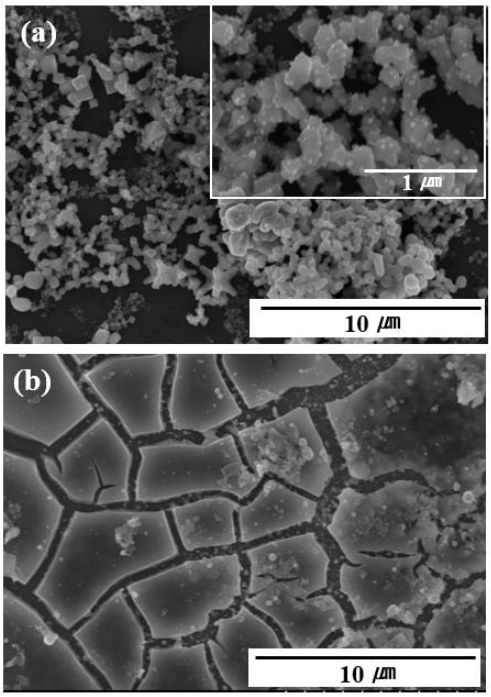

Element	Content (mol%)
Ga	2.02
N	7.10
O	17.01
Si	73.88

Element	Content (mol%)
Ga	26.10
N	6.70
O	65.19
Si	2.01

Fig. 2.9 SEM images and EDX results of the samples deposited at (a) 3.5 mA cm^{-2}; (b) 8 mA cm^{-2}; for 6 h.

Figure 2.9 shows the SEM images and EDX results of the samples deposited at 3.5 mA cm^{-2} and 8 mA cm^{-2} for 6 h, respectively. It was confirmed that more than 6 mol% of N was present on the surface of the samples deposited for 6 h. Furthermore, the mapping micrographs of Fig. 2.10 clearly reveal the presence of Ga and N in the films grown under these conditions. Ga, N, and O are uniformly dispersed in the plate-shaped films formed on the Si substrate.

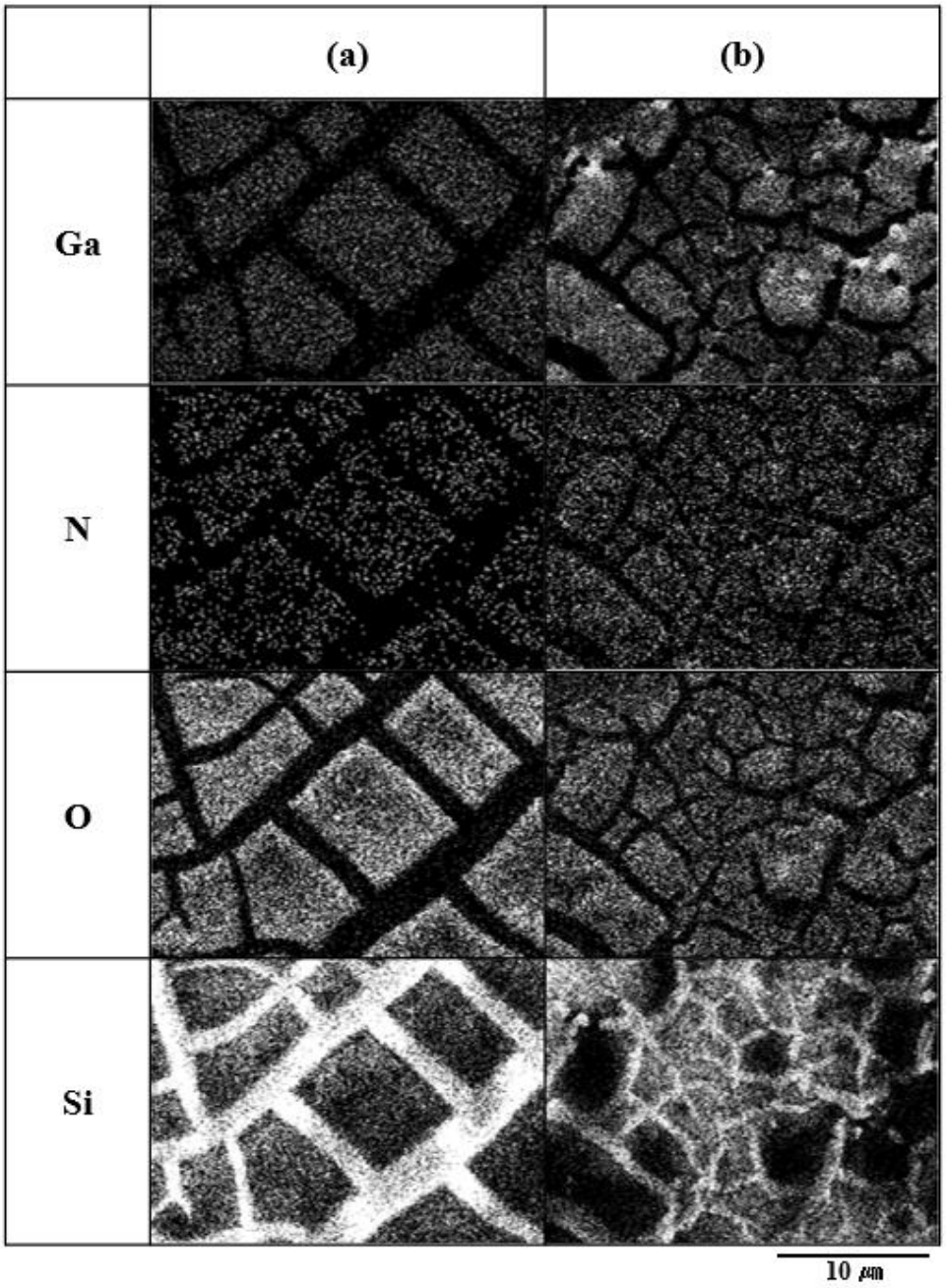

Fig. 2.10 Elemental mapping for the films deposited at different current densities and time of, (a) 3.5 mA cm^{-2} for 24 h; (b) 8 mA cm^{-2} for 6 h.

Figure 2.11 shows the XRD spectra of the above samples. For comparison, the XRD results for crystalline wurtzite GaN powder are shown in Fig. 2.11 (c) [41]. Diffraction peaks were observed at 2θ values of 34.5, 36.8, 48.1, 63.4, and 67.8 degrees in these spectra. These positions are consistent with those observed in the case of wurtzite GaN powder, and the peaks corresponding to cubic-GaN also observed. The strong peaks at $2\theta = 48.1$ and 63.4 degrees are due to reflection from the (102) and (103) planes, and peaks with weak intensities observed at $2\theta = 34.5$, 36.8, and 67.8 degrees correspond to reflections from the (002), (101), and (200) planes, respectively [42, 43]. There are four other peaks at 2θ = 43.0, 57.6, 59.8, and 64.6 degrees corresponding to the (112), (313), (113), and (512) planes of β-Ga_2O_3, respectively [44]. Two other strong peaks could be observed at $2\theta = 38.7$ and 47.1 degrees corresponding to silicon oxide and pure gallium, respectively. Thus, it can be confirmed that the GaN film was formed under these experimental conditions.

However, as is evident from the EDX and XRD results, it was observed that not only GaN but also oxides and metallic Ga were present in the deposited films. These results are similar to the previous reports by K. Al-Heuseen et al [29, 36]. In other words, the deposited film was affected by the oxidation and HER due to the process characteristics performed in the aqueous solution, which caused some drawbacks in the crystallinity and uniformity for the synthesized GaN.

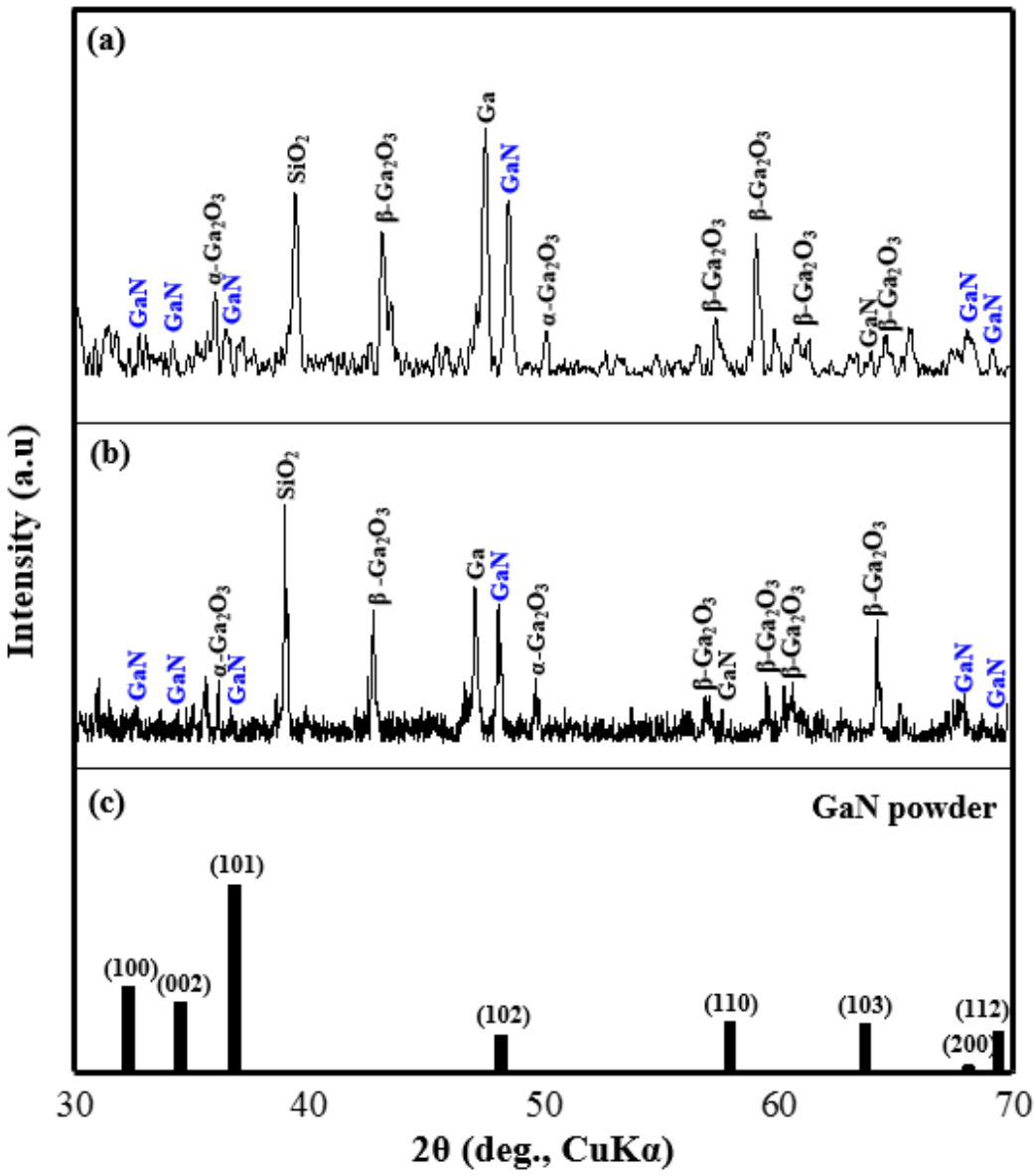

Fig. 2.11 XRD spectra of the films deposited at, (a) 3.5 mA cm^{-2} for 24 h; (b) 8.0 mA cm^{-2} for 6 h; and (c) pure wurtzite GaN powder.

2.3.6 Optical Emission Spectrum

Figure 2.12 shows the results of the PL analysis of the samples. The film deposited at the current density of 3.5 mA cm^{-2} for 24 h showed not only a sharp peak at a wavelength of 380 nm but also broad peaks at wavelengths in the range 490−550 nm. And the film deposited at 8.0 mA cm^{-2} for 6 h showed a sharp peak at a wavelength of 365.5 nm. The band gap energy, E_g, can be calculated from the wavelength of the peak position using the following equation.

$$E_g = hc/e\lambda \approx 1240/\lambda \quad (2.7)$$

Thus, the wavelengths of 380 nm and 365.5 nm correspond to band gap energies of 3.26 eV and 3.39 eV, respectively. It is well known from other reports that h-GaN and c-GaN have band gap energies of 3.39 eV and 3.2 eV, respectively [45, 46]. A slight difference in the values of band gap energy might be caused by the relatively small change in the crystal structure of the sample, which may not be detectable from the XRD measurements. But these band gap energies are good agreement with the band gap energies of GaN. Furthermore, when the sample was irradiated with laser, it emitted blue light at room temperature, as shown in Fig. 2.12 (c). The broad peaks at wavelengths in the range 490–550 nm can be viewed as defects or defect-impurity complexes in GaN and are called yellow luminescence [47]. Although broad peaks appeared in the region of yellow luminescence, the phenomenon of green luminescence did not appear due to very strong intensity at the wavelength of blue light.

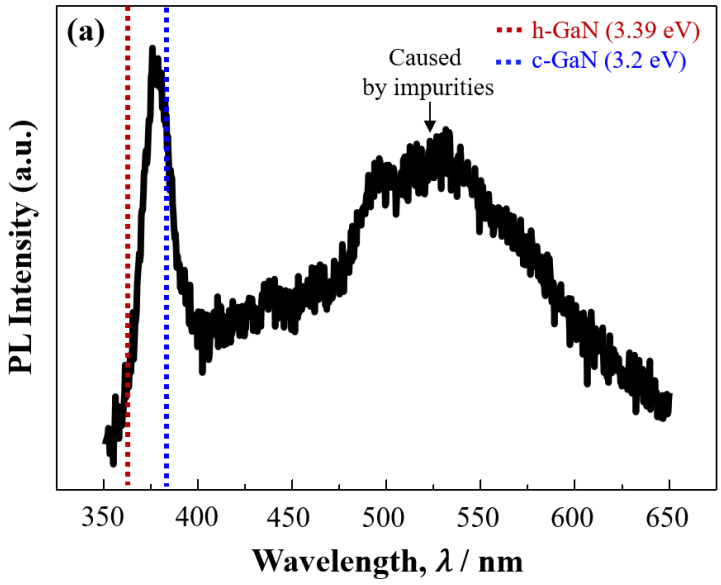

(a) PL Spectrum of the film deposited at 3.5 mA cm^{-2} for 24 h

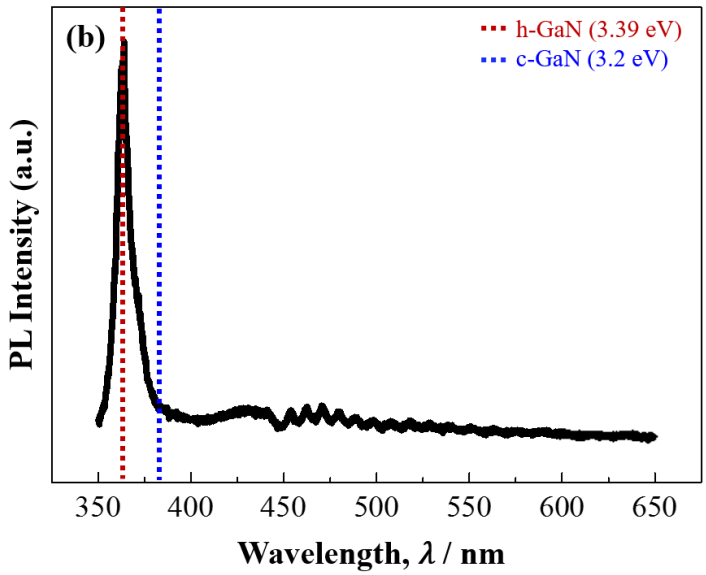

(b) PL Spectrum of the film deposited at 8.0 mA cm^{-2} for 6 h.

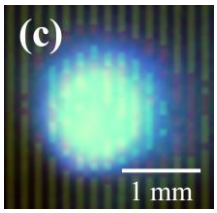

(c) Photograph of light emission observed on the film

Fig. 2.12 Photoluminescence analysis of the films and light emission by He-Cd laser.

2.4 Conclusions

The GaN films were synthesized on n-type Si (111) substrates by electrodeposition below room temperature. The CV analysis revealed that starting from a potential value close to the Ga reduction potential, the NO_3^- and NH_4^+ ions could be transformed to N_{ad}, which combined with Ga_{ad} during deposition, resulting in the formation of GaN films.

The effects of deposition time and current density on the formation of GaN film were examined to determine suitable conditions for synthesis. The surfaces formed at 3.5 mA cm^{-2} or more show a plate-like morphology of various sizes. But these films were observed to have island-shaped structures with many wide cracks caused by hydrogen bubbles generated during deposition process and difference of surface energies. The films contained a mixture of wurtzite GaN and Ga_2O_3 phases. Based on the EDX analysis of the sample formed at 3.5 mA cm^{-2} for 24 h, it was confirmed that Ga, N, and O were uniformly distributed in the film. However, the nitrogen content markedly decreased with increase in deposition current to 8 mA cm^{-2}. When a high current of 10 mA cm^{-2} was applied, Ga_2O_3 was predominant on the surface, and the reaction between Ga and N did not proceed. The PL analysis showed that our samples exhibit blue luminescence and also confirmed the peaks corresponding to the band gap energy of GaN.

The GaN films produced in this work have several drawbacks in terms of composition distribution and uniformity. The films contained a large amount of oxide, and many cracks were found on the surface. Nevertheless, this study shows the possibility of developing cost-effective techniques to synthesize GaN films for application in optoelectronic devices.

Reference

[1] B. Ha, S.H. Seo, J.H. Cho, C.S. Yoon, J. Yoo, G.C. Yi, C.Y. Park, C.J. Lee, *J. Phys. Chem. B* **109** (2005) 11095

[2] V.R. Reddy, P.K. Rao, C.K. *Ramesh, Mater. Sci. Eng. B* **137** (2007) 200

[3] S. Nakamura, M. Senoh, S. Nagahama, N. Iwasa, T. Yamada, T. Matsushita, H. Kiyoku, Y. Sugimoto, *Jpn. J. Appl. Phys.* **35** (1996) 74

[4] S. Nakamura, M. Senoh, S. Nagahama, N. Iwasa, T. Yamada, T. Matsushita, H. Kiyoku, Y. Sugimoto, T. Kozaki, H. Umemoto, M. Sano, K. Chocho, *Appl. Phys. Lett.* **72** (1998) 211

[5] F.A. Ponce, D.P. Bour, *Nature* **386** (1997) 351

[6] M.A. Khan, X. Hu, G. Sumin, A. Lunev, J. Yang, R. Gaska, M.S. Shur, *IEEE Elec. Dev. Lett.* **21** (2000) 63

[7] M.A Khan, M.S Shur, Q.C Chen, J.N Kuznia, *Electron. Lett.* **30** (1994) 2175

[8] J. Verma, S.M. Islam, A. Verma, V. Protasenko, D. Jena, *in A volume in Woodhead Publishing Series in Electronic and Optical Materials, 2nd edn.* (2018) 377

[9] O. Aktas, W. Kim, Z. Fan, A.E. Botchkarev, A. Salvador, S.N. Mohammad, B. Sverdlov, H. Morkoc, *Electron. Lett.* **3** (1995) 1389

[10] D. Reusch, J. Strydom, *IEEE Trans. Power Electron.* **30** (2015) 5151

[11] H.M. Huang, S. Mao, H. Feick, H. Yan, Y. Wu, H. Kind, E. Weber, R. Russo, P. Yang, *J. Science* **292** (2001) 1897

[12] J.C. Johnson, H.J. Choi, K.P. Knutsen, R.D. Schaller, P. Yang, *Nature Mater.* **1** (2002) 106

[13] S. Keller, R. Vetury, G. Parish, S.P. DenBaars, U.K. Mishra, *Appl. Phys. Lett.* **78** (2001) 3088

[13] M.G. Walter, E.L. Warren, J.R. McKone, S.W. Boettcher, Q. Mi, E.A. Santori, N.S. Lewis, *Chem. Rev.* **110** (2010) 6446

[14] S.C. Jain, M. Willander, J. Narayan, R.V. Overstraeten (2000) *J. Appl. Phys.* **87** (2000) 965

[15] H. Amano, T. Tanaka, Y. Kunii, K. Kato, S.T. Kim, I. Akasaki, *Appl. Phys. Lett.* **64** (1994) 1377

[16] Y. Azuma, M. Shimada and K. Okuyama, *J. Chem. Vap. Depos.* **10** (2004) 11

[17] S.A. Nikishin, N.N. Faleev, V.G. Antipov, S. Francoeur, L. Grave de Peralta, G.A. Seryogin, H. Temkin, *J. Appl. Phys. Lett.* **75** (1999) 2073

[18] J. Jasinski, W. Swider, Z. Liliental-Weber, P. Visconti, K.M. Jones, M.A. Reshchikov, F. Yun, H. Morkoç, S.S. Park, K.Y. Lee, *Appl. Phys. Lett.* **78** (2001) 2297

[19] N. Elkashef, R.S. Srinivasa, S. Major, S.C. Sabharwal, K.P. Muthe, *J. Thin Solid Films* **333** (1998) 9

[20] F. Iskandar, T. Ogi, K. Okuyama, *Mater. Lett.* **60** (2006) 73

[21] H. Morkoç, S. Strite, G.B. Gao, M.E. Lin, B. Sverdlov and M. Burns, *J. Appl. Phys.* **76** (1994) 1363

[22] R.K. Roy, A.K. Pal, *Mater. Lett.* **59** (2005) 2204

[23] K. Rajeshwar, *Adv. Mater.* **4** (1992) 23

[24] M.A. Qaeed, K. Ibrahim, K.M.A. Saron, A. Salhin, *Superlattices Microstruct.* **64** (2013) 70

[25] D. Lincot, *J. Thin Solid Films* **487** (2005) 40

[26] J. Katayama, M. Izaki, *J. Appl. Electrochem.* **30** (2000) 855

[27] H. Wang, X.Y. Chen, A.M.C. Ng, F. Fang, A.B Djurišić, W.K. Chan, *2009 IEEE ThO2, 14th OECC* (2009)

[28] K. Al-Heuseen, M.R. Hashim, N.K. Ali, *Mater. Lett.* **64** (2010) 1604

[29] N. Takeno, *Atlas of Eh-pH Diagrams. Intercomparison of Thermodynamic Databases. National Institute of Advanced Industrial Science and Technology.* (2005) 153

[30] D.R. GABE, *J. Appl. Electrochem.* **27** (1997) 908

[31] M.J.N. Pourbaix, *Thermodynamics of Dilute Aqueous Solutions. Edward Arnold and Co.* (1949)

[32] N. Ryan, E.J. Lumley, *J. Electrochem. Soc.* **106** (1959) 388

[33] D. Cubicciotti, *J. Nucl. Mater.* **167** (1989) 241

[34] K. Al-Heuseen, M.R. Hashim, *J. Cryst. Growth* **324** (2011) 274

[35] J.M.M. IIarduya, F. Villafane, *J. Chem. Educ.* **71** (1994) 480

[36] K. Al-Heuseen, *Int. J. Thin Fil. Sci. Tec.* **5** (2016) 113

[37] S. Sarkar, S. Sampath, *Chem. Commun.* **52** (2016) 6407

[38] B.L. Pearce, S.J. Wilkins, T. Paskova, A. Ivanisevic, *J. Mater. Res.* **30** (2015) 2859

[39] S.C. Cruz, S. Keller, T.E. Mates, U.K. Mishra, S.P. DenBaars, *J. Cryst. Growth* **311** (2009) 3817

[40] Joint Committee on Powder Diffraction Standards (JCPDS) (1967) JCPDS File

[41] C.M. Balkaş, R.F. Davis, *J. Ame. Ceram. Soc.* **79** (1996) 2309

[42] J.K. Sprenger, A.S. Cavanagh, H. Sun, K.J. Wahl, A. Roshko, S.M. George, *Chem. Mater.* **28** (2016) 5282

[43] G. Wang, J.S. Park, X. Kong, P.R. Wilson, Z. Chen, J.H. Ahn, *Cryst. Growth Des.* **8** (2008) 1940

[44] H. Zhang, Z. Ye, B. Zhao, *J. Appl. Phys.* **87** (2000) 2830

[45] D.S, Chaudhuri, A.K. Pal, *Mater. Lett.* **53** (2002) 68

[46] J. Neugebauer, C.G. Van de Walle, *Appl. Phys. Lett.* **69** (1996) 503

Chapter 3

Influence of Substrate on Formation of Electrodeposited GaN Film

Chapter 3 – Influence of Substrate on Formation of Electrodeposited GaN Film

3.1 Introduction

GaN is a one of III-V group semiconductors with a wide bandgap energy (3.39 eV), attracting attention as a next-generation material that will lead the optoelectronic device field due to its blue light emission characteristics [1–6]. At present, although high quality GaN is being fabricated by various dry methods [7–12], a low-cost synthesis method for commercialization is further required since the expensive process price of dry process.

Electrochemical methods are currently receiving considerable attention since they are very useful as low-cost processes for the synthesis of next generation materials. In recent years, electrodeposition technique [13–15] has been increasingly researched because it can easily form the films on various types of electrodes relatively, and the thickness and morphology of the film can be simply controlled by electrochemical parameters [16, 17]. Many researchers have reported on the growth of semiconductor materials in bulk or thin film form by electroplating from liquid solutions [18], and there are some reports on the synthesis of III-V semiconductor materials by electrodeposition [19–21]. Several researchers have confirmed the possibility of GaN synthesis at room temperature from aqueous solutions and ionic liquids by electrodeposition [22–26]. However, there still has been little reported to clarify the formation mechanism of GaN film.

The electrodeposition of GaN is carried out in various electrolyte. It is however, extremely difficult to control the composition of films. The difference in the reduction potentials of gallium (Ga) and nitrogen (N) is greater than 1 V, and it is very difficult to deposit nitride films by wet process at room temperature. Especially, the growth of GaN film from aqueous solution is significantly affected by the hydrogen evolution occurring at the cathode electrode. One of the researchers [23] has reported that the

formation of GaN occurs by a combination reaction between trivalent gallium (Ga^{3+}) cations and trivalent nitrogen (N^{3-}) in ammonium (NH_4^+) cation from aqueous solution. However, the reduction reactions of the nitrogen species ions during the electrochemical deposition process are still not clarified [25], and it is difficult to explain the formation of the GaN film because the NH_4^+ ions have the most stable energy state in aqueous solution.

In addition, in most studies, the semiconductor substrates such as silicon (Si), silicon carbide (SiC) have been used to fabricate GaN films by electroplating. Semiconductor substrates have very high resistance values compared to metal substrates and thus do not effectively transfer electrons to the interface between electrode surface and electrolyte during the electrodeposition process [26]. This factor makes the mechanism of the GaN formation by electrodeposition unclear. Therefore, the examination of the behavior of ions occurring at different electrodes and the comparison of the results are important for the low cost / temperature synthesis of GaN film from aqueous solutions.

This chapter reports on the electrochemical behavior of ions from acid aqueous solutions containing various chemicals and presents the effects of substrate materials on the electrodeposition of GaN film. The electrochemical behavior of each ion was investigated by adding chemicals step by step using cyclic voltammetry. Electrodeposition was attempted on each electrode and the influence of the electrode properties on GaN formation was examined by comparison with CV results. The formation mechanism of GaN film in aqueous solutions is discussed and suggest a suitable substrate material.

2. Experimental Details

Gallium nitrate hydrate ($Ga(NO_3)_3 \cdot xH_2O$, ≥99.9%, Sigma Aldrich), ammonium nitrate (NH_4NO_3, ≥98%, Sigma Aldrich) were purchased for using as the source of GaN. Concentrated nitric acid (HNO_3, 70.0%, Nacalai Tesque) was used to adjust the pH level of each solution. Sulfuric acid (H_2SO_4, 70.0%, Nacalai Tesque) was used to obtain the background for confirming the reaction of nitrogen (N) species ions.

In order to CV and electrochemical deposition, a potentiostat/galvanostat (Hokuto Denko, HZ-7000) was used. A three-electrode cell configuration was applied and gallium (Ga), platinum (Pt), aluminum (Al) and titanium (Ti) electrodes were used as the working electrode, separately. These substrate materials were selected in consideration of hydrogen sensitivity and lattice constant. Pt coil was used as the counter electrode and the reference electrode was a silver/silver chloride (SSC = 0.22 V vs. SHE) electrode in a saturated KCl. The liquid gallium dissolved at 60 °C was inhaled with a syringe, transferred on glass plate, and cooled to prepare a plate-shaped Ga electrode. The surface of electrodes was polished using an abrasive paper to a grade from 800 to 2000, gradually. And Pt coil was immersed in HCl to clean the surface and is thereafter washed with distilled water. Finally, all electrodes were washed with distilled water and dried under atmospheric conditions. Prior to experiments, the electrodes and Pt wire were connected and covered with a Nitoflon adhesive tape (Nitto Denko) to yield an electrode area of 1.0×1.0 cm^2.

Cyclic voltammogram was recorded between −2.0 and 2.0 V vs. SSC at a scanning rate of 20 mV s^{-1}. Scans were first swept in the negative direction from the natural potential of electrodes and all potential values were recorded versus SSC electrode.

All electrochemical experiments were conducted in aqueous solutions at room temperature and in unstirred solutions. The working and counter electrodes were separated by a distance of approximately 1.0 cm. The electrodepositions were attempted using the galvanostatic method. The samples were immediately rinsed thoroughly with distilled water after deposition.

The surface morphology of deposited films was characterized with scanning electron microscopy (SEM, Hitachi, S-4800), and the chemical composition was analyzed by energy dispersive X-ray spectroscopy (EDX, HORIBA, EMAX ENERGY, EX-350). The SEM measurement was performed at 10 kV, and the EDX analysis is conducted at an acceleration voltage of 12 kV and current of 10 μA. The examination of the crystal structure of the films was carried out on X-ray diffractometer (XRD, Rigaku, Ultima IV) using Cu–Kα radiation.

3. Results and Discussion

3.1 Behavior of Nitrogen Species on Different Electrodes

The electrochemical behavior of ions onto several electrodes in acid aqueous solutions was examined by CV technique.

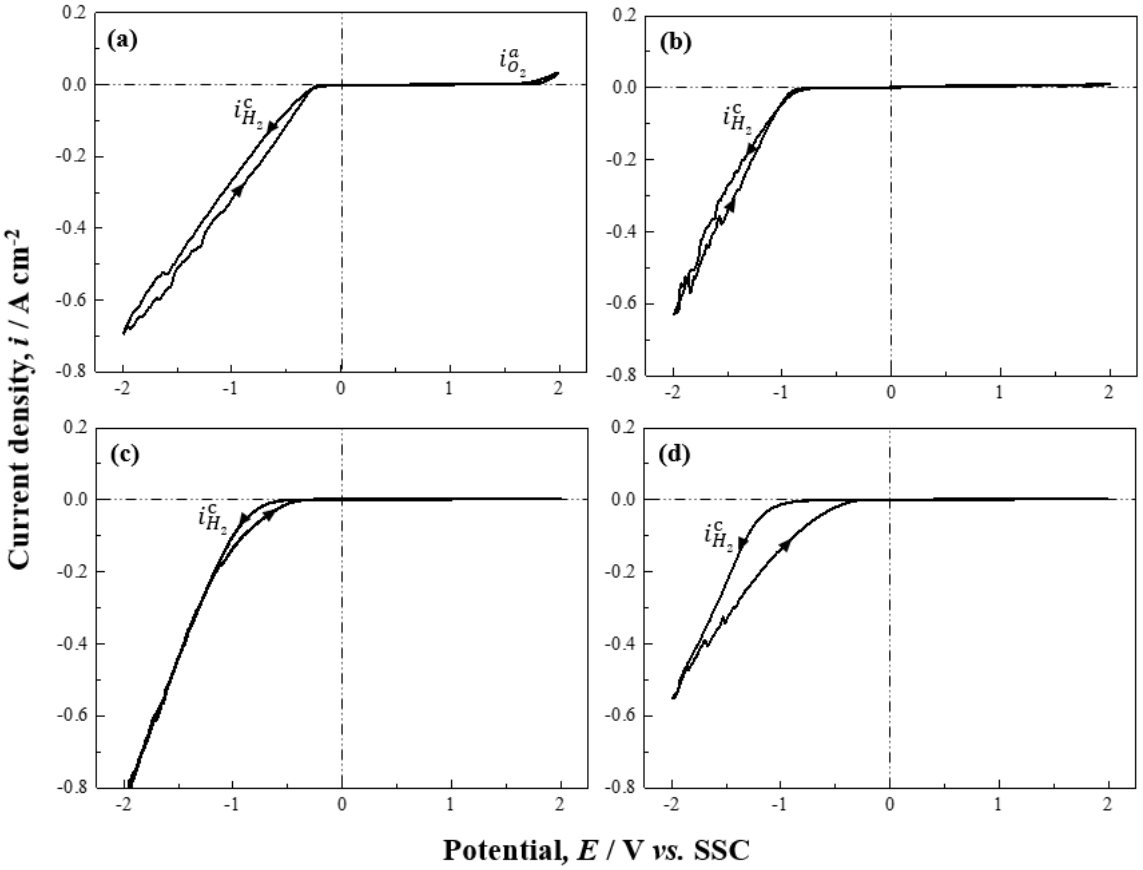

Fig. 3.1 Voltammograms obtained from 1 M H_2SO_4 solution of pH 0.64 for (a) ~(d) Pt, Ga, Al and Ti electrodes, respectively. (i^c_{H2}: hydrogen evolution, i^a_{O2} oxygen evolution)

Figure 3.1 shows the voltammograms obtained from the solutions of pH 0.64 containing only 1 M H_2SO_4 using the aforementioned electrodes (1 M = 1 mol dm^{-3}). The cathodic current is gradually increasing below −0.22 V, which corresponds to the hydrogen evolution reaction (HER), $i^c_{H_2}$, on the Pt electrode (in Fig. 3.1(a)) [27].

$$2H^{+}_{(aq)} + 2e^{-} \rightleftharpoons H_2(g) \qquad (E^0 = -0.22 \text{ V vs. SSC}) \tag{3.1}$$

Hydrogen adsorption processes at the surface of a platinoid metal (Ni, Pt, Pd, etc.) with low hydrogen overvoltage may occur until the formation of a quasi-complete monolayer [28]. And a slight anodic current appears at +1.2 V. This corresponds to the following oxygen evolution reaction (OER), $i^{a}_{O_2}$, that occurs on Pt coil.

$$2H_2O \rightarrow O_2 + 4H^{+} + 4e^{-} \qquad (E^0 = +1.01 \text{ V vs. SSC}) \tag{3.2}$$

Likewise, it can be shown that the cathodic current due to HER appear on the Ga surface (Fig. 3.1(b)), but this current starts from negative potential (ca. −0.87 V) compared to the case of the Pt electrode. In the case of the Al electrode (Fig. 3.1(c)), similarly to the case of the Ga electrode, the HER potential is slightly shifted in the negative direction, but an anodic current corresponding to OER is not observed. At the Ti electrode with the highest hydrogen overvoltage, a cathodic current corresponding to HER occurs at −1.1 V.

The results in Fig. 3.2 show CVs from the solutions of pH 0.9 containing 1 M HNO_3. Comparison of the results in the H_2SO_4 solutions depicted as grey dashed lines can confirm the behavior of nitrate (NO_3^-) ions on each electrode. For the Pt electrode (Fig. 2(a)), the peak due to the HER from −0.2 V is stronger and the other cathodic current is not clearly observed. In the result on the Ga electrode of Fig. 2(b), the cathodic current occurred at a slightly positive potential and weak cathodic current peak is identified at A_1, which may be attributed to the reduction processes of NO_3^- ions that occurred after HER through the following reactions [30, 31]:

$$NO_3^- + 2H^{+} + 2e^{-} \rightarrow NO_2^- + H_2O \qquad (E^0 = +0.62 \text{ V vs. SSC}) \tag{3.3}$$

$$NO_3^- + 4H^{+} + 3e^{-} \rightarrow NO^- + H_2O \qquad (E^0 = +0.73 \text{ V vs. SSC}) \tag{3.4}$$

$$2NO_3^- + 12H^{+} + 10e^{-} \rightarrow N_2 + 6H_2O \qquad (E^0 = +1.02 \text{ V vs. SSC}) \tag{3.5}$$

$$NO_3^- + 10H^{+} + 8e^{-} \rightarrow NH_4^+ + 3H_2O \qquad (E^0 = +0.66 \text{ V vs. SSC}) \tag{3.6}$$

$$NO_2^- + 8H^{+} + 6e^{-} \rightarrow NH_4^+ + 2H_2O \qquad (E^0 = +0.63 \text{ V vs. SSC}) \tag{3.7}$$

All reactions can occur simultaneously at similar potentials and nitrogen species ions are easy to exist as ammonium ions in aqueous solution. It can be confirmed that the reduction reaction of NO_3^- does not occur before HER even though the reduction potential of NO_3^- has more positive value than the standard reduction potential of H^+. In the result on the Al electrode, the trend on a graph is similar with result on Ga, and the current corresponding to the reduction of NO_3^- is found at ca. –1.0 V (A_2). For Ti electrode, a cathodic current start from positive potential. And the anodic currents are observed at A'_1 and A'_2 on the Ga and Al electrodes, respectively. These anodic currents can be thought as dissolution of Ga and Al into solution. As a result, it can be confirmed that NO_3^- ions can be reduced with HER, and the reactions occur at a negative potential than its standard reduction potential by the influence of H_2.

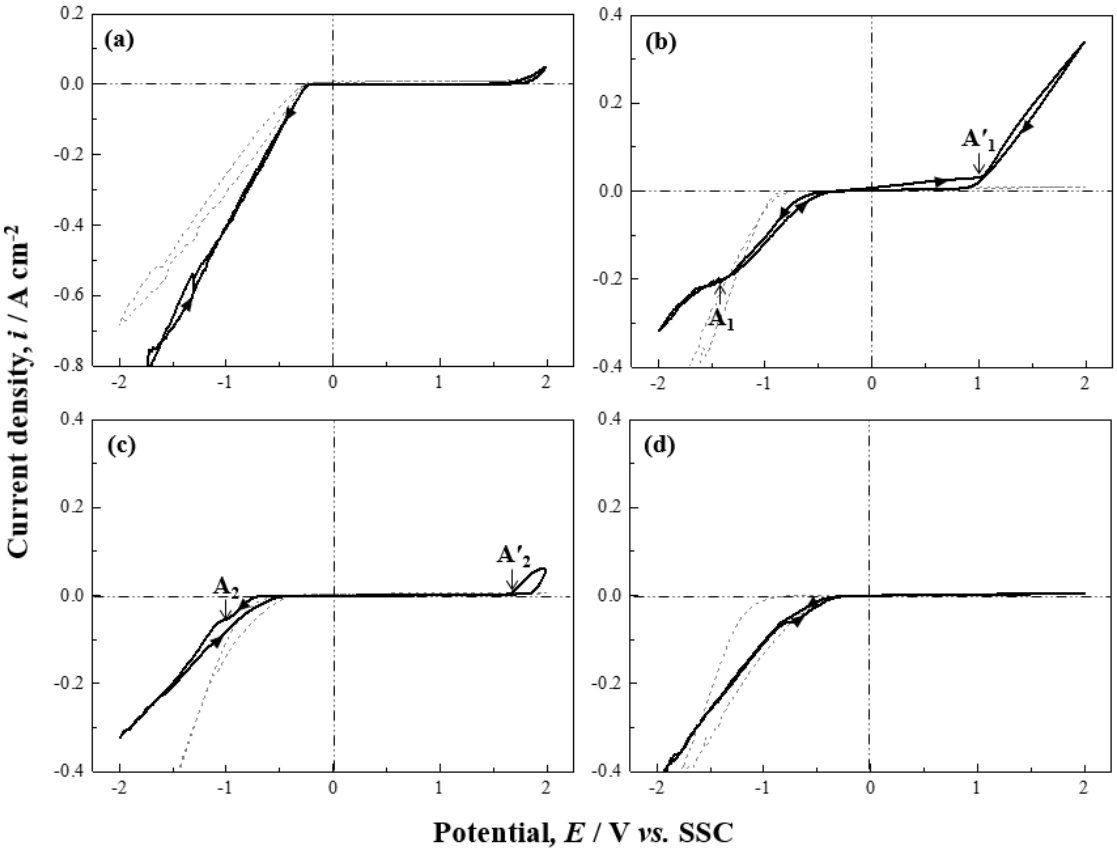

Fig. 3.2 Voltammograms obtained from 1 HNO_3 solution of pH 0.88 for (a)–(d) Pt, Ga, Al and Ti electrodes, respectively. The grey dashed lines represent the CVs obtained from the solution containing 1 M H_2SO_4 on the same electrodes.

Figure 3.3 shows the CV results from 1 M HNO_3 solutions of adding 0.5 M NH_4NO_3 to confirm the influence of NH_4^+ ions. In the Pt electrode, a reduction current other than HER is still not shown, but the noisy signals are detected by adsorption of gases. From the Ga electrode of Fig. 3.3(b), a small cathodic current curve shows at B_1, and more obvious peak appears at the same potential on the Al electrode (B_2). These current curves suggest that the intermediate reactions corresponding to Eqs. (3.3)−(3.5) are accelerated by the NH_4^+ ions present in the solution. In addition, the result on the Al electrode shows another current curve seen at B_3 in Fig. 3.3(c). It may suggest that the formation reactions of nitrite (NO_2^-) ions and adsorbed nitrogen (N_{ads}) are accelerated. Moreover, NO_2^- ions formed during the electrochemical process can cause the next proportional reaction with NH_4^+ ions, thereby forming the N_{ads} [32].

$$NO_2^- + NH_4^+ \rightarrow 2N_{ads} + 2H_2O \quad (3.8)$$

From the graph obtained from the Ti electrode in Fig. 3(d), a weak current change that can be considered as the reduction of NO_3^- appears but clear peak is not detected.

In summary, the electrochemical behavior of N species ions on each electrode can be described as following:

i) The reduction reactions of NO_3^- ions occur at a negative potential than its standard reduction potential with HER. The reduction reaction of NO_3^- does not occur on the surface of Pt electrode where HER is very easy to occur.

ii) When NO_3^- ions and NH_4^+ ions coexist in the solution, the reaction of NO_2^- and N_2 formation can be accelerated, and NO_2^- ions can be changed to N_{ads} by the comproportionation reaction with NH_4^+ ions.

iii) On the Ti electrodes with low hydrogen evolution, a weak signal appears but clear peak is not detected.

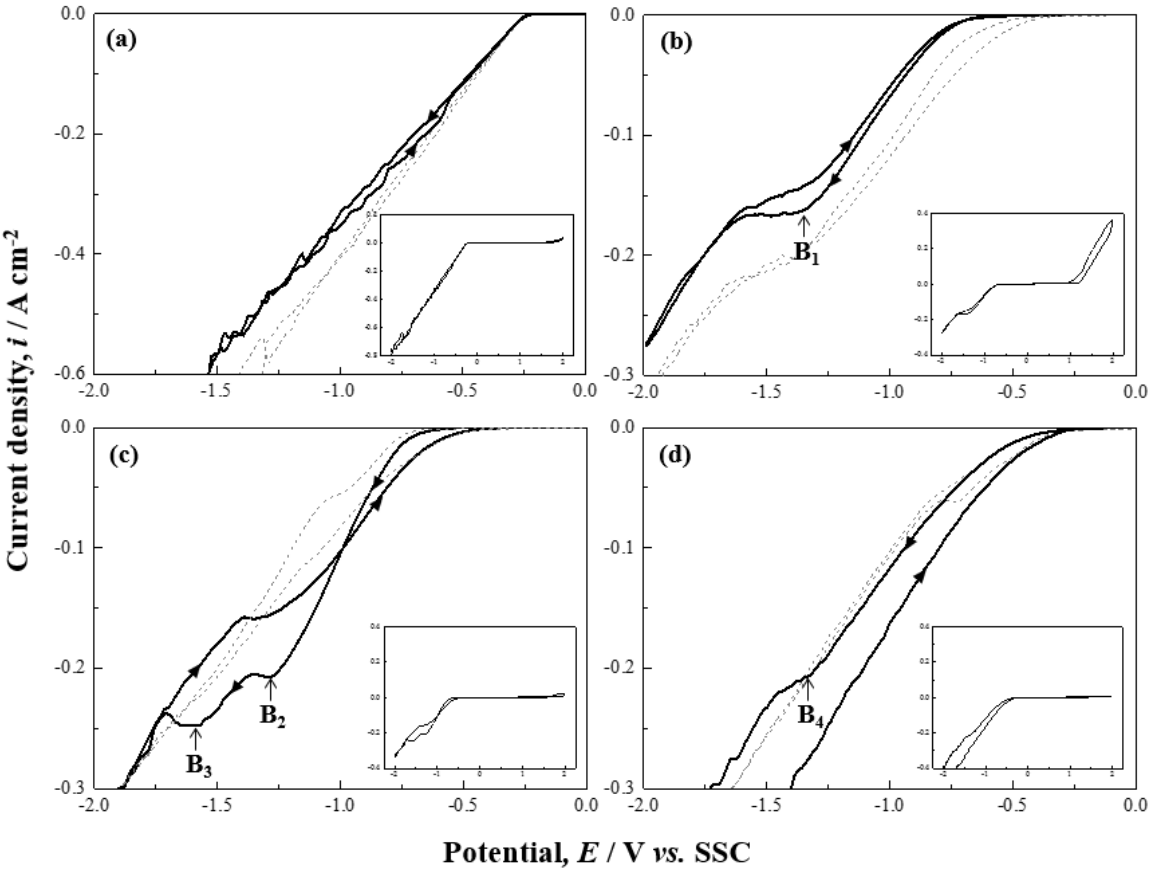

Fig. 3.3 Voltammograms obtained in 1 M HNO_3 + 0.5 M NH_4NO_3 solution of pH 0.78 for (a) –(d) Pt, Ga, Al and Ti electrodes. The grey dashed lines represent the CVs obtained from 1 M HNO_3 solution.

3.2 Behavior of Gallium Ion in Nitrate solutions

The electrochemical behavior of Ga^{3+} ions in acidic solutions was also examined by adding $Ga(NO_3)_3$. Figure 3.4 shows the results obtained from the solutions of pH 0.94 containing 1 M HNO_3 and 0.1 M $Ga(NO_3)_3$. As a result of Fig. 3.4(a), the separated current peak does not appear on the Pt electrode, but a slight increase in current that can be considered as the precipitation of Ga is observed around −0.5 V. In the case of Ga electrode (in Fig. 3.4(b)), it can be seen that a cathodic current density is reduced compared to that in the 1 M HNO_3 solution and HER start more negative potential. And after HER, a slight cathodic current appears corresponding to the following reduction reaction of Ga^{3+} as described follow [33].

$$Ga^{3+} + 3e^{-} \rightarrow Ga_{ads} \quad (E^0 = -0.78 \text{ V vs. SSC}) \tag{3.9}$$

Subsequently, the current flow due to NO_3^- reductions is shown from C_1. For the Al, the increased cathodic current corresponding to the reduction of Ga^{3+} is found at the same potential as for the Ga electrode, and two separated current curves are observed. The formation of metallic Ga starts at positive potential than reduction of NO_3^-, and the reactions of NO_3^- occurs following that. In the result of Fig. 3.4(d) obtained from the Ti electrode, the cathode current significantly decreases and the reduction of NO_3^- proceeds from C_4. After H^+ ions are adsorbed and bound with metal ions on the electrode surface, the metal can be precipitated during the process of H_2 gas evolution. Thus, the cathodic current corresponding to Ga reduction is decreased on the Ti electrode with high hydrogen overpotential [34].

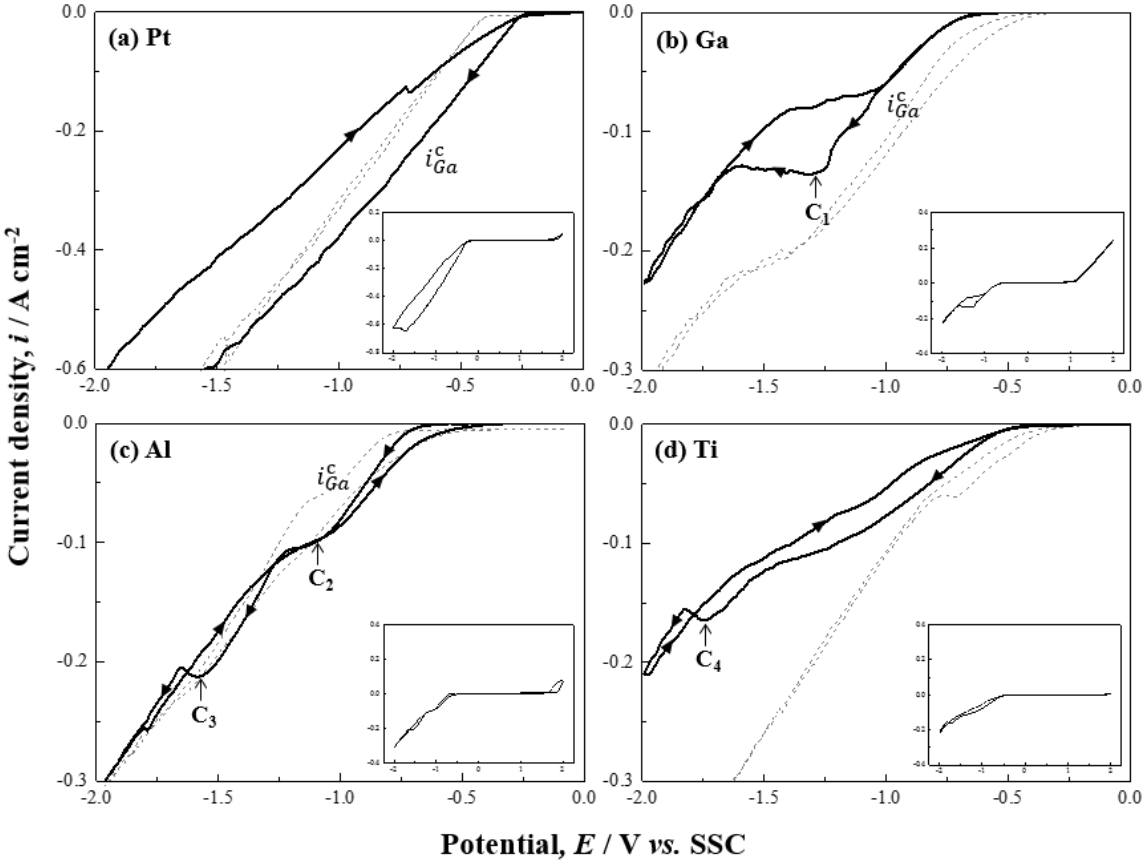

Fig. 3.4 Voltammograms obtained from 1 M HNO_3 + 0.1 M $Ga(NO_3)_3$ solution of pH 0.94 for Pt, Ga, Al and Ti electrodes. The grey dashed lines represent the CVs in 1 M HNO_3 solution on the same electrodes. (i_{Ga}^{c} :reduction of gallium)

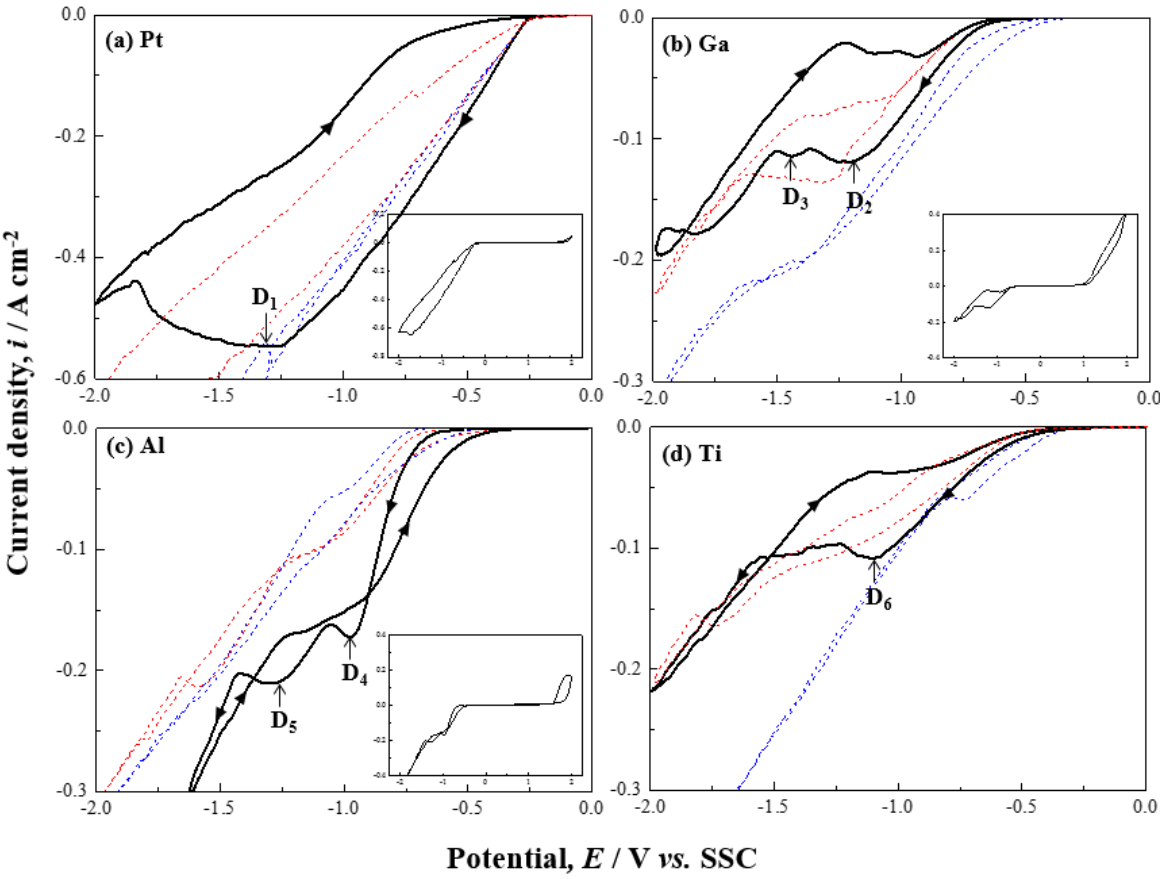

Fig. 3.5 Voltammograms in 1 M HNO_3 + 0.1 M $Ga(NO_3)_3$ + 0.5 M NH_4NO_3 solution of pH 0.85 for Pt, Ga, Al and Ti electrodes. The blue and red dashed lines represent the CVs obtained from 1 M HNO_3 and 1 M HNO_3 + 0.1 M $Ga(NO_3)_3$ solutions, respectively.

Figure 3.5 shows the CVs obtained from the mixed solutions of 1 M HNO, 0.1 M $Ga(NO_3)_3$ and 0.5 M NH_4NO_3. The result for the Pt electrode in Fig. 3.5(a) shows the cathodic current corresponding to HER and Ga precipitation. And a current curve is detected in the results from other solutions is detected at D_1. And a current curve that is not seen in the results obtained from the other solutions is detected. As shown the result in Fig. 3.5(b) and 3.5(c), two cathodic current hills are observed separately (D_2–D_5). The first current curve causes by the reduction of Ga^{3+} and the second curve is due to the intermediate reactions of NO_3^- corresponding to Eqs. (3.3)–(3.5). In the CV on the Ti of Fig. 3.5(d), the cathode current due to Ga reduction is detected (D_6) and a slight current increase corresponding to the reduction

of NO_3^- is observed. Moreover, this increase in current is more apparent on the Al electrode. In other words, it can be known from these results that NH_4^+ ions affect not only reduction of NO_3^- but also the precipitation of Ga^{3+} ions.

3.3 Electrodeposition on Different Substrates

The electrodeposition of GaN film in an aqueous solution is attempted on different substrates, and their morphology and composition are characterized by SEM and EDX. Figure 3.6 shows the SEM images of sample surface deposited at a current density of 3.5 $mA \cdot cm^{-2}$ for 24 h on the above four substrates. And the corresponding EDX results are described in Table 3.1.

As shown from Fig. 3.6, The film surface deposited on the Pt substrate shows that a circular metal Ga is deposited. And EDX result shows little N content. A needle-like morphology is observed in the film surface deposited on Ga substrate and N content of 20 mol% is detected. On the film deposited on Al substrate, a morphology consisting of nanoparticles in the form of circular particles appeared, and it is confirmed that significant amounts of Ga and N are present. A thick titanium oxide (TiO_2) in the form of a plate is formed on the film deposited on the Ti substrate and N is not detected. When a large amount of hydrogen bubble is generated on the electrode surface, only Ga is precipitated. And the film deposited on the Ti substrate having the highest hydrogen overvoltage among the four electrodes, it can be seen that almost TiO_2 is formed. In contrast, the films deposited on Ga and Al electrodes show high ratio of Ga and N contents.

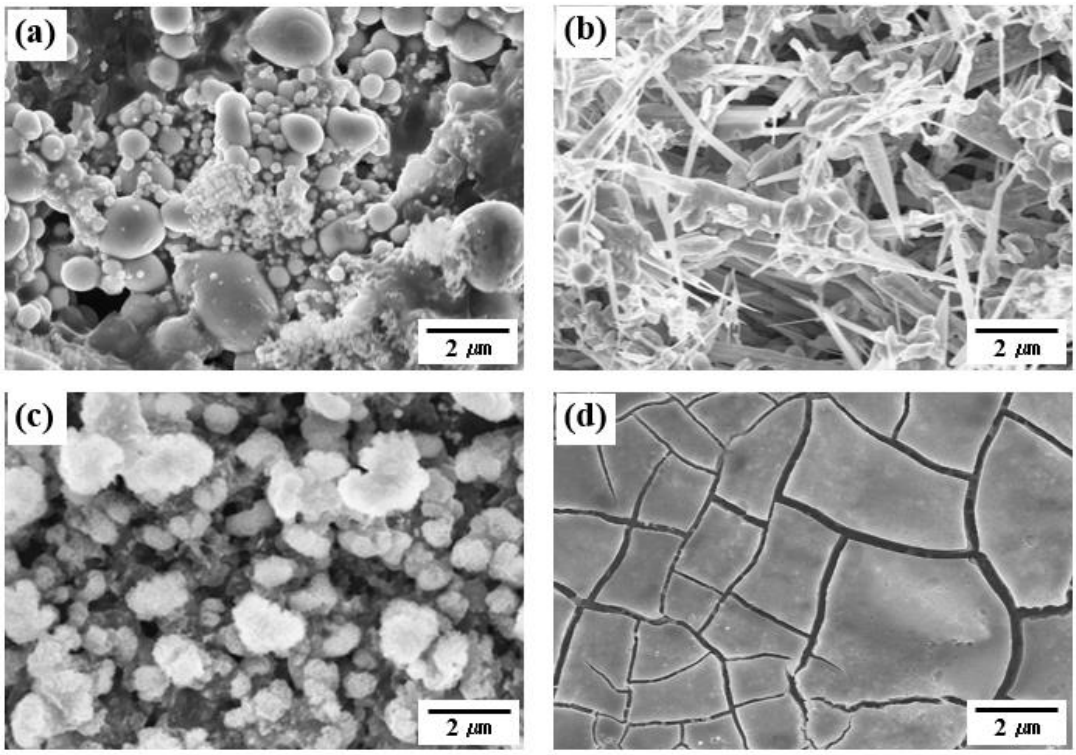

Fig. 3.6 SEM images of the films deposited on (a) Pt plate; (b) Ga plate; (c) Al plate; (d) Ti plate; at 3.5 mA s^{-1} for 24 h from 0.1 M $Ga(NO_3)_3$, + 0.5 M NH_4NO_3 + 1 M HNO_3 solution.

Table 3.1 EDX results of the films deposited on different substrates at 3.5 mA cm^{-2} for 24 h.

Elements (mol%)	(a) on Pt	(a) on Ga	(a) on Al	(a) on Ti
Ga	92.71	71.32	48.14	20.77
N	1.63	20.03	22.74	0.00
O	5.59	8.65	7.56	57.03

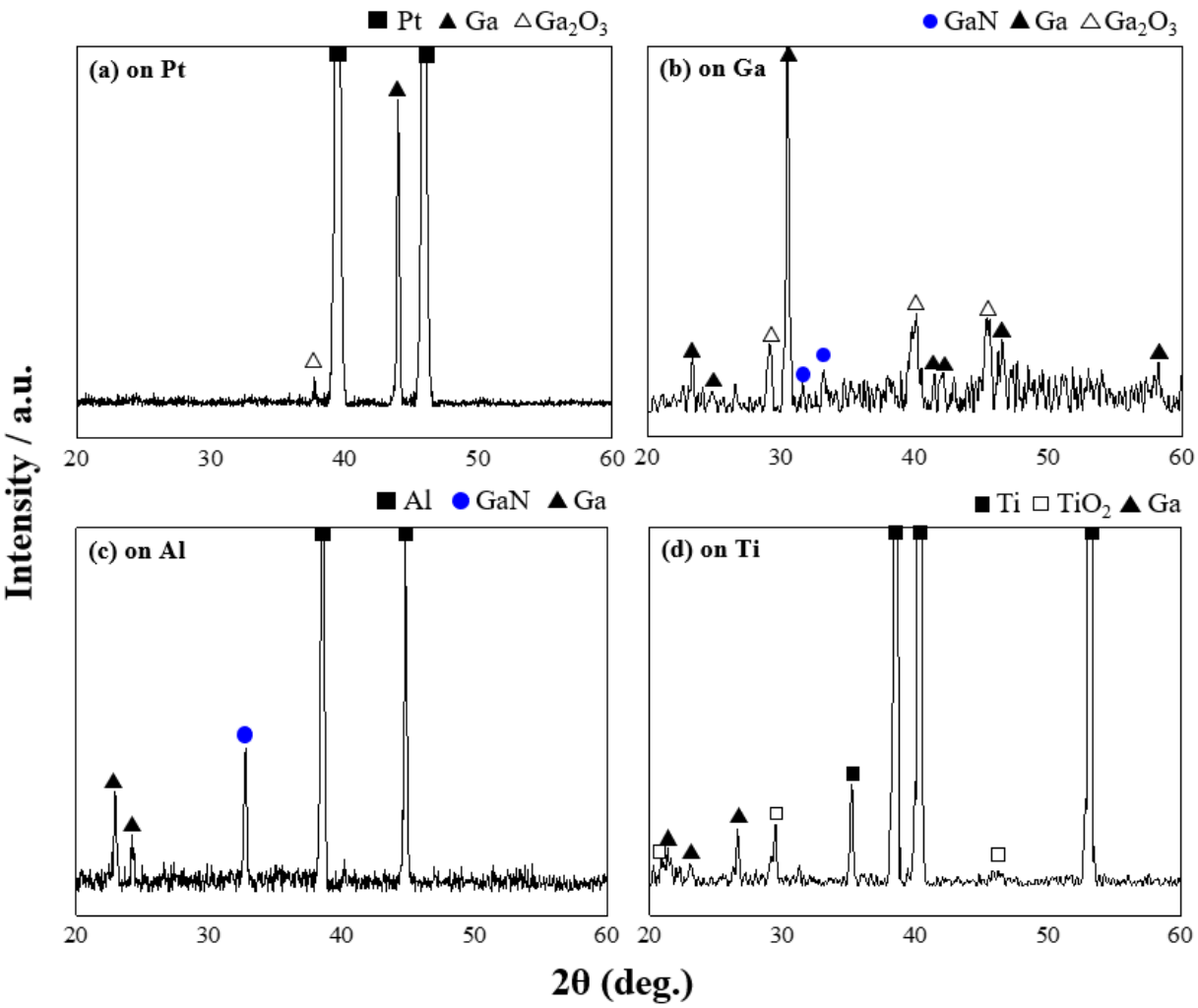

Fig. 3.7 XRD spectra of deposited films on (a) Pt plate; (b) Ga plate; (c) Al plate; (d) Ti plate; at 3.5 mA s^{-1} for 24 h from mixed aqueous solution of 0.1 M $Ga(NO_3)_3$, 0.5 M NH_4NO_3 and 1 M HNO_3.

Figure 3.7 shows the XRD spectra of deposited films on different substrates. A peak correspond to Ga is observed at $2\theta = 43.9$ degree from the film deposited on the Pt substrate in Fig. 3.7(a). A peak that corresponds to the reflection of GaN is observed at $2\theta = 32.7$ degree for the film deposited on the Ga and Al substrates, respectively [35]. On the Ga substrate, the peaks due to gallium oxide (Ga_2O_3) [36] appear and a peak corresponding to GaN appear small, while in the film deposited on the Al, a sharp and clear peak due to GaN is detected. For the film deposited on Ti in Fig. 3.7(d), the peaks at $2\theta = 20.3$, 29.5, 31.2 and 46.1 degrees caused by reflections from TiO_2 [37], and the small peaks due to Ga are detected.

Consequently, GaN compound films are formed on the Ga and Al electrodes in which the separated cathodic current peaks are confirmed by CV. Metallic Ga precipitate on the Pt substrate with high hydrogen evolution, and an oxide is detected on the Ti electrode with low hydrogen evolution. These results indicate that the formation of GaN film by electrodeposition is greatly affected by the substrate material and the composition of solution. That is, it can be considered that the GaN compound film can be formed by the following combination reaction when the reduction reactions of Ga^{3+} and NO_3^- ions occur at the close potential values, and when N_{ads} is formed by the addition of NH_4^+ ions.

$$Ga_{ads} + N_{ads} \rightarrow GaN \tag{3.10}$$

4. Conclusions

The electrodeposition of GaN films have been examined on different substrates below room temperature. CV results revealed that the reduction reaction of Ga^{3+} ions occurred with the HER and is not significantly affected by the electrode properties. NO_3^- ions could be changed to NO_2^-, and N_2 from the potential near the Ga reduction potential in the solutions where NH_4^+ ions are present, resulting in the formation of GaN films through a combination with Ga_{ads} during the deposition process.

Depending on the characteristics of the electrode, reactions of each ions started at different potential values, and the formation of GaN film was confirmed on the Ga and Al electrodes. In the film deposited on the Pt substrate having the lowest hydrogen overpotential, only Ga was precipitated without N, and a large amount of titanium oxide was detected along with some Ga on the surface of Ti substrate having the highest hydrogen overpotential. A large amount of hydrogen bubbles interferes with the reduction of N species ions on the Pt electrode. A low content of Ga was detected on the Ti substrate where the cathodic current appeared at a negative potential.

Reference

[1] T.D. Moustakas, R.J. Molnar, T. Lei, G. Menon, C.R. Eddy, Mater. Res. Soc. Symp. Proc. **242** (1992) 427

[2] T.D. Moustakas, T. Lei, R.J. Molnar, *Physica. B* **185** (1993) 36

[3] S. Nakamura, Jpn. *J. Appl. Phys.* **30** (1991) 1705

[4] S. Nakamura, M.R. Krames, *Proceedings of the IEEE* **101** (2013) 2211

[5] J.O. Akinlami, I.O. Olateju, *in Semiconductor physics quantum electronics & optoelectronics* (2012) p. 281

[6] S.P. Denbaars, *Proceedings of the IEEE* **85** (1997) 1740–1749

[7] D. Ehrentraut, E. Meissner, M. Bockowski, *in Technology of Gallium Nitride Crystal Growth, Springer Series in Materials Science* **133** (2010) pp. 31–272

[8] D. Elwell, M.M. Elwell, *Prog. Cryst. Growth & Charact.* **17** (1988) 53

[9] M. J. Paisley, Z. Sitar, J. B. Posthill, R.F. Davis, *J. Vac. Sci. Technol. A* **7** (1989) 701

[10] R.J. Molnar, W. Götz, L.T. Romano, N.M. Johnson, *J. Cryst. Growth* **178** (1997) 147

[11] D.R. Ketchum, J.W. Kolis, Crystal growth of gallium nitride in supercritical ammonia, *J. Cryst. Growth* **222** (2001) 431–434

[12] H. Angerer, O. Ambacher, R. Dimitrov, Th. Metzger, W. Rieger, M. Stutzmann, *MIJ-NSR* **1** (1996) e15

[13] Daniel Lincot, *Thin Solid Films* **487** (2005) 40

[14] T. T. Ngo, S. Chavhan, I. Kosta, O. Miguel, H. Grande, R. Tena-Zaera, *ACS Appl. Mater. Interfaces* (2014) 2836

[15] J Li, L Jiang, B Wang, F Liu, J Yang, D Tang, Y Lai, *Electrochimica Acta* **87** (2013) 153

[16] R.E. Marotti, P. Giorgi, G. Machado, E.A. Dalchiele, *Solar Energy Mater. Sol. Cells,* **90** (2006) 2356

[17] K. Ghezali, L. Mentar, B. Boudine, A. Azizi, J. *Electroanal. Chem.* **794** (2017) 212

[18] R.E. Marotti, D.N. Guerra, C. Bello, G. Machado, E.A. Dalchiele, *Solar Energy Mater. Sol.*

Cells **82** (2004) 85

[19] S. Zein, E.I. Abedin, F. Endres, *Chem. Phys. Chem.* **7** (2006) 58

[20] Y.C. Lee, T.J. Kuo, C.J. Hsu, Y.W. Su, C.C. Chen, *Langmuir* **18** (2002) 9942

[21] T. Gandhi, K.S. Raja, M. Misra, *Electrochimica Acta* **53** (2008) 7331

[22] R.K. Roy, A.K. Pal, *Mater. Lett.* **59** (2005) 2204

[23] K. Al-Heuseen, M.R. Hashim, N.K. Ali, *Mater. Lett.* **64** (2010) 1604

[24] K. Al-Heuseen, M.R. Hashim, *J. Cryst. Growth* **324** (2011) 274

[25] F.R. Wong, A.A. Ali, K. Yasui, A.M. Hashim, *Nanoscale Res. Lett.* **10** (2015) 233

[26] S. Sarkar, S. Sampath, *Chem. Commun.* **52** (2016) 6407

[27] Y.H. Ogata, K. Kobayashi, M. Motoyama, *Curr. Opin. Solid St. M.* **10** (2006) 163

[28] A. Kahyarian, M. Achour, S. Nesic, *in Woodhead Publishing Series in Energy* (2017) pp. 149–190

[29] F. Martin, X. Feaugas, A. Oudriss, D. Tanguy, L. Briottet, J. Kittel, *in 8-State of Hydrogen in Matter: Fundamental Ad/Absorption, Trapping and Transport Mechanisms Mechanics-Microstructure-Corrosion Coupling* (2019) pp. 171–197

[30] A.J. Bard, R. Parsons, J. Jordan, *in Standard Potentials in Aqueous Solutions, IUPAC (Marcel Dekker)*, New York, USA (1985)

[31] N.N. Greenwood, A. Earnshaw, *in Chemistry of the Elements, 2nd edition, Butterworth-Heinemann,* Oxford, UK, (1997)

[32] N. Ryan and E.J. Lumley, *J. Electrochem. Soc.* **106** (1959) 388

[33] W.M. Saltman, N.H. Nachtrieb, The Electrochemistry of Gallium, *J. Electrochem. Soc.* **100** (1953) 126

[34] B.G. Pound, *Corrosion* **47** (1991) 99

[35] D.R. Gabe, The role of hydrogen in metal electrodeposition processes, *J. Appl. Electrochem.* **27** (1997) 908

Chapter 4

Effect of Heat Treatment of Al Substrate on GaN Film Electrodeposited in Aqueous Solution

Chapter 4 – Effect of Heat Treatment of Al Substrate on GaN Film Electrodeposited in Aqueous Solution

4.1 Introduction

Gallium nitride (GaN) is one of the most promising III-V semiconductor material that uses nitrogen as a group V element [1–5]. In particular, GaN has been recognized to be the most important material for blue and ultraviolet optoelectronic devices and has recently attracted considerable attention after the successful fabrication of high-efficiency blue light-emitting diodes [6–9]. During the last two decades, numerous studies have been conducted on GaN semiconductors, and several reports have been published on the synthesis technology of these semiconductors fabrication [10–19]. Various dry plating methods, such as metal–organic chemical vapor deposition (MOCVD) [20, 21], molecular beam epitaxy (MBE) [22–24], thermal ammoniation [25], physical vapor deposition [26], and chemical vapor deposition [27–29], have been adopted and used. However, the high cost of these equipment is one of the major challenges to be overcome for commercialization and widespread application. Moreover, the use of high-temperature systems and ultra-pure gases for GaN fabrication entails considerable complexity and additional manufacturing cost [30].

A low-cost and simple electrochemical method has been studied by some researchers as an alternative for GaN synthesis. Several reports have also confirmed the possibility of GaN synthesis by electrodeposition [31–37]. Most attempts, nonetheless, have resulted in amorphous GaN containing a large amount of oxygen. And GaN films deposited by electrodeposition showed island-like morphology with many cracks and defects. Most low-temperature GaN syntheses have been conducted on Si substrates because of their high quality, large size, and low cost. But Si and deposited metal usually exhibit a weak interaction that leads to three-dimensional island-like growth or Volmer–Weber mechanism [38, 39]. This is because the rate of electrochemical reaction in Si is slower than in metals

[40]. These island-like structures have been also shown from the GaN film grown on Si by the dry processes because of numerous mismatches in the lattice constant and crystal structure between Si and GaN, and have been recognized as a key problem for high-quality GaN fabrication for decades.

To overcome these problems, the effect of various materials, such as aluminum nitride (AlN) [41, 42], aluminum gallium nitride (AlGaN) [43, 44] and aluminum oxide (γ–Al_2O_3) [45], which can be reduced lattice mismatch between GaN and Si has been studied and reported by many researchers [46, 47]. In particular, practically all high-quality gallium nitrides have been grown on Al-based intermediate layers. It can be considered that Al plays an important role in GaN growth.

Al is a metal with a high electrical conductivity compared to Si, and can be, therefore, considered as a substrate material more suitable for electrochemical processes in aqueous solutions. Among the reported studies on the low-temperature electrochemical synthesis of GaN, however, there has been no report regarding the effect of heat treatment of Al substrate on the formation of GaN. Therefore, in this study, Al is selected as a substrate for the synthesis of GaN by electrochemical method, and the deposition is attempted on Al substrates heat-treated at various temperatures.

4.2 Experimental Procedures

4.2.1. Materials and Reagents

For electrodeposition, a commercial Al plate (99.9% purity) and Pt coil (99.99% purity) are purchased and used as working and counter electrodes, respectively. Gallium nitrate hydrate ($Ga(NO_3)_3 \cdot xH_2O$, ≥99.9%, Sigma Aldrich) and ammonium nitrate (NH_4NO_3, ≥98%, Sigma Aldrich) are used as sources of Ga and N, respectively. Boric acid (H_3BO_3 ≥99.5%, Sigma Aldrich) is purchased and employed to prepare the electroplating electrolyte. Concentrated nitric acid (HNO_3, 70.0%, Nacalai Tesque) is used to adjust the pH level of each solution. Deionized water with a resistivity of 18.2 MΩ·cm is used in all the experiments.

4.2.2. Preparation of Electrodes

The working electrodes are 1.0 × 1.0 cm^2 Al plates with a 99.9% purity, and a Pt coil is used as counter electrode. An Ag|AgCl|sat'd–KCl (SSC= +0.22 V vs. SHE) electrode is employed as reference electrode, and all potentials are referred vs. SCC. The Al substrates are prepared by polishing using emery paper to a grade of 2000. They are ultrasonically cleaned with ethanol for 10 min, followed by deionized water for another 10 min. The Pt coil is immersed in hydrochloric acid (HCl, 35%, Nacalai Tesque) to clean the surface and is thereafter washed with distilled water. Finally, all electrodes are washed with distilled water and thereafter dried under atmospheric conditions. Prior to electrodeposition, the Al plate and Pt wire are connected and covered with a Nitoflon adhesive tape (Nitto Denko) to yield an Al electrode area of 0.5 × 0.5 cm^2.

4.2.3. Heat Treatment of Al Substrates

The influence of electrode conditions, such as the composition and crystallinity of various electrodes, on material synthesis has been widely investigated [48]. In this study, the Al substrates are prepared to examine the influence of crystal structure and Al orientation on the synthesis of GaN film by electrodeposition. The Al substrates, referred to as Al200HT and Al500HT, are heat-treated at 200 and 500 °C for 1 h, respectively, in an atmospheric electric furnace according to the commercial Al plate used. The preferred orientation and crystal structure of each Al substrate are characterized by X-ray diffraction (XRD).

4.2.4. Electrodeposition Process

All the electrochemical depositions are performed using a potentiostat (Hokuto Denko, HA3003A) in a three-electrode cell configuration at atmospheric pressure and temperature of 25 °C. The electrodeposition is conducted in solutions composed of 0.1 M $Ga(NO_3)_3$, 2.5 M NH_4NO_3, and 0.6 M H_3BO_3. To prevent the abrupt change in the pH level of the solution by hydrogen ion (H^+) depletion near the electrode surface during the electrodeposition process, H_3BO_3 is used as buffer. The electrodepositions are attempted using the galvanostatic method at a current density of 3.5 $mA \cdot cm^{-2}$ for

3 h. In our previous study, the best results were obtained at this current density. The working and counter electrodes are separated by a distance of approximately 1.0 cm, and the electrolyte is vigorously stirred during the electrodeposition process. After deposition, the specimens are immediately rinsed thoroughly with distilled water.

4.2.5. Characterization and Tests

The cyclic voltammetry experiments are performed to confirm the electrochemical behavior of each ion on the Al surface. The current response is recorded against the applied voltage (V vs. Ag/AgCl), which is scanned in a triangular waveform. The surface morphology is characterized with scanning electron microscopy (SEM, Hitachi, S-4800), and the chemical composition is analyzed by energy dispersive X-ray spectroscopy (EDX, HORIBA, EMAX ENERGY, EX-350). The SEM measurement is performed at 10 kV, and the EDX analysis is conducted at an acceleration voltage of 12 kV and current of 10 μA. The crystalline quality and the lattice parameter of the samples are characterized by X-ray diffraction (XRD, Rigaku, Ultima IV) with a Cu–Kα_1 radiation source ($\lambda = 1.541$ Å). To examine the chemical bonding states, X-ray photoelectron spectroscopy (XPS) measurements are performed with a PerkinElmer PH1 ESCA system. Monochromatic Mg–Kα ionizing radiation (1254 eV) is used with the X-ray source operating at 300 W (15 kV and 20 mA). Raman measurements are performed using Horiba Jobin Yvon HR system, and an argon ion laser (514.5 nm) is utilized as an excitation source. The Raman scattering experiment is implemented in the z (x, unpolarized) $\bar{z}$ scattering configuration. The resolution of this system is 1 cm^{-1}, and the integral time is 3000 ms.

4.3. Results and discussion

4.3.1 Electrochemical behavior of gallium and nitrogen ions

The CV experiments are performed for aqueous solutions containing several chemicals to examine the electrochemical behavior of ions. The pH level of all solutions is adjusted by HNO_3. Table 4.1 lists the conditions of solutions used in the CV experiment. The CVs are recorded at a scan rate of 20 mV

s^{-1} between −2.0 and 2.0 V vs. Ag/AgCl, start from rest potential to negative direction and repeated 5 cycles.

Table 4.1 Bath conditions for cyclic voltammetry measurement.

	Concentration of chemical additive (M)				
Bath No.	**$Ga(NO_3)_3$**	**NH_4NO_3**	**H_3BO_3**	**HNO_3**	**pH**
(a)	-	-	-	0.032	1.50
(b)	-	2.50	-	0.032	1.50
(c)	0.10	-	-	0.031	1.50
(d)	0.10	2.50	-	0.031	1.50
(e)	0.10	2.50	0.60	0.029	1.50

Figure 4.1 shows the CV results of 5th cycle. In order to easily compare each cathodic curve, the expanded graphs in the range of −2.0 to 0 V is displayed in the graph below. In the solution at pH 1.5 containing only HNO_3 shown in graph (a), a slight reduction current is observed starting from approximately −0.6 V, and then a small curve appears at ca. −1.0 V. From the HNO_3 solution, the first curve seems to correspond to hydrogen evolution reaction (HER), and second curve can be regarded as the reduction of nitrate (NO_3^-) ion. As confirmed from E–pH diagram of nitrogen (N) in Fig. 1(b) [51], NO_3^- ion can be reduced through the following cathodic reactions.

$$NO_3^- + 2H^+ + 2e^- \rightarrow NO_2^- + H_2O \quad (4.1)$$

$$NO_2^- + 8H^+ + 8e^- \rightarrow NH_4^+ + 2H_2O \quad (4.2)$$

Although the reduction potential of NO_3^- ion is very positive than HER, it can be seen that the NO_3^- ion does not reduce easily before HER. And if the reaction continues, N species ion may change to most stable ammonium (NH_4^+) ion.

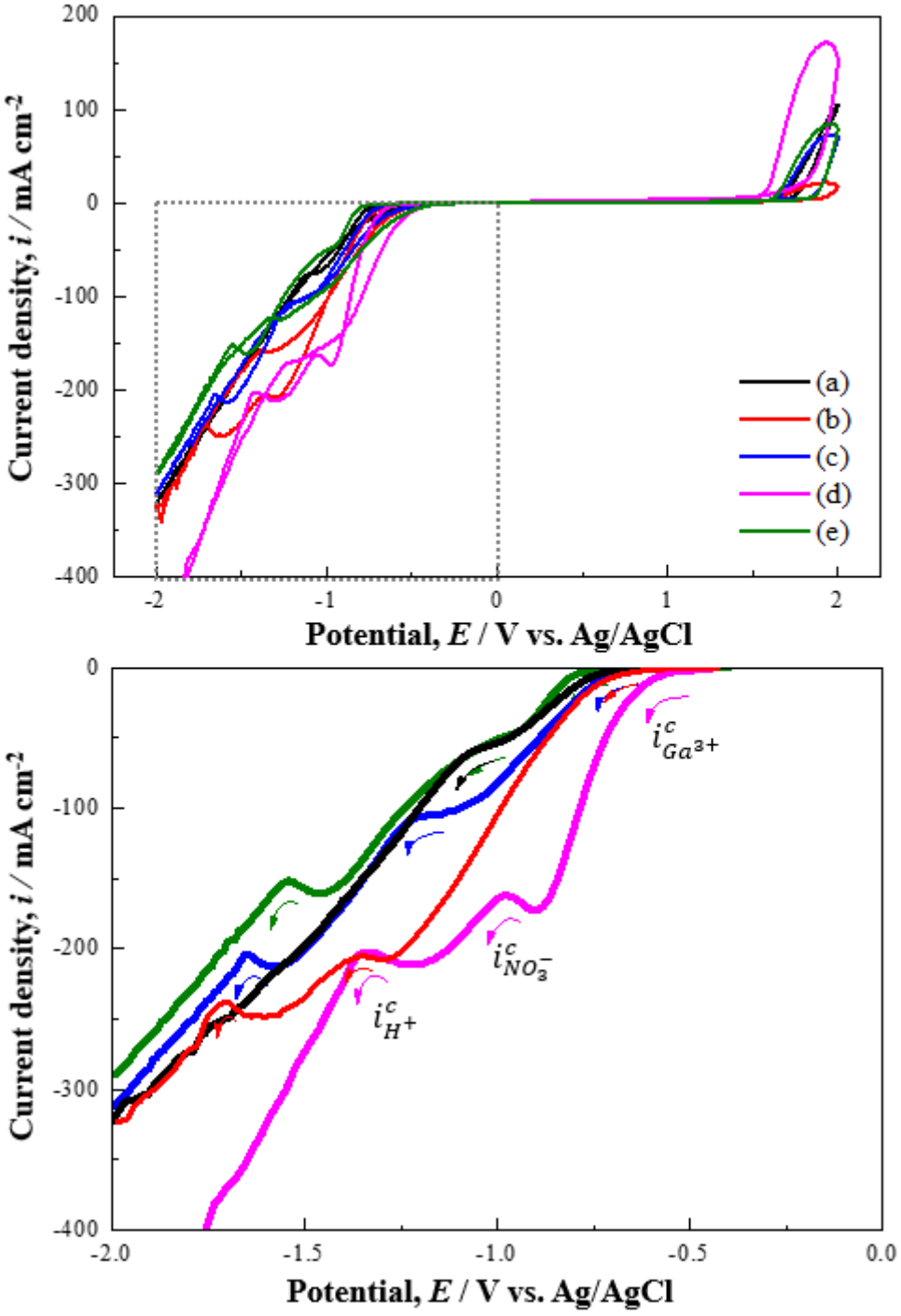

Fig. 4.1 Comparison of CVs from (a)–(e) aqueous solutions in Table 4.1. The graph below shows the cathodic current curves corresponding to a potential region of –2 to 0 V.

In the graph of Fig. 4.1(b) obtained from the solution containing NH_4NO_3, cathodic curves starts at −0.7 and shows two peaks at −1.3 and −1.7 V. Additional curve compared to the graph obtained in the only HNO_3 solution can be expected to the reaction to other nitrogen species such as oxoazanide (NO^-) and adsorbed nitrogen (N_{ads}) by the influence of ammonium (NH_4^+) ion. As known by N. Ryan et al., NO_3^- ion can form N_{ads} in aqueous solutions during the electrodeposition process [52]. Also, the large amount of NH_4^+ ion present in this solution may accelerate the formation of N_{ads} through a comproportionation reaction with NO_2^- ion, as follows:

$$NO_2^- + NH_4^+ \rightarrow N_{ads} + 2H_2O \tag{4.3}$$

In a solution containing 0.1 M $Ga(NO_3)_3$ (graph (c)), the current flow starts at −0.8 V, and a current hill appears at −1.1 V. This start point is close to the potential corresponds to reduction from Ga^{3+} to solid gallium (Ga) in Fig. 1(a), and a current hill can be considered as a result of the consumption of Ga^{3+} at the electrode surface. Therefore, the precipitation of Ga may occur on the Al electrode.

$$Ga^{3+} + 3e^- \rightarrow Ga_{ads} \tag{4.4}$$

It is generally known that hydrogen discharge is preferred for Ga deposition, thus the reduction reaction of Ga^{3+} can therefore occur after the HER on the cathode surface [53]. The curve appearing at −1.7 V thereafter corresponds to the reduction reaction of NO_3^- of Eq. (4.1) and Eq. (4.2). That is, even if Ga is adsorbed on the Al substrate, the reduction reaction of NO_3^- ion can occur, and it can be expected that the reaction of NO_3^- ion occurs at a more negative potential under the influence of the adsorbed gallium (Ga_{ads}).

In the graph (d) obtained from a solution containing Ga^{3+}, NO_3^- and NH_4^+ ions, three clearly separated cathodic peaks appear. After the large current peak corresponding to the precipitation of Ga, $i^c_{Ga^{3+}}$, a distinct reduction peak is found at the potential region corresponding to the reduction reaction of NO_3^-, $i^c_{NO_3^-}$, confirmed from graph (b). In addition, the increased and separated current peak with the addition of Ga^{3+} ion indicates the formation of new phase precipitates on the Al substrate. During the reactions of Eqs. (4.3) and (4.4) on the Al surface, N_{ads} can be combined with Ga_{ads} and finally forms

clusters to form GaN layer.

$$Ga_{ads} + N_{ads} \rightarrow GaN \tag{4.5}$$

Clusters of critical sizes are formed, subsequently leading to the growth of continuous films. These Ga-N bonds cause Ga and N to have electronic states of trivalent Ga cations (Ga^{3+}) and trivalent N anions (N^{3-}), respectively. resulting in secondary growth of GaN with Ga^{3+} and NH_4^+ ions in the solution.

$$Ga^{3+} + NH_4^+ + 4e^- \rightarrow GaN + 2H_2 \tag{4.6}$$

$$Ga^{3+} + N^{3-} \rightarrow GaN \tag{4.7}$$

The third current may be considered to correspond to the reduction of H^+ ion caused by the consumption of NH_4^+ ion, $i_{H^+}^c$.

When H_3BO_3 is added (graph (e)), the current density decreases, and the amount of hydrogen gas bubbles generated on the Al surface is reduced, and also the bubble size becomes smaller. Boric acid thus acts as a surface agent and may be expected to function as a buffer to retard the generation rate of hydrogen ion (H^+) as well as prevent hydrogen adsorption, which can interfere with the permeation of N source ion on the Al surface [53].

4.3.2 Crystallographic Properties of Al Substrates

Figure 4.2 shows the XRD spectra of Al samples treated at different temperatures. Four main diffraction peaks are observed at 2θ values of 38.5, 44.8, 65.1 and 78.3 degrees, corresponding to the reflections of Al (111), Al (200), Al (220), and Al (311) in the Al plate (Fig. 4.2(a)). In the XRD results of heat-treated Al samples (Figs. 4.2(b), (c)), the diffraction patterns indicate the existence of gibbsite ($Al(OH)_3$) and gamma (γ) phase of alumina (Al_2O_3) on the Al surface. The peaks caused by the reflection of γ-Al_2O_3 are strongly observed at 2θ = 29.6, 39.8 and 47.7 degrees, respectively, and the small peaks caused by the reflection of $Al(OH)_3$ are observed at 2θ = 26.8, 35.6, 48.6 and 50.3 degrees.

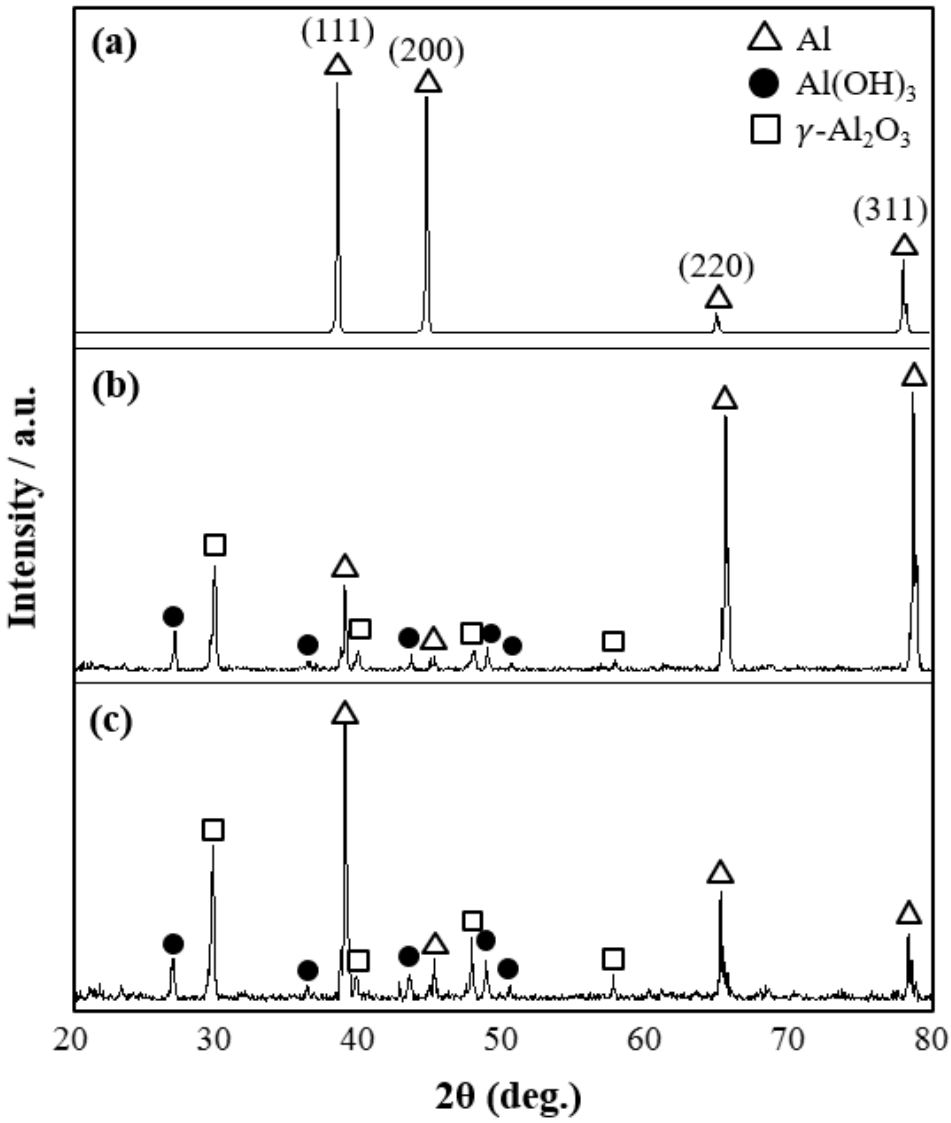

Fig. 4.2 XRD spectra of Al plates heat-treated at different temperature; (a) Free; (b) 200 °C for 1h; (c) 500 °C for 1h.

The orientation of the obtained Al samples is examined by analyzing the XRD results shown in Fig. 4.2. The normalized integrated intensities, $P_{h\,k\,l}$, corresponding to the (111), (200), (220), and (311) planes is calculated using the following expression [54]:

$$P_{hkl} = \frac{I_{hkl}/\sum I_{hkl}}{Ir_{hkl}/\sum Ir_{hkl}} \tag{4.7}$$

where $I_{h\,k\,l}$ is the peak intensity of ($h\,k\,l$) reflection from the Al samples; $\sum I_{h\,k\,l}$ is the sum of peak

intensities; $Ir_{h\,k\,l}$ is the peak intensity of (h k l) reflection for JCPDS card no. 01-089-2769; $\sum Ir_{h\,k\,l}$ is the sum of peak intensities. The calculated results of the preferred orientation of each Al substrate are plotted in Fig. 4.3. As shown in Fig. 4.4(a), the Al plate exhibits a preferred (111) orientation. In contrast, a (220) reflection is relatively weak. For Al200HT (Fig. 3.3(b)), the orientations of (220) and (311) are considerably preferred over (111) and (200). The orientation of (111), however, is preferred for the Al500HT (Fig. 3.3(c)). As a result, the preferred orientations of Al samples gradually change to (220) and (311) with increasing temperature and eventually returns to (111). The XRD pattern also confirms that no additional contamination exists on the Al samples

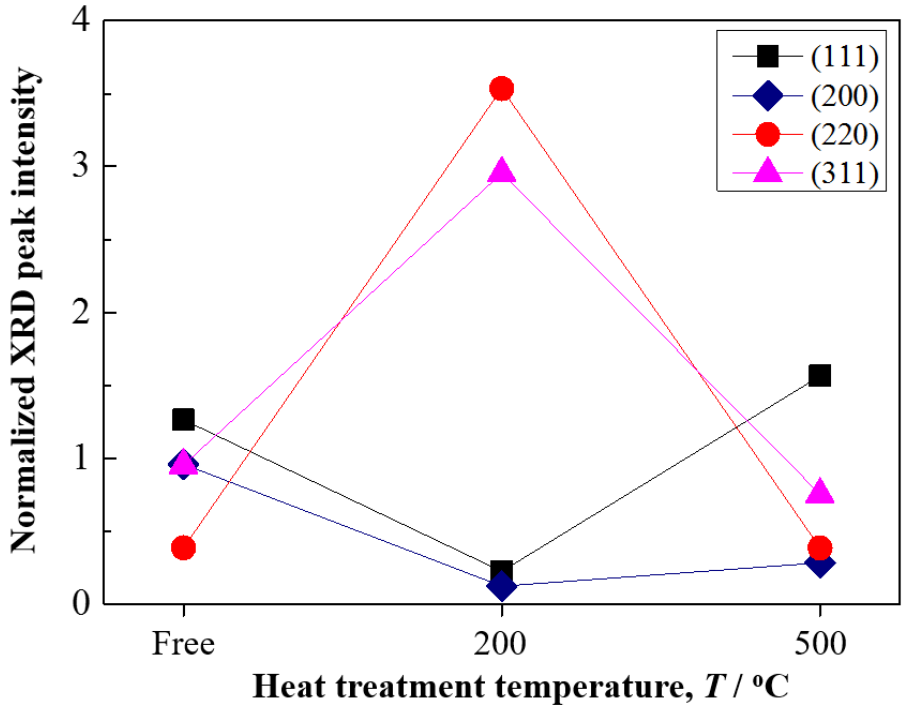

Fig. 4.3 Normalized peak intensity, $P_{h\,k\,l}$, from XRD reflections of Al plates heat-treated at different temperatures.

4.3.3 Electrodeposition and Characterization

The electrodeposition of GaN film in an aqueous solution is attempted on Al substrates, and their morphology and composition are characterized by SEM and EDX. Figure 4.4 shows the SEM images of GaN films deposited with a current density of 3.5 mA·cm^{-2} for 3 h. The corresponding EDX analysis

data are summarized in Table 4.2.

As shown in Fig. 4.4, the film formed on the Al plate exhibit an island-like morphology. And the island-like particles are connected and grow in the form of a thick plate for the film deposited on Al200HT (Fig. 4.4(b)). In the film deposited on Al500HT, a cauliflower-like structure, which was found in the Ga_2O_3 samples, is further formed on the island-like particles [55].

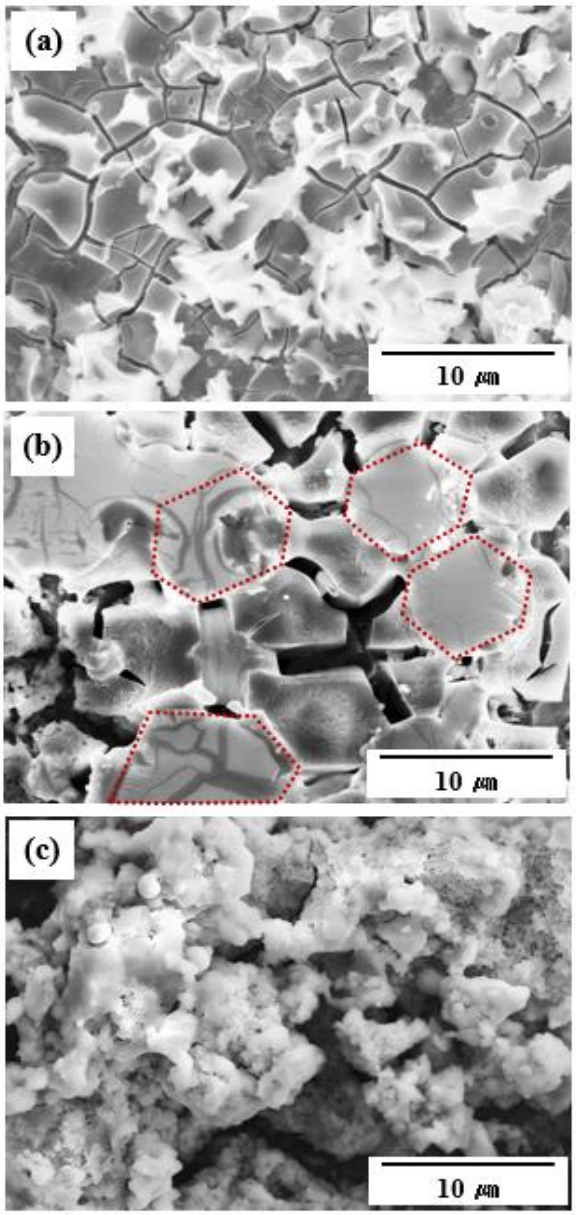

Fig. 4.4 SEM images of the film surfaces deposited at 3.5 mA cm^{-2} for 3 h on, (a) Al plate; (b) Al200HT; (c) Al 500 HT.

The EDX results summarized in Table 4.2 clearly reveal that more than 35 mol% of N and Ga are present with O in the GaN film grown on the Al substrate. This indicates that the GaN compound film is formed according to Eq. (4.6). The mapping micrographs of Fig. 4.5 clearly reveal the presence of Ga and N on the Al substrate. These elements are uniformly dispersed in the deposited films. Similarly, the N content is more than 28 mol% at any given position in the films that form on Al200HT and Al500HT. On the other hand, O increases by more than 20%, which can be attributed to Ga_2O_3. However, it can be seen that the amount of O is lower than the previous result (see Table 3.1). This can be considered to be due to the fact that the addition of H_3BO_3 suppressed the vigorous hydrogen evolution on the substrate surface and so a sudden pH change is not occurred. The mapping results in Fig. 4.5 also show that the films containing a large amount of N are formed on the Al substrates, and Ga, N and O coexist.

Table 4.2 EDX results of the films deposited on Al substrates at 3.5 mA cm^{-2} for 3 h.

Elements (mol%)	Al plate	Al200HT	Al500HT
Ga	35.02	33.99	14.28
N	37.85	33.27	28.40
O	12.58	26.70	20.88
Al	14.55	6.05	36.44

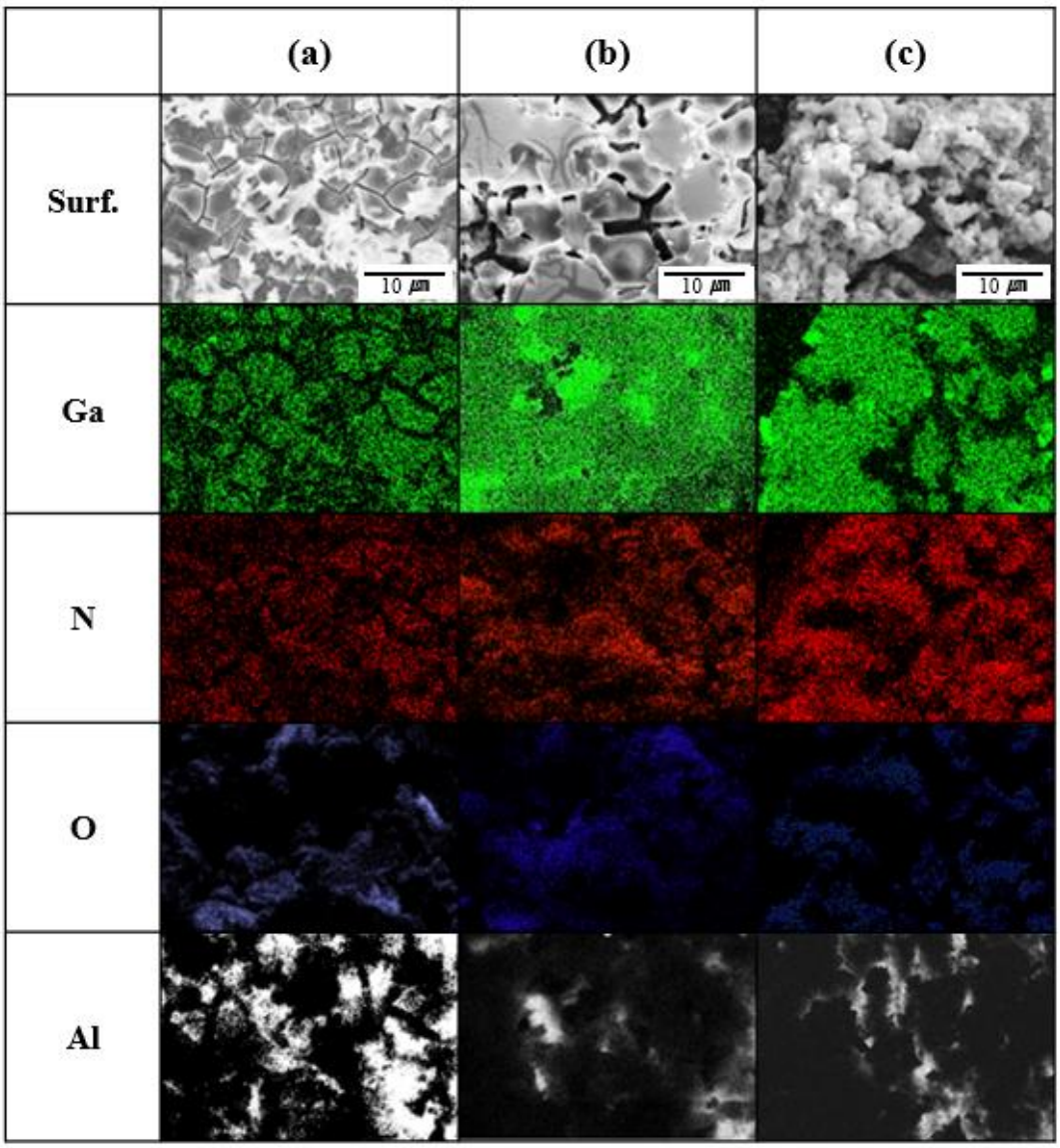

Fig. 4.5 Mapping micrographs via EDX for films deposited on (a) Al plate; (b) Al200HT; (c) Al 500 HT.

Figure 4.6 shows the XRD spectra of GaN films that are prepared by electrodeposition. Two peaks that correspond to the reflection of h-GaN are observed at $2\theta = 32.7$ and 36.8 degrees; these peaks are caused by reflections from the $(1\bar{1}00)$ and $(10\bar{1}1)$ planes for the film deposited on the Al plate, respectively [55, 56]. In contrast, a strong peak corresponding to the reflection of (0002) plane is detected at $2\theta = 34.4$ degree in the diffraction result for the film deposited on Al200HT (Fig. 4.6(b)). In the film formed on Al500HT (Fig. 4.6(c)), the peaks caused by the reflection of h-GaN at the three

aforementioned positions are detected, and the peak corresponding to the reflection of the h-GaN $(1\bar{1}00)$ plane appears to be the strongest. The strong peaks at $2\theta = 38.1$ and $2\theta = 45.4$ degrees are caused by reflections from Al (111) and (200), respectively, and a peak at $2\theta = 29.3$ degree is caused by the reflection of γ–Al_2O_3. The weak intensity peaks corresponding to Ga and β-Ga_2O_3 are also confirmed. Based on the XRD measurement of all samples, it can be observed that the h-GaN film is formed under the experimental conditions used in this study.

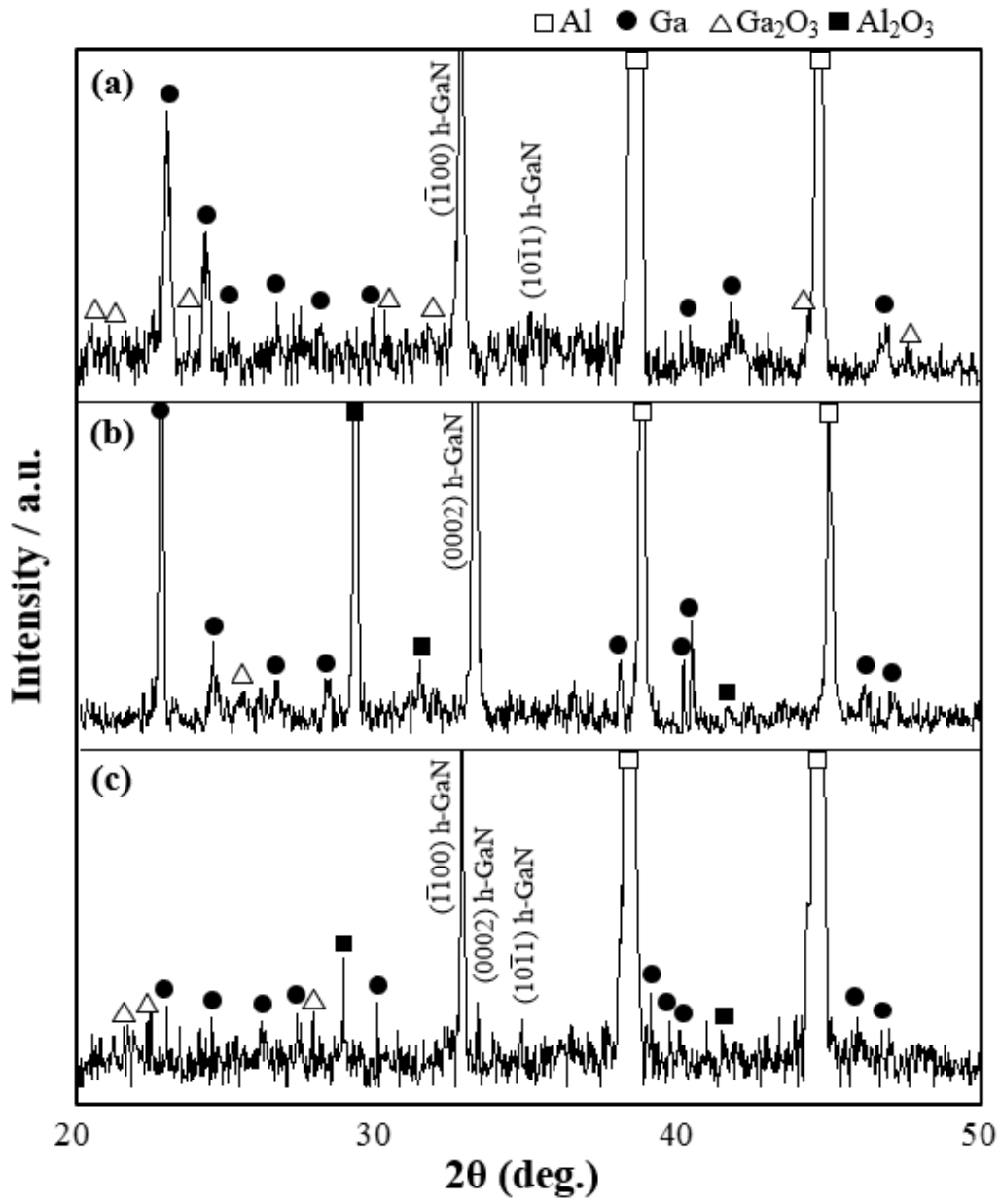

Fig. 4.6 XRD spectra of the films deposited on (a) Al plate; (b) Al200HT; (c) Al500HT.

The surface of the as-deposited material is characterized by XPS studies. Figure 4.7 shows the evolution of XPS spectra of Ga 3*d* and N 1*s* on the surface of the films. All spectra are deconvoluted using a Gaussian–Lorentzian function with background subtraction. Three main peaks are detected in the spectra of Ga 3*d* at 18.1, 22.4, and 26.4 eV corresponding to Ga, GaN, and Ga_2O_3, respectively, as shown in Fig. 4.7(a) –(c) [56]. These peaks are higher than those observed in GaN (Ga 3*d* at 19.6 eV), but three separated peaks corresponding to each chemical bonding are clearly observed [57, 58]. The binding energy of N 1*s* at 399.7 eV clearly shows the presence of nitride (N^{3-}) (Fig. 4.7(e)–8(f)), and peaks corresponding to N–O bonds appear at a binding energy of 408.6 eV [59]. In the deposited film on the Al plate without Al_2O_3 layer (Fig. 4.7(d)), only peaks corresponding to N–Ga–O bonds appear, and there are no peaks corresponding to Ga–N bonds. Despite the inclusion of H_3BO_3 in the electrodeposition solution, there is no detected peak caused by boron in all samples.

Figure 4.8 shows the Raman spectrum of films deposited on Al substrates. Three Raman active optical phonon modes corresponding to h-GaN have been observed from GaN film deposited on the Al plate. One mode is at 144 cm^{-1} because of E_2 (LO), and two bands are at 518 and 718 cm^{-1} of modes A_1 (TO) and E_1 (LO), respectively [60]. In the film formed on Al200HT, the band that corresponds to A_1 (TO) is intensified, and the signal at 570 cm^{-1} that corresponds to E_1 (TO) is also detected. In contrast, weak bands are detected from the film deposited on Al500HT because of the influence of a thick oxide layer. As can be observed from Figs. 4.8(b), (c), strong bands corresponding to Al_2O_3 are also detected in the films deposited on heat-treated Al substrates. The small bands that appear at 359 and 427 cm^{-1} may be caused by the acoustic phonons of Al_2O_3.

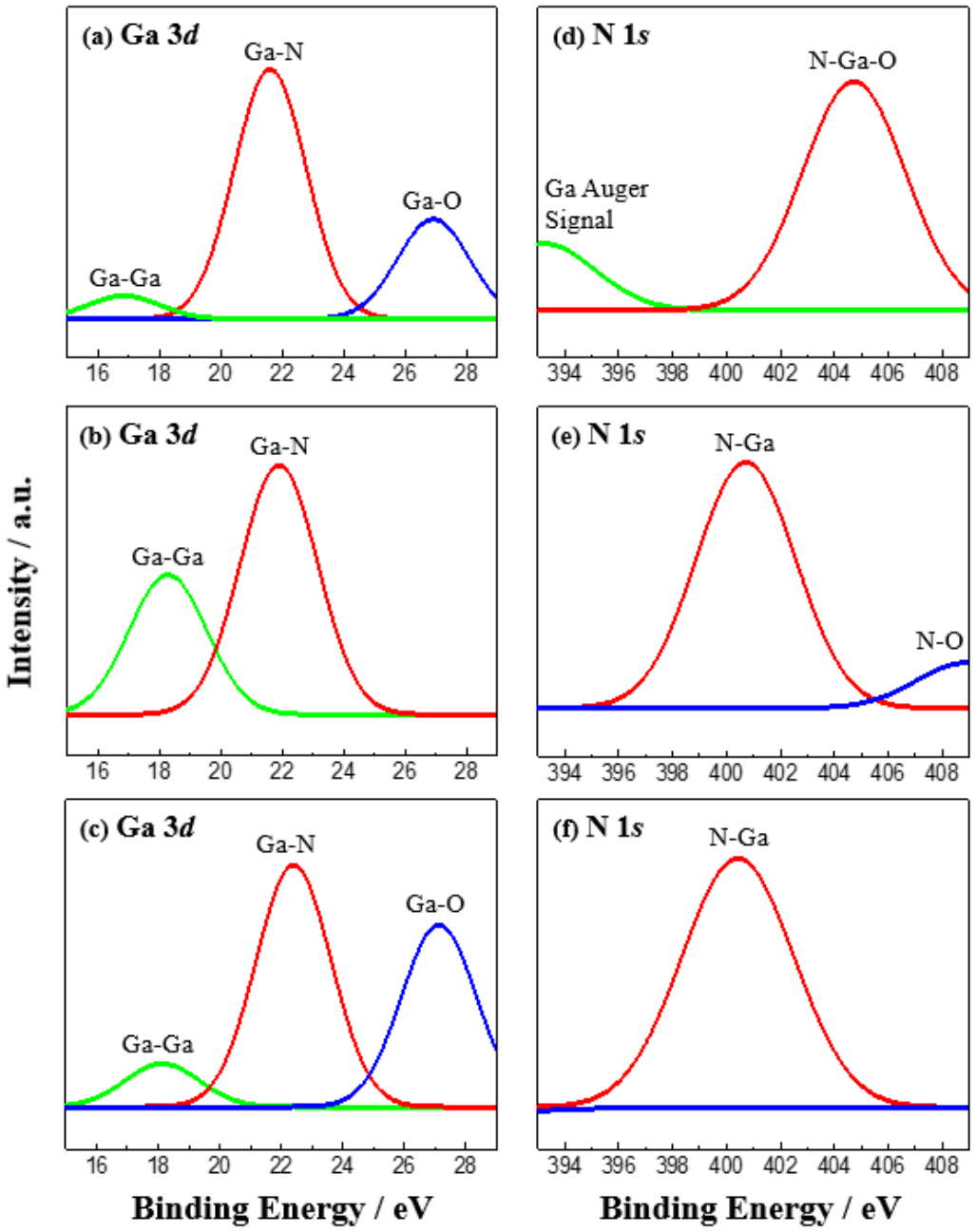

Fig. 4.7 XPS spectra of Ga 3*d* photoelectron peak of GaN films deposited on (a) Al plate; (b) Al200HT; (c) Al 500 HT, and spectra of N 1*s* photoelectron peak for the same samples; (d)–(f).

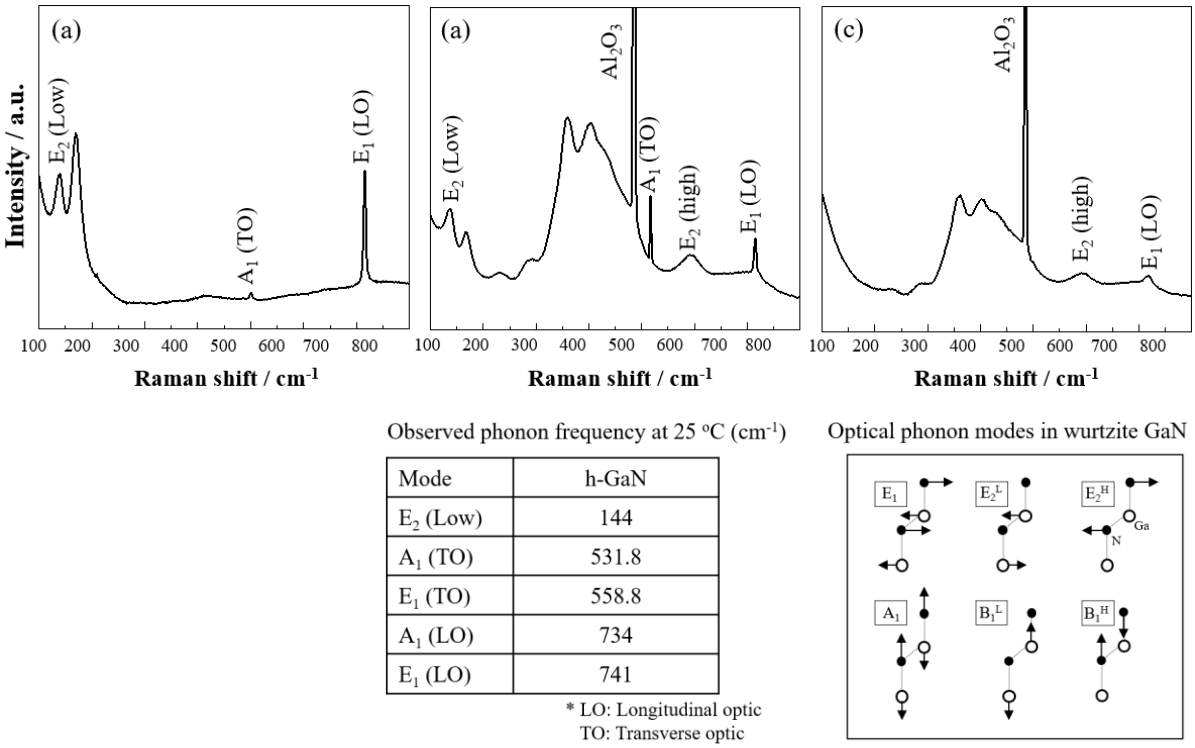

Observed phonon frequency at 25 °C (cm^{-1})

Mode	h-GaN
E_2 (Low)	144
A_1 (TO)	531.8
E_1 (TO)	558.8
A_1 (LO)	734
E_1 (LO)	741

* LO: Longitudinal optic
TO: Transverse optic

Optical phonon modes in wurtzite GaN

Fig. 4.8 Raman spectroscopy of GaN films deposited on (a) Al plate; (b) Al200HT; (c) Al500HT.

4.3.4 Effect of Crystal Orientation of Al on GaN Formation

The effects of the Al substrate on GaN film formation by electrodeposition are considered. It is confirmed that the Al plate and Al500HT are mainly oriented with the (111) plane, and the preferred orientations of Al200HT are Al (220) and (311) planes. In addition, peaks that correspond to Al_2O_3 are also detected on the heat-treated Al samples.

The SEM photographs of GaN films on the aforementioned Al substrates show that the film formed on Al200HT substrate has the densest structure. It is well known that the substrate surface conditions exhibit different sensitivities to various chemical treatments [61–64]. It can be considered that lower surface energy by oxidation make it easy to generate the Ga–N combining reaction.

The effect of each crystallographic parameters should also be considered. The XRD results of the GaN film shown in Fig. 4.6 confirm that the $(1\bar{1}00)$ plane of h-GaN grown on Al prefer the (111) plane as the main orientation, and the (0002) plane prefers the (220) plane. Figure 4.9 shows the crystal

structures and preferred orientation planes of Al and h-GaN [39, 65–66]. The lattice mismatch between the deposition film and substrate is an important factor for film growth [67, 68]. It is well-known that the lattice constant of cubic Al (a_{Al}) is $a = b = c = 4.05$ Å. By measuring the spacing of diffraction spots, the lattice constants of GaN (a_{GaN}) are found to be 3.19 Å (*a* and *b*-axes lattice constant) and 5.19 Å (*c*-axis lattice constant). In the atomic distribution of GaN viewed from the *c*-plane, the lattice space between Ga atoms is 5.52 Å. The lattice parameters of each axis are shown in Fig. 3.10 along with the atomic distribution viewed from each orientation. The lattice mismatch, *f*, at the interface can be characterized by the following simple equation defined by Trampert *et al.* [69].

$$f = 100 \times (a_{Al} - a_{GaN}) / a_{GaN} \tag{3.8}$$

It can be assumed that the c-axis of GaN begins to grow parallel to the orientation plane of Al because the adsorption of Ga and N occurs simultaneously. If *m*-planes of GaN grow on Al (100), then the lattice mismatch between the *c*-axis lattice constants of GaN and Al can be calculated as 22.0%. When *m*-planes of GaN lie along the Al (111), however, the mismatch becomes 10.4%. On another orientation, if polar *c*-plane of GaN grow on Al (110), the lattice mismatch of GaN (0001)/Al (110) can be calculated to be 3.6%. These values are significantly lower than those of GaN on Si (17%) [70]. During the electrodeposition process, therefore, it can be regarded that nucleation of GaN starts along the Al orientation plane in the direction of making mismatch small, and then film growth proceeds in the vertical direction. A schematic of this growth theory of GaN is shown in Fig. 3.11.

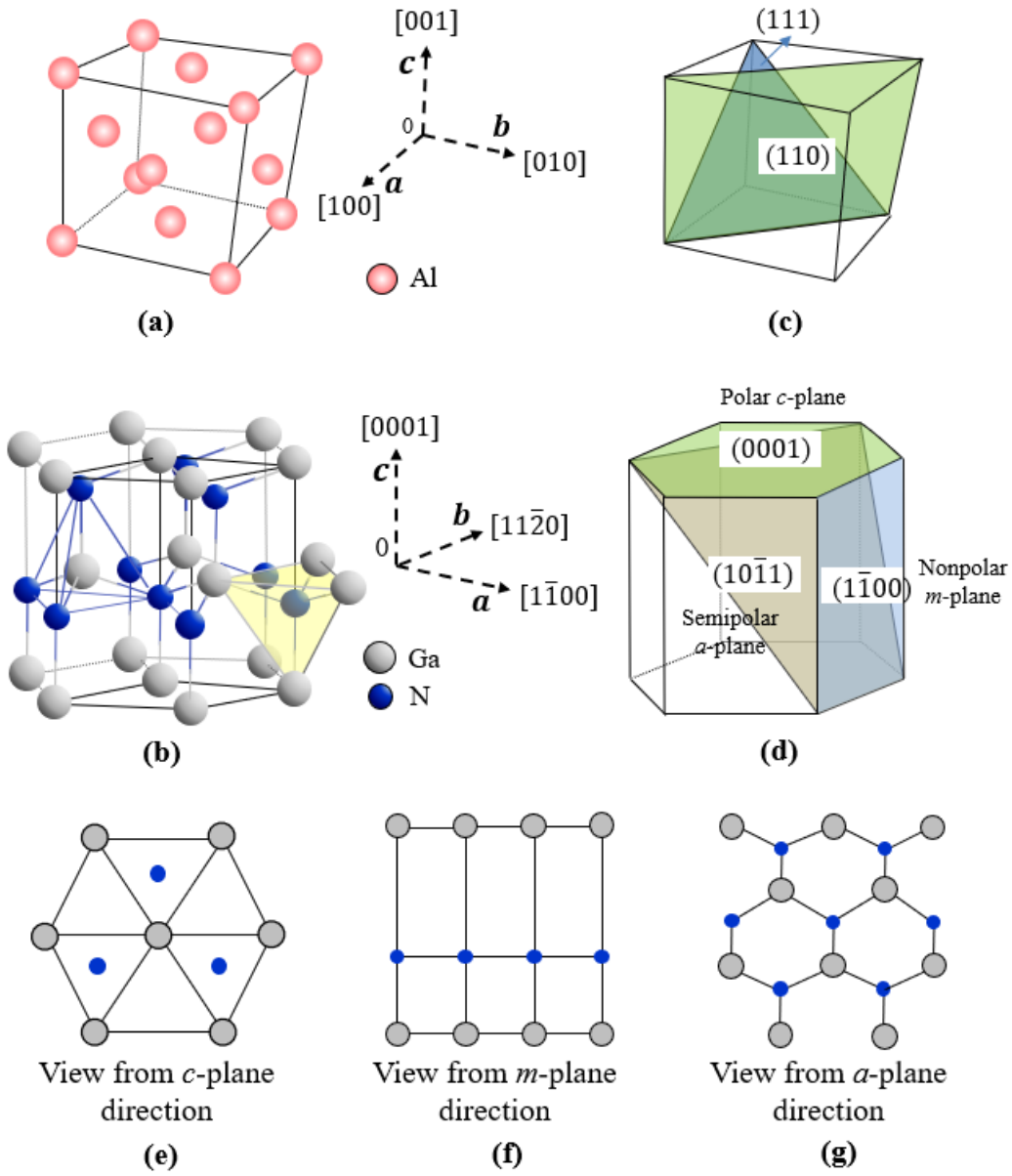

Fig. 4.9 Crystal structures of (a) cubic Al and (b) Wurtzite GaN, and crystallographic main planes of (c) Al substrates and (d) GaN films characterized by XRD. Schematic illustration of the atomic distribution of GaN planes view from each direction are presented in (e) – (g).

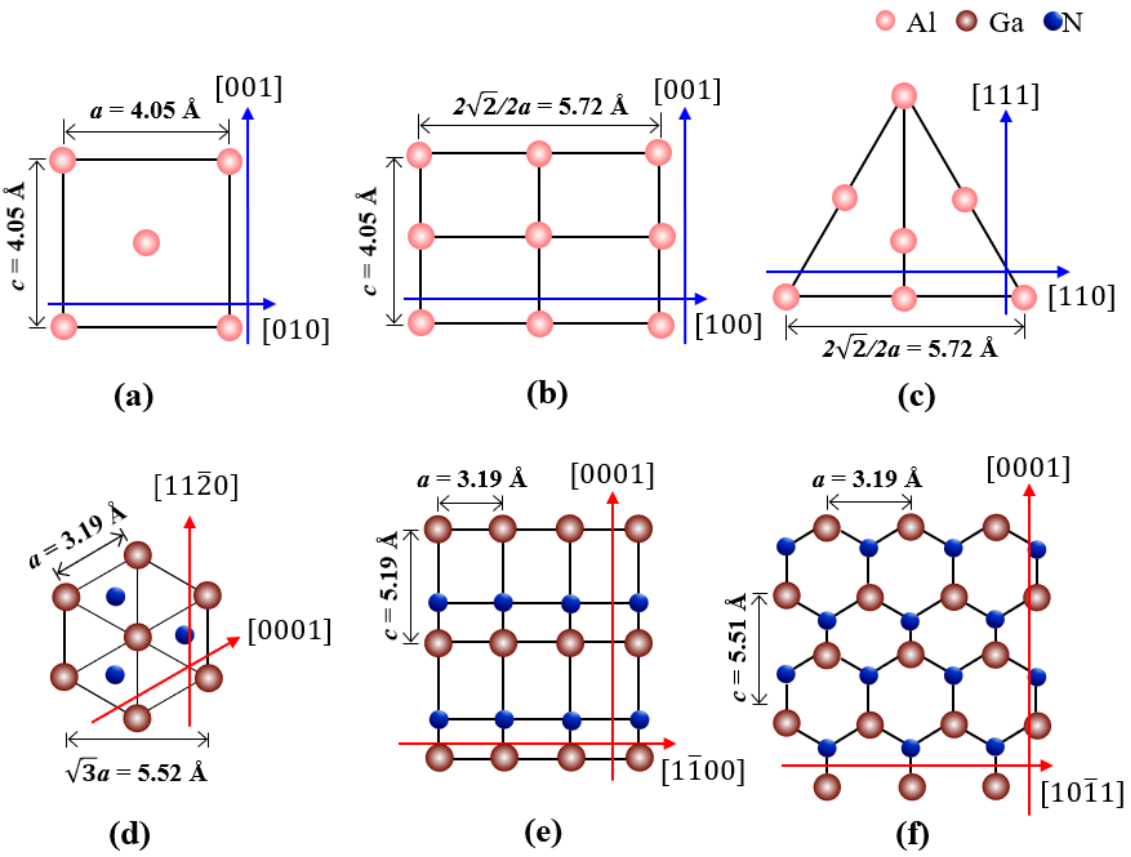

Fig. 4.10 Schematic illustration of the atomic distribution of Al and GaN in each crystal plane. Top views of Al viewed from (a) <100>; (b) <110>; (c) <111>; directions and hexagonal GaN view from (d) <0001>; (e) <1$\bar{1}$00>; (f) <10$\bar{1}$0>; directions are represent, respectively.

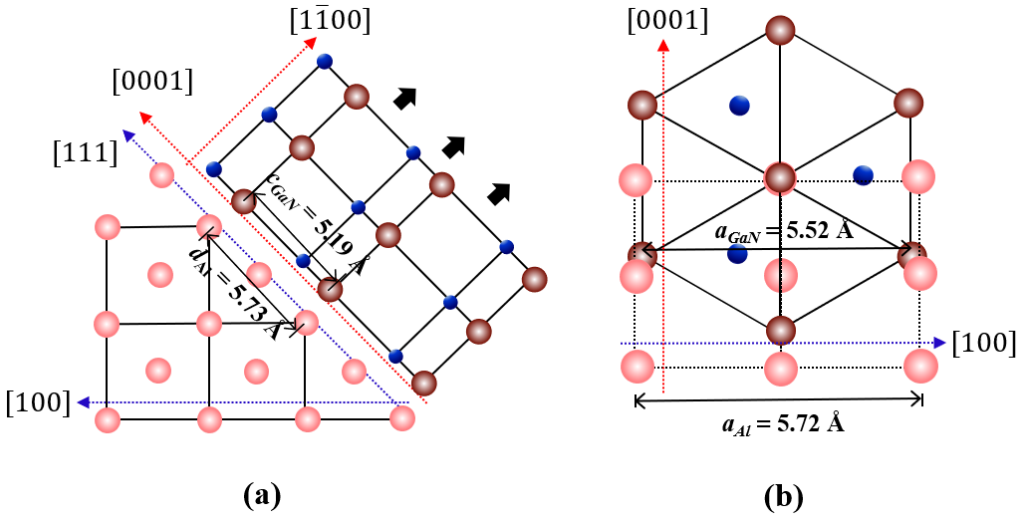

Fig. 4.11 Schematic presentations of atom arrangements in growth plane for the case of $(1\bar{1}00)_{GaN}/(100)_{Al}$ and $(0002)_{GaN}/(110)_{Al}$.

4.4 Conclusions

The GaN films are synthesized on Al substrates with different preferred orientations by electrodeposition under ambient temperatures. In the CV analysis, the cathodic current started from the potential value close to the Ga reduction potential and the current peak corresponding to the reduction reaction of the NO_3^- ion was identified. The adsorbed Ga and N generated here can be combined, which resulting the formation of GaN film.

The GaN films are prepared by applying a current density of 3.5 mA cm^{-2} for 3 h on Al substrates heat-treated at different temperatures. The deposited GaN films contain a mixture of h-GaN and Ga_2O_3 phases. The film formed on the Al substrate heat-treated is found to change from the island-like structure to the thick plate-like structure. Through EDX analysis, it is confirmed that Ga, N, and O are uniformly distributed in the film. Oxygen is reduced by the addition of H_3BO_3 and a high content of N is detected. Raman analysis, XRD, and XPS are also revealed the presence of h-GaN. In addition, the grown GaN films exhibit different growth characteristics depending on the composition and crystal orientation of Al substrates.

The GaN films produced in this work contain a considerable amount of O and exhibit insufficient crystallinity compared to single-crystal GaN. After the formation of GaN, additional processing, such as annealing at a high temperature in the presence of ammonia, may be required because the addition of O to the GaN film may cause lattice deformation or diminish material properties. Nevertheless, the possibility of synthesizing GaN on Al substrate using a low-cost temperature method that can replace the current expensive process has been confirmed. The fact that GaN films can be formed on metals other than semiconductors will have many advantages for various potential applications.

Reference

[1] S. Nakamura, T. Mukai, M. Senoh, *Appl. Phys. Lett.* **64** (1994) 1687

[2] S. Nakamura, T. Mukai, M. Senoh, *J. Appl. Phys.* **76** (1994) 8189

[3] M.A. Khan, Q. Chen, R.A. Skogman, J.N. Kuznia, *Appl. Phys. Lett.* **66** (1995) 2046

[4] R.J. Molnar, R. Singh, T.D. Moustakas, *Appl. Phys. Lett.* **66** (1995) 268

[5] J. I. Pankove, *J. Lumin.* **7** (1973) 114

[6] S. Strite, H. Morkoç. *J. Vacuum Sci. Technol. B* **10** (1992) 1237

[7] S. Nakamura, *Solid State Commun.* **102** (1997) pp. 237

[8] S. Nakamura, M. Senoh, T. Mukai, *Appl. Phys. Lett.* **62** (1993) 2390

[9] S. C. Jain, M. Willander, J. Narayan, R. Van Overstraeten, *J. Appl. Phys.* **87** (2000) 965

[10] I. Akasaki, *IEEJ Trans. FM.* **124** (2004) 107–113

[11] I Akasaki, H Amano, M Kito, K Hiramatsu, *J. Lumin.* **48&49** (1991) 666

[12] H. Amano, M Kito, K Hiramatsu, I Akasaki, *Jpn. J. Appl. Phys.* **28** (1989) 2112

[13] S. Nakamura, T. Mukai, M. Senoh, *J. Appl. Phys.* **30** (1998) 1998

[14] S. Nakamura, M. Senoh, N. Iwasa, S. Nagahama, T. Yamada, T. Mukai, *Jpn. J. Appl. Phys. Lett.* **34** (1995) 1332

[15] S. Nakamura, M. Senoh, S. Nagahama, N. Iwasa, T. Yamada, T. Matsushita, H. Kiyoku, Y. Sugimoto, *Jpn. J. Appl. Phys.* **35** (1996) 217

[16] S. Nakamura, M. Senoh, S. Nagahama, N. Iwasa, T. Yamada, T. Matsushita, H. Kiyoku, Y. Sugimoto, *Jpn. J. Appl. Phys.* **68** (1996) 2105

[17] D.N. Talwar, D. Sofranko, C. Mooney, S. Tallo, *Mater. Sci. Eng. B.* **90** (2002) 269

[18] M. Funato, M. Ueda, Y. Kawakami, Y. Narukawa1, T. Kosugi, M. Takahashi, T. Mukai, *Jpn. J. Appl. Phys.* **45** (2006) 659

[19] Nakamura, N Isawa, M Senoh, T Mukai, *Jpn. J. Appl. Phys.* **31** (1992) 1258

[20] W.G. Jung, S.H. Jung, P. Kung, M. Razeghi, *Nanotechnology,* **17** (2006) 54

[21] C. Saidi, N. Chaaben, A. Bchetnia, A. Fouzri, N. Sakly, B. El Jani, *Superlatt. Microstruct.* **60** (2013) 120

[22] Y.S. Park, T.W. Kang, R. Taylor, *Nanotechnology,* **19** (2008) 1

[23] W Kim, O Aktas, A.E Botchkarev, A Salvador, S.N Mohammad, H. Morkoc, *J. Appl. Phys.* **79** (1996) 7657

[24] K. Bao, L. Wang, H. Sun, R. Guo, Y. Wu, *J. Alloys Compd.* **552** (2013) 26

[25] S. Xue, X. Zhang, R. Huang, D. Tian, H. Zhuang, C. Xue, *Mater. Lett.* **62** (2008) 2743

[26] K. Saron, M. Hashim, *Superlatt. Microstruct.* **56** (2013) 55

[27] Y. Tang, Z. Chen, H. Song, C. Lee, H. Cong, H. Cheng, W. Zhang, I. Bello, S. Lee, *Nano Lett.* **8** (2008) 4191

[28] Q.N. Abdullah, F.K. Yam, Z. Hassan, M. Bououdina, *Superlatt. Microstruct.* **54** (2012) 215

[29] Q.N. Abdullah, F.K. Yam, J.J. Hassan, C.W. Chin, Z. Hassan, M. Bououdina, Int. J. Hydrogen Ener. **38** (2013) 14085

[30] F. Iskandar, T. Ogi, K. Okuyama, *Lett.* **60** (2006) 73

[31] J.K. Sprenger, A.S. Cavanagh, H. Sun, K.J. Wahl, A. Roshko, S.M. George, *Chem. Mater.* **28** (2016) 5282

[32] R.K. Roy and A.K. Pal, *Mater. Lett.* **59** (2005) 2204

[33] K. Al-Heuseen, M.R. Hashim, N.K. Ali, *Mater. Lett.* **64** (2010) 1604

[34] M.A. Qaeed, K. Ibrahim, K.M.A. Saron, A. Salhin, *Superlatt. Microstruct.* **64** (2013) 70

[35] K. Al-Heuseen and M.R. Hashim, *J. Cryst. Growth.* **324** (2011) 274

[36] K. Al-Heuseen, Int. J. Thin. Fil. *Sci. Tec.* **5** (2016) 113

[37] S. Sarkar and S. Sampath, *Chem. Commun.* **52** (2016) 6407

[38] Q. Huang, H. Deligianni, L.T. Romankiw, *J. Electrochem. Soc.* **153** (2006) 332

[39] E. Budevski, G. Staikov, W.J. Lorenz, *in Electrochemical phase formation and growth, Weinheim: VCH* (1997) 294

[40] Y.H. Ogata, K. Kobayashi, M. Motoyama, *Curr. Opin. Solid St. Mater. Sci.* **10** (2006) 163

[41] H. Amano, N. Sawaki, I. Akasaki, Y. Toyoda, *Appl. Phys. Lett.* **48** (1986) 353

[42] P. Chena, R. Zhang, Z.M. Zhao, D.J. Xia, B. Shen, Z.Z. Chen, Y.G. Zhou, S.Y. Xie, W.F. Lu, Y.D. Zheng, *J. Cryst. Growth* **225** (2001) 150

[43] C.C. Huang, S.J. Chang, R.W. Chuang, J.C. Lin, Y.C. Cheng, W.J. Lin, *Appl. Surf. Sci.* **256** (2010) 6367

[44] M.H. Kim, Y.G. Do, H.C. Kang, D.Y. Noh, S.J. Park, *Appl. Phys. Lett.* **79** (2001) 2713

[45] L. Wang, X. Liu, Y. Zan, J. Wang, D. Wang, D. Lu, Z. Wang, *Appl. Phys. Lett.* **72** (1998) 109

[46] K. Cheng, M. Leys, S. Degroote, M. Germain, G. Borghs, *Appl. Phys. Lett.* **92** (2008) 192111

[47] C.L. Wu, J.C. Wang, M.H. Chan, T.T. Chen, S. Gwo, *Appl. Phys. Lett.* **83** (2003) 4530

[48] M. Akiyama, K. Nagao, N. Ueno, H. Tateyama, T. Yamada, *Vacuum* **74** (2004) 699

[49] D.R. Gabe, *J. Appl. Electrochem.* **27(8)** (1997) 908

[50] N. Takeno, *in Atlas of Eh-pH Diagrams. Intercomparison of Thermodynamic Databases. National Institute of Advanced Industrial Science and Technology* (2005) 153

[51] M.J.N. Pourbaix, *in Thermodynamics of Dilute Aqueous Solutions, Edward Arnold and Co.* (1949)

[52] N. Ryan and E.J. Lumley, *J. Electrochem. Soc.* **106** (1959) 388

[53] T. Tsuda, T. Nohira, Y. Ito, *Electrochim. Acta* **47** (2002) 2817

[54] E Huang, *RSC Adv.* **7** (2017) 47898

[55] J.H. Boo, S.A. Ustin, W. H, *J. Cryst. Growth* **189–190** (1998) 183

[56] C.C. Yang, I. Lo, Y.C. Hsu, H.Y. Yang, *in Epitaxy* (2017) Chap. 7

[57] Z.L. Fang, J.Y. Kang, W.Z. Shen, *J. Phys. Chem. C* **112** (2008) 17652

[58] C.C. Hu, H. Teng, *J. Phys. Chem. C* **114** (2010) 20100

[59] Y.P. Song, H.Z. Zhang, C. Lin, Y.W. Zhu, G.H. Li, F.H. Yang, D.P. Yu, *Phys. Rev. B: Condens. Matter Mater. Phys.* **69** (2004) 075304

[60] H. Harima, *J. Soc. Mat. Sci. Japan* **51(9)** (2002) 983

[61] S. Kalpakjian, *in Manufacturing process for engineering materials, Pearson Edu. India* (1984) 5th

edition

[62] I. Akasaki, H. Amano, M. Kito, K. Hiramatsu, *J. Cryst. Growth* **98** (1989) 209

[63] V. Srikant V. Sergo, D.R. Clarke, *J. Am. Ceram. Soc.* **78(7)** (1995) 1931

[64] S.K. Hong, B.J. Kim, H.S. Park, Y. Park, S.Y. Yoon, T.I. Kim, *J. Cryst. Growth* **191** (1998) 275

[65] M. Frentrup, S. Ploch, M. Pristovsek, M. Kneissl, *Phys. Status Solidi B* **248(3)** (2011) 583

[66] M. Yoshizawa, A. Kikuchi, M. Mori, N. Fujita, K. Kishino, *Jpn. J. Appl. Phys.* **36** (1997) 459

[67] I. Ruach-Nir, H.D. Wagner, I. Rubinstein, G. Hodes, *Adv. Funct. Mater.* **13(2)** (2003) 159

[68] R.R. Reeber, K. Wang, *J. Mater. Res.* 15 (2000) 40

[69] A. Trampert, F. Schippan, L. Däweritz, K. H. Ploog, *Appl. Phys. Lett.* **78** (2001) 2461

[70] A. Watanabe, T. Takeuch, K. Hirosawa, H. Amano, K. Hiramatsu, I. Akasaki, *J. Cryst. Growth* **128** (1993) 391

Chapter 5

Summary and Future work

Chapter 5 – Summary and Future Work

5.1 Summary

As increasing demand for GaN and its alloy materials for wide application market, the manufacturing techniques is also receiving a great deal of interest. However, cost reduction of manufacturing technology is essential for the commercialization of expensive GaN devices. In this study, electrochemical deposition has been applied for the synthesis of GaN film, and all deposition process is conducted from aqueous solution at normal temperature and pressure. All experimental results has been discussed in detail Chapter 2–4. Concluding remarks for each Chapter are as follows:

Chapter 2 describes the low-temperature synthesis of GaN films from aqueous solution by electrodeposition. The GaN films were synthesized on n-Si (111) substrates by electrodeposition below room temperature. The electrochemical behavior of ions was confirmed by cyclic voltammetry. Results revealed that reduction reaction of gallium occurs on the Si substrate, and nitrate ion could be transformed to adsorbing nitrogen in the solution including ammonium ion. The combination reaction between adsorbed gallium and adsorbed nitrogen formed GaN film. The films deposited by galvanostatic method showed a plate-like morphology. But these film surfaces had island-shaped structures with many wide cracks. The films contained a mixture of wurtzite GaN, cubic GaN and Ga_2O_3 phases. EDX results revealed that gallium, nitrogen, and oxygen were distributed in plate-like structure. The PL analysis showed that films deposited by electrodeposition exhibit blue luminescence and also confirmed the peaks corresponding to the band gap energy of GaN.

Chapter 3 focuses on the influence of substrate conditions on the formation of GaN film from aqueous solution. According to the characteristics of each electrode, the reduction reaction of gallium and nitrogen species ions showed different behaviors in the solutions. When three separated cathodic current

peaks appeared in CV, it was confirmed that nitrogen was present in the deposited film. Most of the metallic gallium was precipitated on the Pt electrode with low hydrogen overpotential, and an oxide layer was formed on the Ti electrode with high hydrogen overpotential. If the reduction reaction of nitrogen occurred along with the precipitation of gallium according to the electrode characteristics, nitrogen adsorbed onto the gallium being adsorbed was generated, and as a result, GaN compound film can be formed.

Chapter 4 presents the synthesis of GaN film on heat-treated aluminum substrate by room temperature electrodeposition. The GaN films are synthesized on aluminum substrates with different preferred orientations by electrodeposition. The GaN films are prepared by applying a current density of 3.5 mA cm^{-2} for 3 h on aluminum substrates heat-treated at different temperatures of 200 and 500 °C. The deposited GaN films contain a mixture of hexagonal GaN and Ga_2O_3 phases. Through EDX analysis, it is confirmed that gallium, nitrogen and oxygen are uniformly distributed in the film. In addition, the nitrogen and gallium contents were more than 30%, which is significantly higher compared to those contained in GaN films electrodeposited on silicon substrates. Raman analysis, XRD, and XPS clearly showed the presence of hexagonal GaN on the deposited films. It is also confirmed that the GaN film grows in a direction perpendicular to the preferred orientation of aluminum and the formation of GaN grows from the preferred orientation plane of aluminum in the direction of making mismatch small. In other words, the crystal structure of the GaN is considerably influenced by the orientation and composition of Al substrates.

5.2 Future Work

This study demonstrated the possibility of the synthesis of GaN film by electrodeposition technique from room temperature aqueous solution. This technique, however, is difficult to obtain a single crystal GaN film and it is difficult to confirm the reproducibility. Moreover, the polycrystalline GaN film produced here showed luminescent characteristics different according to the analysis position. Therefore, it is obvious that this film produced by electrodeposition is not capable of industrial applications. Along with the vigorous hydrogen evolution that occurs during the deposition process in solution, the film surface has a lot of cracks and defects, and the substrate and deposited film do not have sufficient adhesion.

However, it has been confirmed that GaN film can be formed from an aqueous solution at room temperature, and that the film growth is improved by changing the solution and substrate conditions. And I would like to note that the properties of GaN can be improved by post-treatment such as high temperature heat treatment after electrodeposition. Of course, additional processes may deviate from the purpose of this study, but further processing is inevitable for the production of GaN with sufficient properties. In addition, if a substrate such as graphene, which is more conductive than Si and has a small lattice mismatch with GaN, is applied, it is expected that the synthesis of GaN film having better characteristics than the currently synthesized film is possible.

The post-treatment is considered to be very advantageous because it is possible to grow additional nitride layers through high temperature heat treatment in a nitrogen atmosphere. In this study, experiments were performed considering only one-step process at room temperature. However, the synthesis of high quality GaN may be sufficiently possible through post-treatment and multi-step processes.

Achievements

List of publication

1. Jae-wook Kang, Takuaki Mitsuhashi, Kensuke Kurode, Masazumi Okido, “Low-Temperature Synthesis of GaN Film from Aqueous Solution by Electrodeposition”, J. Appl. Electrochem. 49 (2019) pp.871–881

2. Jae-wook Kang, Kensuke Kurode, Masazumi Okido, “Influence of Substrate on Formation of Electrodeposited GaN Film”, Mater. Trans., Submitted

3. Jae-wook Kang, Kensuke Kurode, Masazumi Okido, “Effect of Heat Treatment of Al Substrate on GaN Film Electrodeposited in Aqueous Solution”, J. Surf. Eng. Mater. Adv. Technol., Submitted

Other papers

4. Jae-wook Kang, Jun-Mu Park, Sung-Hwa Hwang, Seung-Hyo Lee, Myeong-Hoon Lee, “Influence of Heat Treatment and Magnesium Content on Corrosion Resistance of Al-Mg Coated Steel Sheet, J. Korean Inst. Surf. Eng. 49 (2016) 202–210

5. Jun-Mu Park, Jae-wook Kang, Seung-Hyo Lee, Kyung-Man Moon, Myeong-Hoon Lee, “The Characteristic Analysis of Calcareous Deposit Films Formed on Steel Plate by Cathodic Current Process in Marine Environment”, J. Korean Inst. Surf. Eng. 49 (2016) 166–171

6. Myeong-Hoon Lee, Yeon-Won Kim, Jae-Wook Kang, Seul-Gi Lee, Jun-Mu Park, Kyung-Man Moon and Yun-Hae Kim, “Influence of Annealing Temperatures on Corrosion Resistance of Magnesium Thin Film Coated Electrogalvanized Steel” (2015) Mod. Phys. Lett. B 29

List of presentation in international conferences

1. J.W. Kang, S. Nomura, K. Kurode, M. Okido, “Electrodeposition of GaN film in aqueous solution, International Conference on Materials and Systems for Sustainability (ICMass 2019), Nagoya, Japan (Nov. 2019)

2. J.W. Kang, K. Kurode, M. Okido, “Electrochemical behavior of Ga^{3+}, NO_3^- and NH_4^+ ions in aqueous solution for synthesizing GaN using by electrodeposition method”, The Electrochemical Society (235th ECS), Dallas, USA, (May 28, 2019)

3. J.W. Kang, T. Mitsuhashi, K. Kurode, M. Okido, “Electrodeposition of Ga from $GaCl_3$ in DMSO bath and influence of NH_4NO_3”, International Symposium on Surface Treatment & Modification Technologies (STMT 2017), Jeju, Korea, (Nov. 23, 2017)

Other presentations

4. J.W. Kang, J.M. Park, J. Kang, Y.S. Yun, M.H. Lee, “The Effect of CO_2 Gas for Electro-deposit Films Formation in Seawater and Crystal Structures”, 7th International Symposium on Advanced Plasma Science and its Applications for Nitrides and Nanomaterials (ISPlasma2015), Nagoya, Japan (Mar. 26, 2015)

5. J.W. Kang, Y.W. Kim, J.M. Park, S.H. Hwang, J. Kang, M. H. Lee, “Effect of Heat Treatment on Corrosion Resistance of Magnesium Alloy Coatings on Electrogalvanized Steel”, 7th International Symposium on Advanced Plasma Science and its Applications for Nitrides and Nanomaterials (ISPlasma2015), Nagoya, Japan (Mar. 26, 2015)

6. J.W. Kang, J.M. Park, J. Kang, Y.S. Yun, M.H. Lee, “Corrosion Behavior of Al-Mg Coated Steel with Different Mg Contents Prepared by PVD Method”, 7th International Symposium on Advanced Plasma Science and its Applications for Nitrides and Nanomaterials (ISPlasma2015), Nagoya, Japan (Mar. 26, 2015)

7. J. Kang, Y.S. Yun, J.W. Kang, J.M. Park, M.H. Lee, “Parametric Studies of the Formation of Calcareous Deposits on Steel Protected with Cathodic Protection in Seawater”, 7th International Symposium on Advanced Plasma Science and its Applications for Nitrides and Nanomaterials (ISPlasma2015), Nagoya, Japan (Mar. 26, 2015)

8. J.M. Park, J.W. Kang, Y.H. Kim, K.M. Moon, M.H. Lee, “Tribological Properties of the Basalt Fiber Reinforced Composites based on Fiber Orientaion and PTFE-Coating process”, 15th International Symposium on Biomimetic Materials Processing (BMMP-15), Nagoya, Japan (Jan. 25, 2015)

9. J.M. Park, J.W. Kang, J. Kang, K.M. Moon, M.H. Lee, “Effective Characteristics of Calcareous Deposit Films on Steel Pipe Prepared by Application Principle of Cathodic Protection in Natural Seawater”, 15th International Symposium on Biomimetic Materials Processing (BMMP-15), Nagoya, Japan (Jan. 25, 2015)

10. J.M. Park, J.W. Kang, J. Kang, K.M. Moon, M.H. Lee, “Prarametric Studies of the Formation of Calcareous Deposits on Steel Protected with Cathodic Protection in Seawater”, 15th International Symposium on Biomimetic Materials Processing (BMMP-15), Nagoya, Japan (Jan. 25, 2015)

11. J. W. Kang, J.M. Park, J. Kang, Y.S. Yun, M.H. Lee, “Corrosion Resistance of Al-Mg Alloy Films with Different Mg Contents Prepared by PVD Method”, 15th International Symposium on Biomimetic Materials Processing (BMMP-15), Nagoya, Japan (Jan. 25, 2015)

12. J.M. Park, H.M. Kim, J.W. Kang, M.H. Lee, “Tribological Properties of the Basalt Fiber Reinforced Composites by PTFE-Coating”, 2nd International Workshop on Solution Plasma and Molecular Technologies (SPM-2), Goyang, Korea (May. 16, 2014)

13. J.W. Kang[a], S.J. Lee, H.M. Kim, J.M. Park, M.H. Lee, “Calcareous Deposit Films Formed by Electro-deposition Method in Natural Seawater with Dissolved CO_2”, 2nd International Workshop on Solution Plasma and Molecular Technologies (SPM-2), Goyang, Korea (May. 16, 2014)

14. S.J. Lee, H.M. Kim, S.G. Lee, J.W. Kang, M.H. Lee, “Calcium Carbonate Films Formed by Eletro-deposition Method in Seawater with Dissolved Carbon Dioxide”, 14th International Symposium on Biomimetic Materials Processing (BMMP-14), Nagoya, Japan, (Jan, 25, 2014)

15. S.G. Lee, H.M. Kim, J.W. Kang, K.M. Moon, M.H. Lee, “Corrosion Resistance of Al-Mg Alloy Films on Steel Substrate Prepared by Sputtering Method”, 14th International Symposium on Biomimetic Materials Processing (BMMP-14), Nagoya, Japan, (Jan. 25, 2014)

16. S.J. Lee, H.M. Kim, S.G. Lee, J.W. Kang, M.H. Lee, “Environmentally Friendly Hybrid Coating Formed by Eletrodeposition Method in Seawater with Dissolved Carbon Dioxide”, The 1st International Conference on Surface Engineering 2013(ICSE-2013), Busan, Korea (Nov. 20, 2013)

List of presentation in domestic conference

1. 中垣まどか, 粂野翔太, 姜 在煜, 黒田健介, 興戸正純, “軽金属塩化物を 含む 炭酸プロピレン 浴からの 電析挙動, 軽金属学会第 136 回春季大会, 2019.03.18–19

Acknowledgements

Here is my acknowledgement page of my PhD thesis. It would not have been possible to write this doctoral thesis without the help and support of the people around me. I would like to thank all people who have helped and inspired me during my doctoral study.

Firstly, I am cordially grateful to my academic supervisor, Prof. Dr. Masazumi Okido, and my second academic supervisor, Prof. Dr. Kensuke Kuroda, for giving me the opportunity to study at the Surface & Interface Engineering Laboratory, and for their appreciated supervision, valuable guidance, and supports to follow the right path for my research works. Special thanks go to 1. Prof. Dr. Masazumi Okido, 2. Tetsuji Hirato, 3. Ryoichi Ichino, and 4. Kensuke Kuroda for being judges of my thesis committee.

I would also like to express my appreciation and thank to Mrs. Otsuka Tominaga for her assistances during staying in Japan.

I thank all the before & present members of the Okido & Kuroda group including students and researchers for all their kindness and assistances. The group provides a warm working atmosphere and convivial place to study.

Special Thanks to Prof. Dr. Myeong-Hoon Lee for referring me to Prof. Dr. Masazumi Okido and offering unstinting supports to fulfill my dream of studying abroad.

I am grateful to Prof. Jong-Do Kim, Prof. Yong-Sub Yun, Prof. Jeong-Hyun Yang, Prof. Jun Kang, Prof. Yeon-Won Kim, Dr. Hye-Min Kim and all members of the S.C.C.C who gave me a lot of advice. Especially, I would like to special thanks to Dr. Jun-Mu Park, Mr. Kyung-Min Lim, Mr. Han-Bin Kim and Jae-Hyuk Park who have been a big help to me for a long time.

The financial support from the Japan Society for the Promotion of Science (JSPS) is acknowledged for helping my focus on the research.

Finally, my personal thanks to dear parents and my sister You-Jin Kang, for their wait, understanding, and absolute love. Their love provided my inspiration and was my driving force. I wish they knew how much I love and appreciate them.

Jae-Wook Kang

Department of Materials Science and Engineering,

Graduate School of Engineering,

Nagoya University

Jan. 2020